2020

The Role of Adipocytes in the Tumor Microenvironment in Obesity-Driven Breast Cancer Progression

Sarah Ackerman

THE ROLE OF ADIPOCYTES IN THE TUMOR MICROENVIRONMENT IN OBESITY-DRIVEN BREAST CANCER PROGRESSION

A Thesis Presented to the Faculty of

The Rockefeller University

in Partial Fulfillment of the Requirements for

the degree of Doctor of Philosophy

by

Sarah Ackerman

June 2020

THE ROLE OF ADIPOCYTES IN THE TUMOR MICROENVIRONMENT IN OBESITY-DRIVEN BREAST CANCER PROGRESSION

Sarah Ackerman, Ph.D.

The Rockefeller University 2020

Obesity affects more than 1 in 3 adults in the United States and has been shown to increase the relative risk of death for women with breast cancer and to increase the risk of developing breast cancer in post-menopausal women. Breast cancer develops in an environment containing white adipose tissue (WAT) which predominately consists of mature white adipocytes. In obesity, WAT undergoes hypertrophy and hyperplasia and can ultimately develop hypoxia, insulin resistance, inflammation, and dysregulated endocrine function. Since obesity directly affects WAT, we hypothesized that molecular changes in white adipocytes in the tumor microenvironment contribute to breast cancer progression. We developed mouse models of obesity-driven breast cancer using diet induced obesity (DIO) and orthotopic models of breast cancer. From one of these models, we performed RNA sequencing of peritumoral mammary fat pads and uninvolved contralateral fat pads. Pathway analysis showed an upregulation in transcripts involved in polyamine and creatine biosynthesis in the obese tumor microenvironment. We have found that the rate limiting enzyme in creatine synthesis, Gatm, is upregulated in adipocytes in the tumor microenvironment of obese mice and plays a key role in breast tumor progression. Using an adipocyte-specific knockout of Gatm (Adipo-Gatm KO), we found a significant reduction in obesity-driven breast tumor growth relative to littermate controls. We have also found that knocking down the creatine transporter (Slc6a8) in breast cancer cells fully attenuates obesity-driven tumor progression. These data support a central role for creatine metabolism in breast tumor

progression in mice and suggest that adipocyte-derived creatine is utilized by the tumor to support its growth. We also examined mammary adipose tissue from human breast cancer patients and found that Gatm is increased in the mammary adipose tissue of obese/overweight relative to normal weight breast cancer patients, supporting the translational relevance of our findings. Overall, we have established models of obesity-driven breast cancer, identified key gene candidates and pathways that affect obesity-dependent breast cancer, and have investigated underlying mechanisms.

This work is dedicated to all of my friends and family who have supported me through this project.

ACKNOWLEDGMENTS

Thank you to Paul Cohen for all of your guidance and support as my mentor. You have allowed me to grow and think on my own while still keeping me on the path forward. Your patience and kindness are much appreciated! To my co-workers, thank you for motivating me and talking through so many bumps in the road of my project. Without you guys lab life would be much less fun! I will miss you all very much!! Thank you specifically to Olivia Maguire and Aarthi Maganti-Vijaykumar for your help with experiments to push my project towards publication.

Thank you to my committee members, Kivanc Birsoy and Sohail Tavazoie for your help throughout this project. Thank you to Celeste Simon for your input on my thesis and traveling from UPenn to act as my external examiner.

Thank you to Andrew Dannenberg, Neil Iyengar, Kathy Zhou and Cathy Liu for all of your help with the human studies in my project. I appreciate you sharing samples and space in your laboratory to broaden the scope of my project.

To Lawrence Kazak, Janane Rahbani and Bozena Samborska for your assistance with the Gatm project. Thank you for providing me with the Gatm floxed mice and processing many samples for mass spec analysis.

Thank you to the Rockefeller Genomics, Bioinformatics and Hospital Statistics Resource Centers for all of your help with my project. Thank you to Tom Carroll for your patience teaching me in your course. Thank you to Caroline Jiang for all of your help with the statistical analysis for this project.

Thank you to Marta Delgado for all of your guidance and help running the Science and Education Policy Association (SEPA). And to Cris Rosario and Stephanie Fernandez for your help

and support. Thank you to all of the Dean's Office for making it possible for me to be a student here, your continuous support and continuing to say yes to all of my crazy ideas for SEPA.

I also really appreciated the opportunities granted to me by Jesse Ausubel and Mandë Holford through the Rockefeller Science Diplomacy course. This course set me on track to pursue the AAAS fellowship and my current career goal of working in science policy.

To my friends in graduate school, thank you for always taking the time to do things outside of science. We rocked some Harry Potter trivia and game nights. To Amy Dunn for always coming with me to gym class and cheering me up when science gets me down. And to Tim Blanchfield for running a kickass gym class which I desperately need to destress.

To the ladies of A2A. Thank you for always being there for me. You all bring fun to my life and I miss living with you all in our old crappy house. Thank you to Eliza for listening to me rant and rave about all manner of issues during my PhD. You are a good listener and always bring perspective to my stress.

Finally, to my parents and brother, thank you for always believing in my ability. Thank you to my mom for talking me off the ledge more than once and always thinking I'm a good scientist even when everything seems to be going wrong. And to my dad for driving in loads of paper towels, snacks and other random things to get me through the weeks. I love you.

TABLE OF CONTENTS

LIST OF FIGURES

CHAPTER 5

CHAPTER 6

LIST OF TABLES

LIST OF ABBREVIATIONS

AAV8 – Adeno-associated virus serotype 8
Adipo-CrT KO or Adipo-Slc6a8 KO – Adipocyte-specific creatine transporter (Slc6a8) knockout mouse
Adipo-Gatm KO – Adipocyte-specific Gatm knockout mouse
Adipo-Odc1 KO – Adipocyte-specific Odc1 knockout mouse
Adipo-Prdm16 KO – Adipocyte-specific Prdm16 knockout mouse
aP2-Prdm16 Tg – Adipocyte protein 2 driven Prdm16 transgenic mouse
BAT – Brown adipose tissue
Beige / beiging – Presence of beige adipocytes / stimulation of beige adipocytes in white adipose tissue
BMI – Body mass index
C57Bl/6J or B6 – Black 6 mice from Jackson Labs
cDNA – Complementary DNA
CLS – Crown like structures
Contra – Contralateral (non-tumor bearing) adipose
Cr - Creatine
CrT – Creatine transporter
DFMO – Difluoromethylornithine, inhibits Odc1
DIO – Diet induced obesity
Gatm – Glycine amidinotransferase, rate limiting step in creatine synthesis
HFD – High fat diet (60% Research diets)
i.p. - intraperitoneal injection
LFD – Low fat diet (10% Research diets)
Odc1 – Ornithine decarboxylase 1, rate limiting step in polyamine synthesis
PCr – Phosphocreatine
PCA – Principle component analysis
Peri – Peritumoral adipose
Prdm16 – PR domain containing 16, master regulator of beige adipose
qPCR – Quantitative PCR
Slc6a8 – Solute carrier family 6, member 8 (creatine transporter)
Slc6a8 KD - Creatine transporter knockdown in E0771 cells
TRAP – Translating ribosome affinity purification
TZD – Thiazolidinediones (rosiglitazone)
WAT – White adipose tissue

INTRODUCTION

1.1 Obesity and society

Obesity currently affects 39.8% of adults in the United States (Hales et al. 2017). In 2008, the U.S. hospitalization and health care costs attributable to obesity were estimated to be $147B/year (Finkelstein et al. 2009). It has been estimated that this amount will increase by $48-66 billion/year by 2030 (Wang et al. 2011). Obesity is presenting a major public health concern in the U.S. and worldwide (Finucane et al. 2011).

Obesity occurs when more calories are consumed than are expended. Body mass index (BMI) is a common measure used to indicate someone as overweight (25 – 30) or obese (greater than or equal to 30). Overweight and obese individuals are at increased risk of developing type 2 diabetes, hypertension, cardiovascular disease and non-alcoholic fatty liver disease (Global BMI Mortality Collaboration et al. 2016; Goossens 2017). Recently it has become apparent that obesity is also liked to cancer. Epidemiologic evidence shows obesity increases a patient's risk of developing many types of cancers (ex. breast, kidney, ovarian and colon cancer) and is associated with worse outcome of these cancers (Calle et al. 2003; Renehan et al. 2008).

1.2 Epidemiological data

A seminal paper in 2003 by Calle et al. showed that cancer patients with a BMI above 40 had mortality rates that were 52% higher for men and 62% higher for women (Calle et al. 2003). In 2008, a meta-analysis of prospective observational studies showed BMI is associated with increased risk of many tumor types (Renehan et al. 2008). These included esophageal, thyroid and renal cancers in men and endometrial, gallbladder, esophageal and renal cancers in women (Renehan et al. 2008). These two papers established that obesity is a risk factor for both developing

cancer and for adverse outcomes from many types of cancer. More recently, Arnold et al. showed that in 2012, 3.6% of new adult cancer cases were attributable to high BMI (Arnold et al. 2015) and in 2014, Bhaskaran et al. showed BMI was positively associated with risk of developing liver, colon, ovarian and postmenopausal breast cancer (Bhaskaran et al. 2014).

1.3 Breast cancer and obesity

Breast cancer is the most common cancer in women regardless of race or ethnicity and is the second most common cause of death from cancer ("Breast Cancer Statistics | CDC" 2019). Breast cancer develops in an environment that predominantly consists of mammary white adipocytes. These mammary adipocytes become dysfunctional in the obese state and may impact breast tumor progression.

Calle et al. showed that obese women (BMI>40) with breast cancer have a 2.12-fold increased relative risk of death (Calle et al. 2003). A study in 2014 showed that obese post-menopausal women have an increased hazard ratio of 1.05 for breast cancer per every 5kg/m2 increase in BMI (Bhaskaran et al. 2014). Interestingly, this increased hazard ratio was not present for obese premenopausal women. Another group showed an increased hazard ratio for post-menopausal women but also examined premenopausal women and found that excess body weight confers increased risk both pre- and post-menopause (Renehan et al. 2008). Current studies also point to the increased relative risk of breast cancer in obese post-menopausal women to be estrogen receptor driven (Cleary and Grossmann 2009).

While BMI is one measure of obesity, it is not necessarily the most accurate. Post-menopausal women with a normal BMI but relatively high body fat levels were found to have an elevated risk of invasive breast cancer and altered levels of circulating metabolic inflammatory

factors (Iyengar et al. 2018). These investigators also found that, regardless of menopausal state, white adipose tissue inflammation, which was defined by the presence of dead/dying adipocytes surrounded by macrophages forming crown-like structures (CLS), is associated with a hazard ratio of 1.83 for worse breast cancer prognosis compared to women without inflamed mammary adipose tissue (Iyengar, Zhou, et al. 2016).

Overall, the current consensus is that there is an increased risk of developing breast cancer for obese postmenopausal women, specifically ER positive breast cancer. Relative risk of death from breast cancer is increased for obese women regardless of menopausal state and hormone receptor status. It is also becoming exceedingly clear that BMI is not a sufficient measurement of adipose tissue health and that lean patients (defined by BMI) with excess adiposity and adipose tissue inflammation may also be at an increased risk for breast cancer and related mortality.

1.4 Adipose tissue

Adipose tissue consists of adipocytes, immune cells, stromal cells, blood vessels and nerve projections. There are three distinct types of adipocytes: white, brown, and beige. White adipocytes store excess nutrients as triglyceride (Rosen and Spiegelman 2014). In contrast, brown and beige adipocytes have high levels of uncoupling protein 1 (UCP1), which uncouples oxidative phosphorylation from ATP synthesis, thereby dissipating energy as heat (Cohen and Spiegelman 2015). Beige adipocytes appear within white adipose tissue (WAT) and can be stimulated by cold exposure, PPARγ agonists and exercise (Harms and Seale 2013). Beige and brown adipocytes are associated with improvements in glucose and lipid homeostasis, and are generally associated with favorable metabolic health (Kajimura, Spiegelman, and Seale 2015).

In the setting of obesity, adipose tissue becomes dysfunctional. Brown adipose tissue (BAT), predominantly made up of brown adipocytes, develops a more "white fat" like phenotype with higher levels of inflammation (Alcalá et al. 2019). White adipose tissue (WAT) exhibits increased white adipocyte cell number (hyperplasia) and the cells themselves grow larger (hypertrophy). These changes are associated with elevated levels of free fatty acids (FFA) and triglycerides, increased blood glucose, and insulin resistance (Martyn, Kaneki, and Yasuhara 2008).

Adipose tissue also becomes hypoxic in obesity with lower oxygen consumption and correspondingly lower capillary density (Engin 2017). It has also been shown that local adipose tissue hypoxia results in dysregulated adipokine production (Hosogai et al. 2007). Increased expression of hypoxia-inducible transcription factor alpha (HIF1α) promotes chemokine release from adipocytes, leading to adipose inflammation (Lee et al. 2014). This environment of low oxygen and increased inflammation is thought to help promote tumor growth through chronic inflammation remodeling the extracellular matrix (ECM) (Seo et al. 2015).

White adipose tissue traditionally is considered a lipid storage organ, but it also acts as an endocrine organ by secreting adipokines which can have local and systemic effects (Coelho, Oliveira, and Fernandes 2013). Leptin and adiponectin are the best characterized adipokines. Leptin expression increases with obesity, while adiponectin expression decreases (Stern, Rutkowski, and Scherer 2016). White adipose tissue (WAT) also produces inflammatory cytokines such as tumor necrosis factor alpha (TNFα), interleukin 6 (IL-6), interleukin 1 beta (IL-1β) and transforming growth factor beta (TGFβ) (Osborn and Olefsky 2012).

1.5 Current molecular links between obesity and cancer (Figure 1.1)

There are many studies examining the connections between obesity and cancer. Here we describe the main factors (adipokines, inflammatory cytokines, immune cells, insulin/IGFs etc.), which have been shown to link obesity and cancer.

1.5.1 Leptin

Leptin is an adipose-derived hormone that coordinates energy homeostasis by signaling from adipose to the hypothalamus (Maffei et al. 1995). Plasma leptin is correlated with BMI in rodents and humans (Maffei et al. 1995). Higher circulating leptin is associated with increased risk of postmenopausal breast cancer (Harris et al. 2011; Ollberding et al. 2013) and patients with breast cancer that overexpresses the leptin receptor have an unfavorable prognosis (Miyoshi et al. 2006).

Leptin can upregulate metalloprotinease-13 (MMP-13) which can in turn enhance the invasiveness of pancreatic cancer. Additionally, deleting the leptin receptor in the brain (db/db $^{Nse/Nse}$) dramatically reduced tumor burden in a spontaneous model of breast cancer through reduction of the ERK1/2 and JAk2/STAT3 pathways (J. Park et al. 2010). Chang et al. also showed that the leptin-STAT3 pathway regulates breast cancer stem-like cells which can promote malignant breast cancer progression (Chang et al. 2015).

1.5.2 Adiponectin

Adiponectin is an adipokine associated with the "healthy" expansion of adipose tissue (Stern, Rutkowski, and Scherer 2016). Adiponectin has been shown to act on hepatocytes to increase insulin sensitivity (Berg et al. 2001) and also has anti-inflammatory effects (Kadowaki et al. 2006). In the setting of obesity, adiponectin levels are reduced and are inversely correlated with

the progression of several cancers, including breast, pancreatic, and colorectal cancer (Grote et al. 2012; Shahar et al. 2010; An et al. 2012). In a meta-analysis Wei et al. found that levels of circulating adiponectin were significantly downregulated in patients with cancer compared to those without (Wei et al. 2016). Interestingly, most breast cancer cell lines express the adiponectin receptor (ex. MCF7, MDA-MB-231 and SKBR3) (Parida, Siddharth, and Sharma 2019) and adiponectin can signal through this receptor, reducing cellular proliferation and inducing apoptosis (Bråkenhielm et al. 2004).

1.5.3 Endotrohpin

In the setting of obesity, adipocytes secrete ECM molecules such as COL6a3 to support hypertrophy. Endotrophin (ETP) is the carboxy-terminal proteolytic cleavage product of the COL6a3 chain and abundantly expressed in adipose tissue (J. Park and Scherer 2013). Human endotrophin enhances epithelial-mesenchymal (EMT) transition in breast cancer cells and chemotherapy resistance (Bu et al. 2019). Bu et al. developed neutralizing monoclonal antibodies against human endotrophin which limit breast tumor growth and enhance chemosensitivity in a nude mouse model carrying human breasts (Bu et al. 2019).

1.5.4 Insulin and Insulin-like growth factor

Levels of insulin and insulin-like growth factors are increased in obese patients. Hyperinsulinemia is an independent risk factor for breast cancer development in women (Gunter et al. 2009) and prostate cancer mortality in men (Ma et al. 2008). In a mouse model injected with a mammary carcinoma cell line (Mvt1), hyperinsulinemia promoted breast cancer metastasis to the lung (Ferguson et al. 2012). Several cancer cell types also express the insulin receptor. Thus,

in the hyperinsulinemic condition, tumor cells activate the phosphatidylinositol-4,5-bisphosphate 3-kinase (PI3K) pathway, leading to proliferation and tumor progression (Ulanet et al. 2010).

Insulin-like growth factor 1 (IGF-1) and insulin-like growth factor 2 (IGF-2) have a similar molecular structure to insulin and are regulated by insulin (Pollak 2008). Circulating levels of IGF-1 are associated with an increased risk of prostate cancer and premenopausal breast cancer (Renehan et al. 2004). IGF-2 is found in the colonic mucosa of 30% of colorectal cancer patients compared to 10% in healthy individuals (Cui et al. 2006), suggesting it may also play a role in cancer incidence or progression.

The IGF-1 receptor (IGF1R) is elevated in many types of cancer cells, specifically in human breast cancer (Papa et al. 1990) and colorectal carcinomas (Weber et al. 2002). When stimulated, IGF1R can activate the mitogen-activated protein kinase (MAPK) pathway, promoting many types of cancer, including skin and pancreatic cancer initiation and progression *in vitro* (Bol et al. 1997; Lopez and Hanahan 2002). IGF1R can also activate Akt (McCampbell et al. 2006), which is a crucial for progression of diabetes, cancer and aging (Zoncu, Efeyan, and Sabatini 2011).

Many obese patients also have type 2 diabetes with insulin resistance and increased circulating insulin. In 2008, a meta-analysis showed that cancer patients who are diabetic are at an increased risk for all-cause mortality compared to non-diabetic cancer patients (Barone et al. 2008). Overall the insulin/IGF axis plays a key role in obesity and in turn has been implicated in tumor incidence and progression.

1.5.5 Inflammatory Cytokines

Tumor necrosis factor alpha (TNFα) is proinflammatory and stimulates lipolysis and release of free fatty acids (FFAs) from resident immune cells in WAT (Iyengar, Gucalp, et al. 2016). NF-κb is activated by TNFα, and this activation has been shown to be important for cancer development (Khandekar, Cohen, and Spiegelman 2011). Specifically, deletion of NF-κb inhibitor-α (NFKBIA) promotes development of glioblastoma (Bredel et al. 2011), NF-κb is necessary for the development of colitis and colonic epithelial cell turnover in colitis-associated carcinogenesis (Burkitt et al. 2015), and NF-κb is an anti-apoptotic factor which promotes hepatocellular carcinoma (Kern et al. 2018).

IL-6 is a pro-inflammatory cytokine which activates the immune system. It is also secreted by resident adipose immune cells and further activates the immune system. IL-6 also activates the JAK/STAT pathway. Specifically, IL-6 and TNFα cause hepatic inflammation which activates STAT3, promoting hepatocellular carcinoma (E. J. Park et al. 2010). Interestingly, in thyroid cancer, STAT3 is a negative regulator of tumor growth (Couto et al. 2012).

1.5.6 Inflammation and Immune Cells

Adipose tissue contains resident immune cells such as macrophages, T cells and NK cells. In the obese state, there is an accumulation of these immune cells, which increases inflammation through the secretion of proinflammatory cytokines. Adipose inflammation is associated with increased breast tumorigenesis (Seo et al. 2015) and worse progression (Iyengar, Zhou, et al. 2016; Pierce et al. 2009). Inflammation can affect a myriad of factors which affect cancer progression such as TNFα and IL-6 secretion, insulin resistance and altered angiogenesis (Hursting et al. 2012).

Adipose tissue macrophages (ATMs) accumulate in obese WAT and produce inflammatory cytokines. Proliferating ATMs are associated with poor clinical outcome from breast cancer (McCampbell et al. 2006) and protect tumors from the effects of radiation treatment (De Palma and Lewis 2013). Mechanistically, Kolb et al. demonstrated that activated ATMs in obese adipose tissue have activated NLCR4 inflammasomes, which produce IL-1b thereby promoting breast cancer progression (Kolb et al. 2016).

Crown-like structures are rings of macrophages which surround dead or dying adipocytes. The presence of CLS is an important measure of adipose inflammation. An increase in CLS in mammary adipose tissue is associated with a worse prognosis in patients with breast cancer (Morris et al. 2011; Iyengar, Zhou, et al. 2016). A retrospective study showed that increased CLS density in the local white adipose is associated with worse disease-specific survival and overall survival for patients with squamous cell carcinoma of the tongue (Iyengar, Ghossein, et al. 2016). CLS are an important indicator of adipose tissue inflammation but the mechanism by which these macrophages affect tumorigenesis and progression is unclear.

1.5.7 Free Fatty Acids (FFA) and Fatty Acid Oxidation (FAO)

Free fatty acids (FFA) are elevated in obesity and can promote insulin resistance and inflammation (Boden 2008). Fatty acid oxidation (FAO) is the breakdown of fatty acids for energy. Lazar et al. showed that adipose-derived exosomes contain proteins related to fatty acid oxidation (FAO). In the setting of obesity, the number of exosomes increases and they can traffic to nearby melanoma cells altering FAO metabolism within the tumor (Lazar et al. 2016). Zhang et al. demonstrated that adipocytes in the melanoma tumor microenvironment. transfer lipids to

melanoma cells increasing the levels of fatty acids fueling melanoma proliferation and invasion (Zhang et al. 2018)

1.5.8 Vegf and vasculature

In humans, obesity promotes resistance to anti-VEGF therapy in breast cancer (Incio et al. 2018) and renal cell carcinoma (Ladoire et al. 2011). There is controversy over whether or not all obesity-driven tumors are relatively resistant to anti-VEGF or if only certain patients have this characteristic (Gati et al. 2014; Cao 2018).

However, in a mouse model of post-menopausal obesity-driven breast cancer, VEGF levels are higher in ovariectomized obese mice compared to ovariectomized non-obese controls (Gu et al. 2011). Gu et al. proposed that postmenopausal obesity promotes tumor angiogenesis and breast cancer progression possibly through increased adipose tissue mass and adipokines such as VEGF that could systemically and locally affect breast cancer progression (Gu et al. 2011).

Another study in 2012 also found an increase in expression of TNFα, VEGF, IKKB and mTOR in mammary tumors of obese mice. Inhibitors (rapamycin, bevacizumab and aspirin) that target members of the IKKB/mTOR/VEGF pathway suppressed tumorigenesis and prolonged survival more effectively in obese than in nonobese mice (Chen et al. 2012).

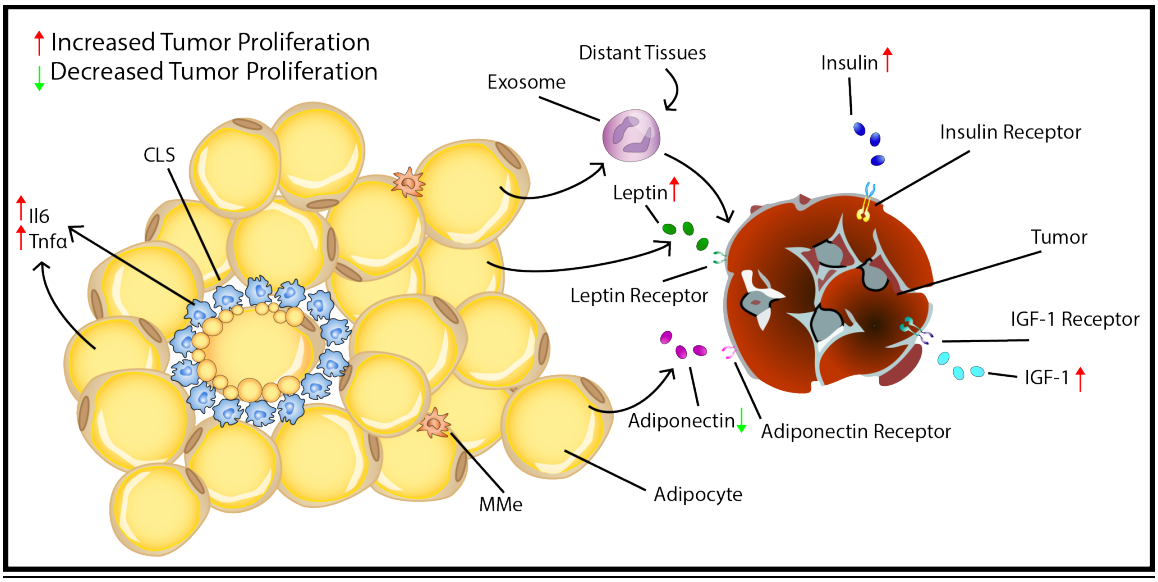

Figure 1.2 Mechanisms linking obesity and cancer growth. Figure previously published in *Insights into the Link Between Obesity and Cancer* Current Obesity Reports (2017) (Ackerman et al. 2017), copyrights procured from Springer Nature.

1.6 Summary

Obesity and cancer are now widely accepted to be linked, and some cancers such as breast cancer show a particular worsened outcome in obese patients. A large number of interconnected pathways have been identified connecting obesity and breast cancer. Many papers have presented promising mechanisms (Lazar et al. 2016; Kolb et al. 2016; Bu et al. 2019) yet none have solved the question entirely. It seems most likely to us that there is not one answer and that multiple interventions will be required to treat the condition in humans.

In our studies, we take a unique approach by examining the white adipocytes which predominate in the breast tumor microenvironment. We hypothesize that molecular changes in obese white adipocytes in the tumor microenvironment accelerate breast tumor progression. We developed mouse models of obesity-driven breast cancer and examined the transcriptome of the adipose tissue. We have identified key genes expressed in obese peritumoral adipocytes which

affect breast tumor progression and have begun to investigate the mechanism of action. We have also extended our findings to breast cancer patients and see that the pathways we have discovered may be relevant for human disease.

Overall, our study has discovered novel pathways connecting breast tumor progression and obesity in a mouse model. Breaking the link between breast cancer and obesity is key to treating patients especially considering that 1 in 3 adults in the U.S. are obese and 1 in 8 women will develop breast cancer. Factors involved in the pathways described here have the potential to be implemented in translational medicine.

CHAPTER 2

MODELING OBESITY-DRIVEN BREAST CANCER AND ANALYSING ADIPOSE TISSUE IN THE MODEL

2.1 Developing a model to study obesity-driven breast cancer

2.1.1 E0771 model

Obesity and breast cancer are epidemiologically linked, yet the mechanism underlying this association is not well understood. We were interested in addressing this question from an adipose perspective. Since we know that adipose tissue is more than just a repository for fat and we know that adipose tissue is abundantly present in the breast tumor microenvironment, we hypothesized that unhealthy adipose tissue in the tumor microenvironment can promote obesity-driven tumor growth.

C57Bl/6J (B6) mice are susceptible to diet induced obesity (DIO) when fed a 60% high fat diet (HFD). On average after 12 weeks on a HFD, female B6 mice weighed 50% more ($p<0.01$) than chow fed control mice (Figure 2.1A). HFD mice also had a 480% ($p<0.0001$) increase in fat mass compared to chow control mice, while the amount of lean mass remained similar (Figure 2.1B). Levels of blood glucose and insulin were 40% ($p<0.0001$) and 200% ($p<0.01$) greater respectively, in HFD mice compared to chow controls (Figure 2.1C and D). This was expected as DIO is often used as a model for insulin resistance.

We started by studying an orthotopic breast cancer model using the E0771 breast cancer cell line. E0771 cells are syngeneic on B6 and produce rapidly growing, obesity-dependent tumors. After 9 weeks on a HFD or chow diet, 50,000 E0771 cells were injected into the fourth mammary fat pad. Tumors in HFD mice showed increased progression compared to tumors in chow mice ($p<0.01$) (Figure 2.1E). At endpoint, tumors in the HFD mice were 500% greater ($p<0.01$) in

Figure 2.1 Establishing E0771 as a model of obesity-driven breast cancer

A. Weight of wild-type B6 mice on chow and HFD. B. Lean and fat mass of chow and HFD mice. C. Blood glucose of chow and HFD fed mice with E0771 tumors. D. Insulin levels of chow and HFD fed mice with E0771 tumors. E. Progression of E0771 tumor growth in chow and HFD fed mice. F. Final tumor weight of chow and HFD tumors at necropsy. Data shown here represent mean +/- standard error of the mean (SEM). ** $p<0.01$, *** $p<0.001$, **** $p<0.0001$.

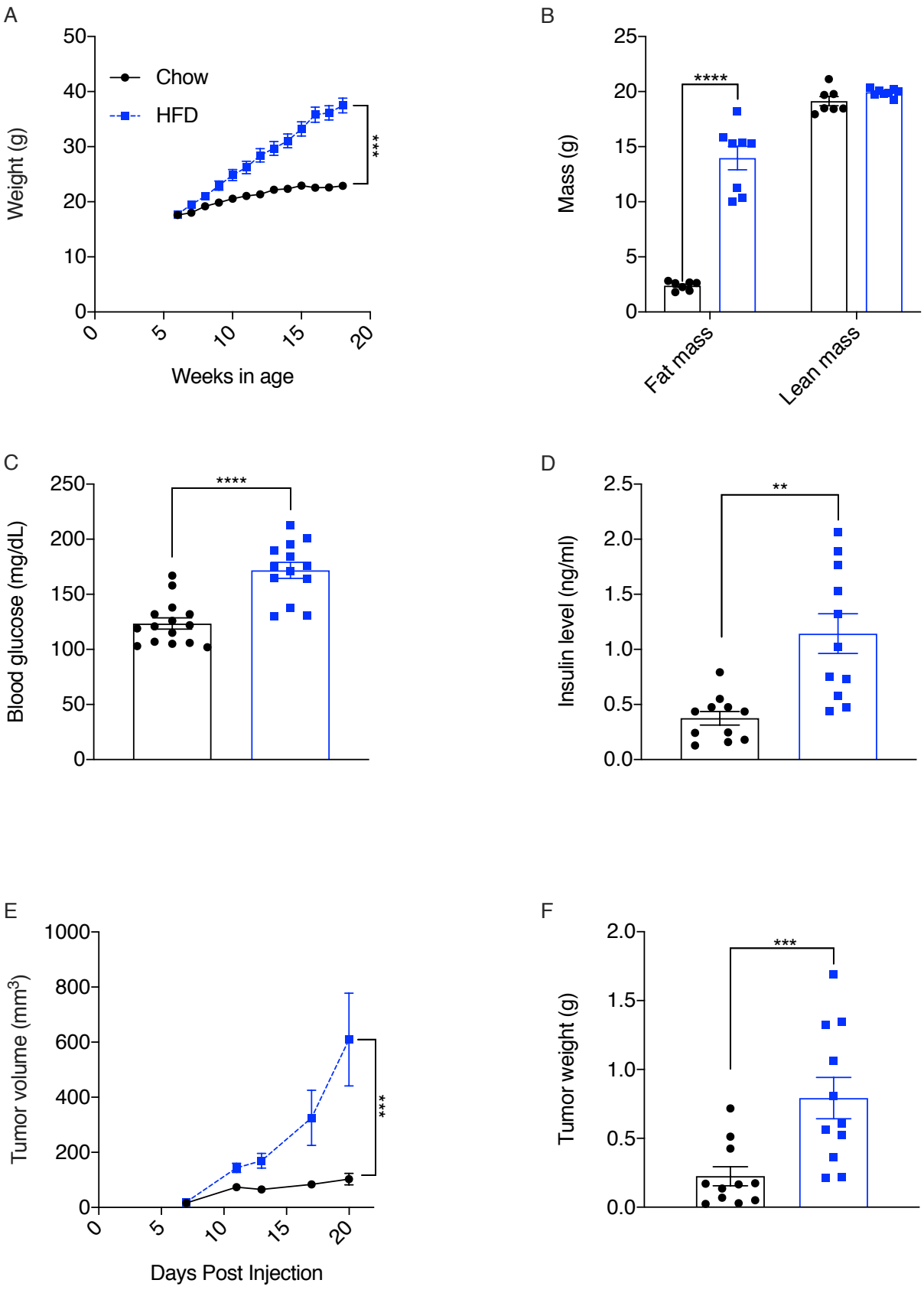
A
Weight (g)
Chow
HFD
***
Weeks in age
B
Mass (g)
****
Fat mass
Lean mass
C
Blood glucose (mg/dL)
****
D
Insulin level (ng/ml)
**
E
Tumor volume (mm3)
***
Days Post Injection
F
Tumor weight (g)
***

volume compared to tumors in the chow controls (Figure 2.1E). Endpoint final tumor weight was also 250% greater ($p<0.001$) in the HFD mice compared to chow controls (Figure 2.1F).

2.1.2 Pair feeding study

We wanted to investigate whether the obesity-driven tumor growth we observed was due to obesity *per se* or possibly due to a dietary component. To answer this question, we set up a pair feeding experiment in which a group of mice was fed HFD but only provided the same number of calories as LFD controls voluntarily consumed (see methods). Mice on a HFD gained 50% more weight ($p<0.0001$) than either the low-fat diet (LFD) mice or the HFD pair fed mice (Figure 2.2A). The fat mass of the HFD mice was also significantly greater than the LFD (440%, $p<0.0001$) and pair fed groups (220%, $p<0.0001$) (Figure 2.2B). Interestingly, the fat mass of the pair fed mice was twice ($p<0.05$) the LFD group suggesting that even though these mice were calorie-matched, the adipose tissue was expanded (Figure 2.2B).

These three groups of mice were then injected with 50,000 E0771 cells. Tumors in HFD mice showed increased progression compared to tumors in LFD or HFD pair fed mice ($p<0.001$). Tumors grew 290% larger ($p<0.001$) in volume in HFD mice compared to tumors in the LFD and HFD pair fed mice by endpoint (day 20). There was no difference in tumor growth between the LFD and HFD pair fed groups (Figure 2.2C). At endpoint, tumor weight was 230% increased ($p<0.05$) in the HFD group, and there was no difference in tumor weight between the LFD and HFD pair fed mice (Figure 2.2D). These data indicate that it was obesity and not the diet that was responsible for increased tumor progression.

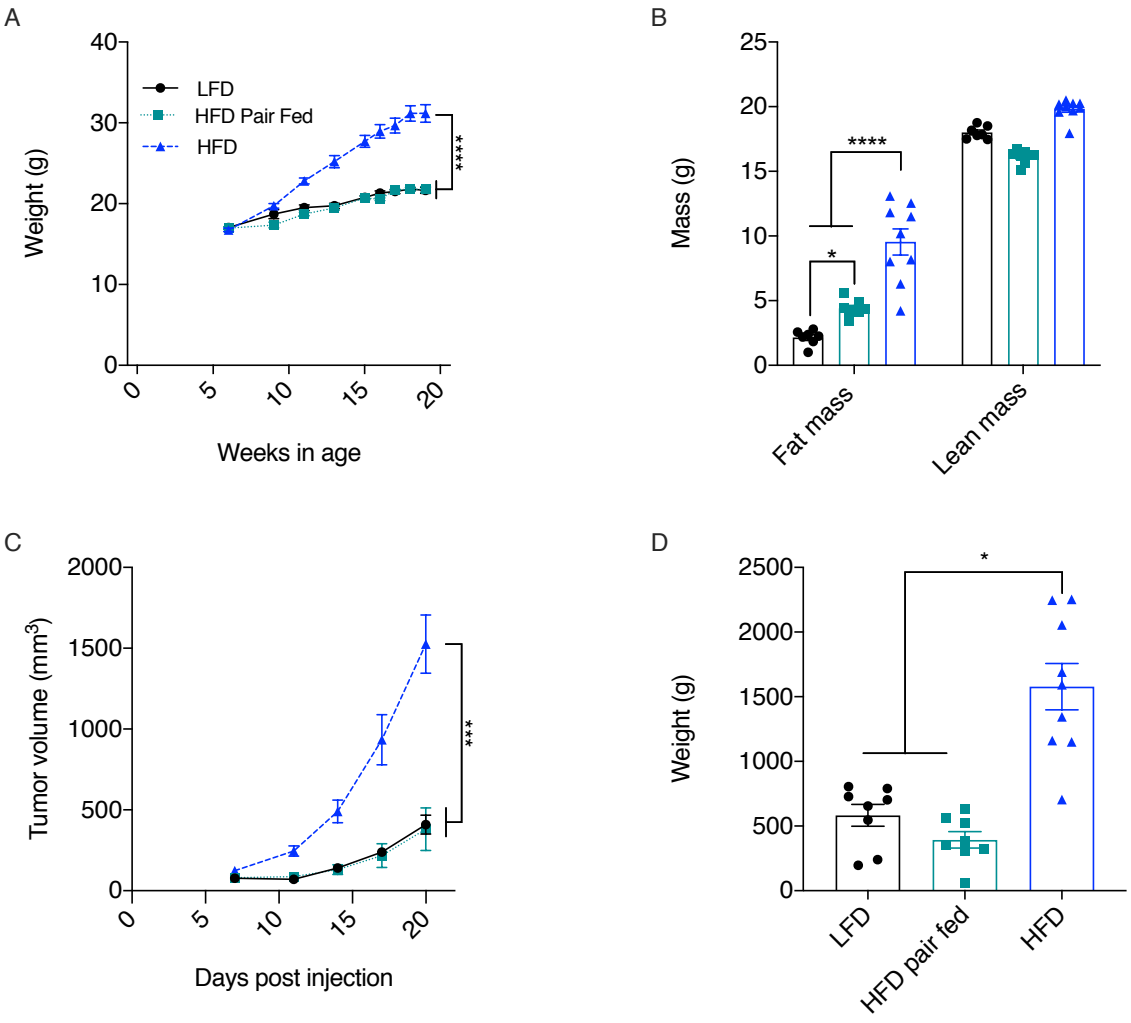

Figure 2.2 HFD pair-fed mice had similar tumor progression to chow fed mice

A. Weight of chow, HFD pair fed (starting at 14 weeks of age) and HFD fed mice. B. Fat and lean mass at necropsy. C. Progression of E0771 tumor growth in chow, HFD pair fed and HFD mice. D. Final weight of chow, HFD pair fed and HFD fed tumors at necropsy. Data shown here represent mean +/- standard error of the mean (SEM). * $p< 0.05$, *** $p<0.001$, **** $p<0.0001$.

2.2 Transcriptomic analysis to identify molecular mechanisms

In both our mouse model and in humans, breast cancer develops in close proximity to mammary adipose tissue. Thus, we were interested in how adipose tissue in the tumor microenvironment might be affecting breast tumor progression. To answer this question, we

performed RNA sequencing of peritumoral (immediately surrounding the tumor) and contralateral mammary fat from the E0771 model (Figure 2.3A).

RNA was isolated from bulk adipose tissue from the following six groups: chow peritumoral, chow contralateral, HFD peritumoral, HFD contralateral, chow non-tumor bearing and HFD non-tumor bearing. Libraries were prepared and RNA sequencing was performed (n=4 per group). Principal component analysis illustrated that the data clustered by diet (PCA 1) and the presence of the tumor (PCA 2) (Figure 2.3B). The HFD peritumoral fat was most distinct from the chow fed mice as well as HFD contralateral and HFD non-tumor bearing groups (Figure 2.3B).

We were most interested in gene expression changes in the HFD peritumoral adipose tissue, as we reasoned these pathways might be involved in obesity-driven tumor growth. GSEA KEGG pathway analysis was performed to compare HFD peritumoral to HFD contralateral adipose tissue and identified a list of significantly upregulated pathways (Figure 2.3C). One pathway that has not previously been studied for its role in cancer progression is the Arginine and Proline Metabolism pathway.

Within the Arginine and Proline Metabolism pathway were the genes encoding the rate-limiting enzymes in polyamine and creatine biosynthesis, both of which were upregulated in HFD peritumoral adipose tissue. Ornithine decarboxylase 1 (Odc1) was upregulated 459% ($p<0.0001$) and glycine amidinotransferase (Gatm) was upregulated 350% ($p<0.0001$) in peritumoral vs. contralateral mammary fat. These genes were also slightly upregulated (154% Odc1 and 116% Gatm) in chow fed peritumoral vs. contralateral fat, but these differences did not reach statistical significance ($p=0.5$ Odc1 and $p=0.8$ Gatm). There was no difference in Odc1 or Gatm expression between chow and HFD fed non-tumor bearing mice.

Odc1 and Gatm are the rate limiting steps in polyamine and creatine biosynthesis respectively. They are also connected through arginine and ornithine (Figure 2.3D). The fact that both of these genes were upregulated in HFD peritumoral adipose tissue and that they are in interconnected pathways was intriguing. Furthermore, we noticed that many of the other genes in the polyamine pathway were upregulated in HFD peritumoral fat (see Chapter 4). This suggested to us that there was an upregulation in these pathways in obese mammary adipose tissue in the tumor microenvironment. We hypothesized that these molecular alterations play a role in obesity-dependent tumor growth.

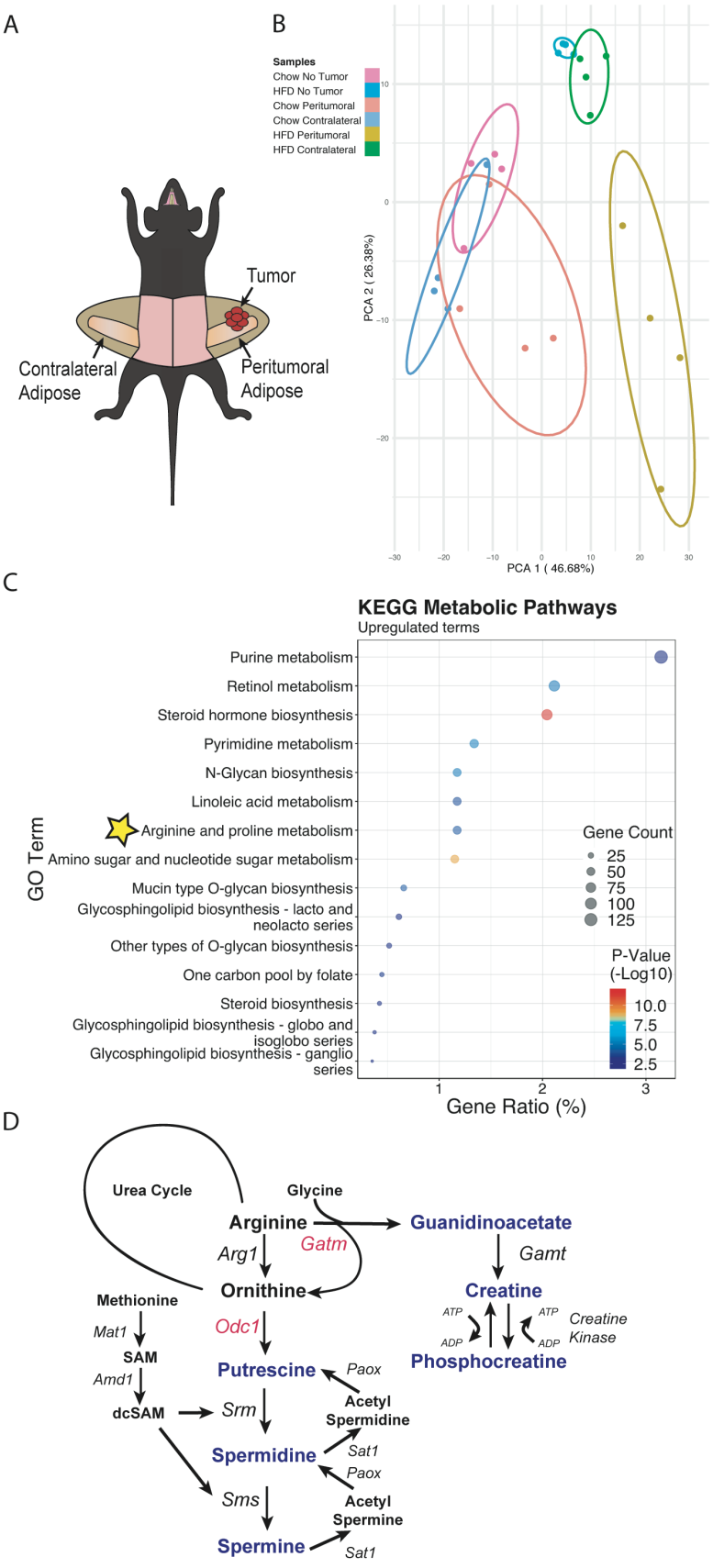

Figure 2.3 Transcriptomic analysis of adipose tissue from obesity-driven breast cancer model

A. Diagram of tumor location in left 4th mammary fat pad (peritumoral) and corresponding contralateral fat pad. B. PCA plot of RNA sequencing of adipose tissue from peritumoral and contralateral adipose from chow and HFD fed mice. C. GSEA KEGG Pathway analysis of HFD Contralateral vs. HFD Peritumoral adipose. D. Segment of the Arginine and Proline Metabolism KEGG pathway demonstrating the link between polyamine and creatine synthesis.

2.3 Additional models of obesity-driven breast cancer

2.3.1 Py8119 model

As we began to create tools to modify Gatm and Odc1 in our model of obesity-driven breast cancer, we felt it was important to develop additional models of obesity-driven breast cancer. The Py8119 line was derived from the MMTV-PyMT transgenic mouse line (see below) which develops genetically-driven breast tumors (Biswas et al. 2014; Gibby et al. 2012). Py8119 is negative for the expression of estrogen receptor, progesterone receptor and Her2 (Biswas et al. 2014). Py8119 has also been shown to be obesity dependent (Kolb et al. 2016).

We performed a similar experiment to the E0771 study above. 50,000 Py8119 cancer cells were injected into mice on a chow or HFD (Figure 2.4A). Py8119 tumors in HFD mice showed increased progression compared to tumors in chow mice ($p<0.001$). At endpoint, tumors in the HFD mice grew 160% ($p<0.001$) larger in volume than tumors in the chow fed controls (Figure 2.4B).

2.3.2 PyMT model

We also studied the effect of obesity in a genetic model of breast cancer: MMTV-PyMT transgenic mice. The PyMT model has mammary gland specific expression of the polyomavirus middle T antigen driven by the mouse mammary tumor virus promoter/enhancer (MMTV-PyMT)

(Guy, Cardiff, and Muller 1992). This mouse line is known to produce tumors in all of the mammary fad pads and to metastasize to the lungs (Fantozzi and Christofori 2006). This mouse line has also been shown to have obesity dependent tumor growth. Body weight, visceral fat weights, primary mammary tumor growth and terminal total tumor weights have been shown to increase in PyMT mice on a HFD (Cowen et al. 2015).

PyMT mice on a HFD weighed 20% ($p<0.01$) more than chow fed controls (Figure 2.4C). Interestingly, the difference in weight between chow and HFD fed PyMT mice was smaller than in our cohorts of wild-type B6 mice. Primary tumors in HFD mice trended towards increased progression compared to primary tumors in chow mice ($p=0.7$). At endpoint, primary tumor volume was 60% larger in HFD mice compared to chow controls, though this was not statistically significant ($p=0.75$) (Figure 2.4D). Overall tumor burden was also increased in HFD mice, but this was not statistically significant (data not shown). This suggested that the PyMT model may not be obesity dependent or perhaps the limited weight gain in these mice attenuated the effect of excess adiposity on these tumors.

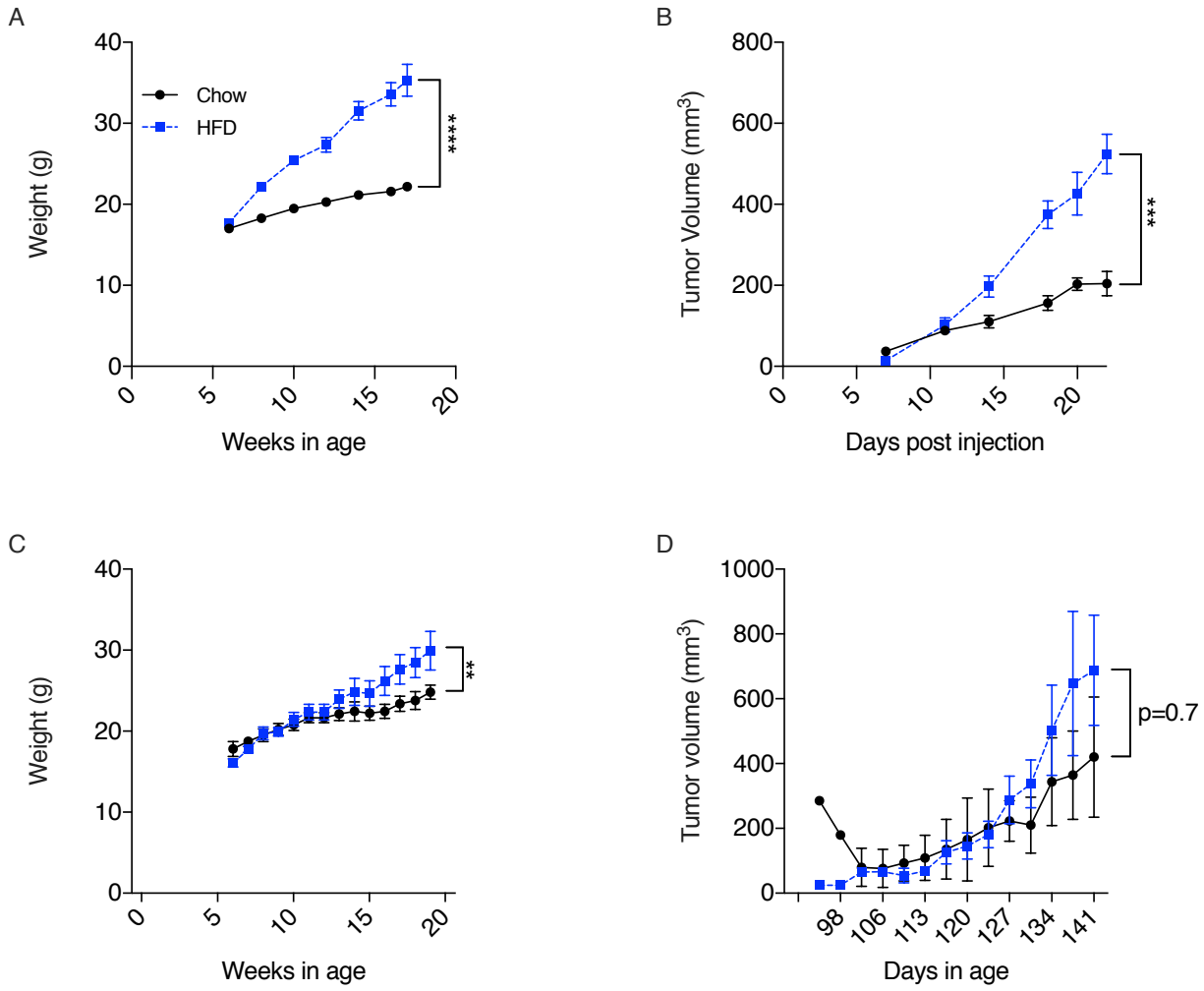

Figure 2.4 Py8119 and MTTV-PyMT models of obesity-driven breast cancer

A. Weight of C57Bl6 mice on chow and HFD. B. Py8119 tumor growth in chow and HFD mice. C. Weight of MMTV-PyMT Bl6 mice on chow and HFD. D. Progression of primary tumors in MMTV-PyMT Bl6 mice on chow and HFD. Data shown here represent mean +/- standard error of the mean (SEM). ** $p<0.01$, *** $p<0.001$, **** $p<0.0001$.

2.4 Confirmation of Gatm and Odc1 and TRAP analysis

2.4.1 qPCR confirmation

RNA sequencing clearly showed that Odc1 and Gatm were upregulated at the mRNA level in HFD peritumoral adipose tissue. In order to confirm this result, we completed an independent study, identical to the E0771 study described in Figure 2.1E. Levels of Odc1 and Gatm were increased significantly in HFD peritumoral adipose tissue (400% and 590%) as compared to HFD contralateral adipose tissue (Figure 2.5A and B). Both genes were also increased in the chow peritumoral adipose tissue (400% and 280%) as compared to chow contralateral adipose, though these differences were not statistically significant (Figure 2.5A and B).

We also examined peritumoral and contralateral adipose tissue from the orthotopic Py8119 and genetic PyMT transgenic models described in Figure 2.4. Odc1 and Gatm levels were also increased in the HFD peritumoral adipose tissue in the orthotopic Py8119 model (Figure 2.5A and B). The RNA level of Gatm but not that of Odc1 was increased in the HFD peritumoral adipose tissue in the PyMT genetic model (Figure 2.5A and B). The less robust transcriptional changes in the PyMT genetic model may have been due to the lack of obesity-dependent growth in this model. Additionally, PyMT transgenic mice develop multifocal tumors, making it more challenging to clearly demarcate peritumoral from distant adipose tissue.

2.4.2 Translating ribosome affinity purification (TRAP)

Adipose tissue is made up of many cell types including adipocytes, immune cells and fibroblasts. The bulk RNA sequencing which we performed included all of these cell types. To determine whether our genes of interest showed altered expression specifically in adipocytes we used translating ribosome affinity purification (TRAP). Rosa TRAP; Adiponectin cre positive

mice, that express a GFP tagged ribosomal protein in adipocytes, were placed on chow or HFD for 10 weeks and then injected with E0771 tumor cells. Mice on HFD gained significantly more weight, and tumors grew significantly larger in the HFD mice, just as in wild-type B6 mice (data not shown). Ribosomes from adipocytes were pulled down using anti-GFP antibody conjugated magnetic beads, allowing for the isolation of adipocyte RNA from peritumoral and contralateral adipose tissue. Gatm was highly expressed in adipocytes in HFD mice; specifically, Gatm was 1003% higher in peritumoral adipocytes compared to the bulk peritumoral adipose tissue (input) (Figure 2.5D).

Odc1 expression was not significantly increased in peritumoral adipocytes from HFD mice but was increased 130% ($p<0.05$) in HFD contralateral adipocytes compared to input from HFD contralateral bulk adipose tissue (input) (Figure 2.5F). These data suggest that Odc1 is expressed both in adipocytes and other cell types in adipose tissue, such as immune cells.

In the chow fed groups, we found that Gatm RNA levels were decreased in adipocytes compared to input (Figure 2.5C), while Odc1 RNA levels appeared to be relatively similar between adipocytes and input (Figure 2.5E). Overall, we concluded that Gatm was most adipocyte specific in HFD peritumoral adipose and that Odc1 can likely be expressed in both the adipocytes and other cell types in HFD peritumoral adipose.

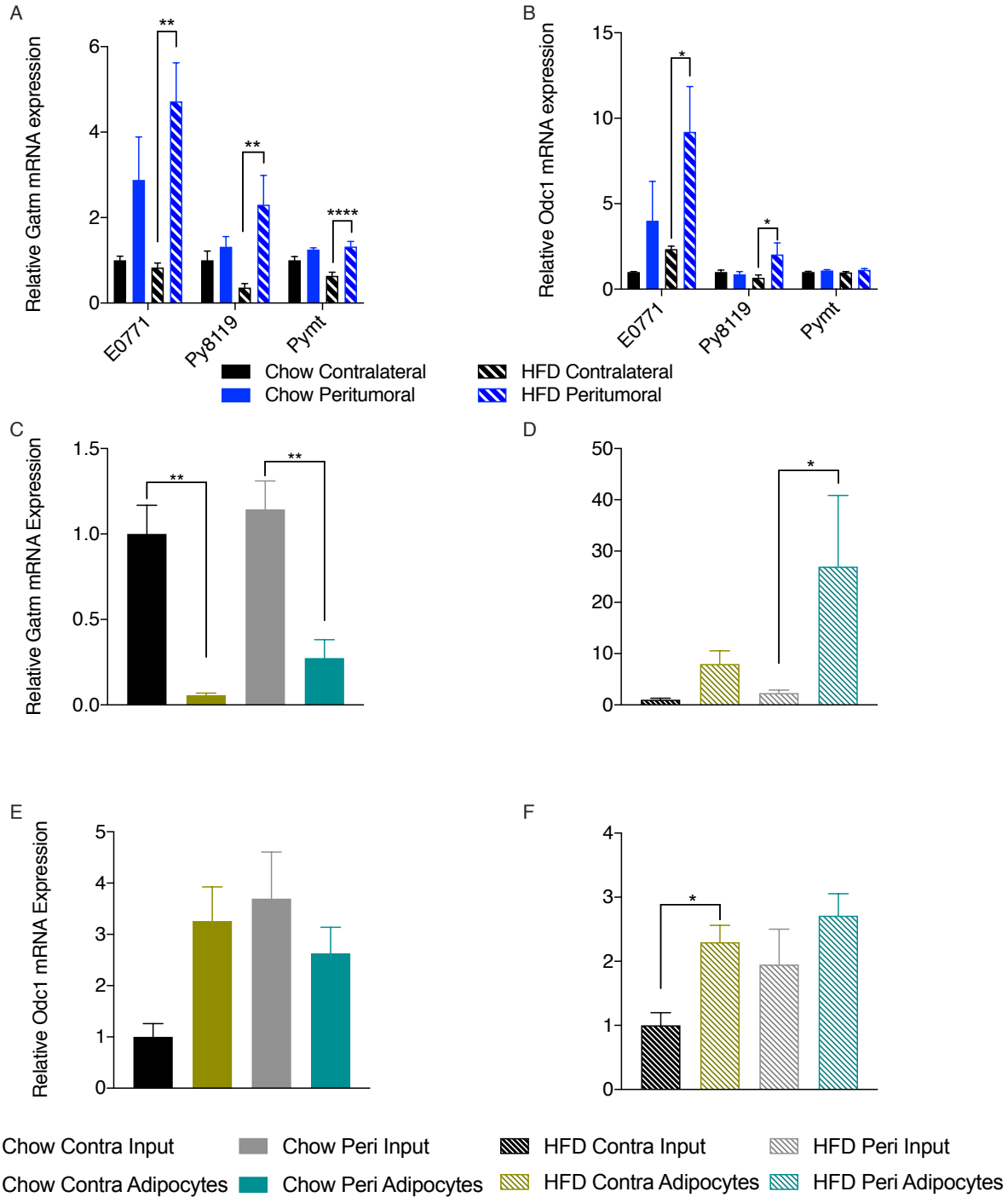

Figure 2.5. mRNA levels of key regulatory genes from qPCR confirmation and adipocyte-specific TRAP

A. mRNA expression of Gatm from adipose tissue in E0771, Py8119 and MMTV-PyMT models of driven breast cancer. B. mRNA expression of Odc1 from adipose tissue in E0771, Py8119 and MMTV-PyMT models of breast cancer. C and D. Expression of Gatm from adipocyte-specific TRAP of peritumoral and contralateral adipose tissue from chow and HFD mice. E and F. Expression of Odc1 from adipocyte-specific TRAP of peritumoral and contralateral adipose tissue from chow and HFD mice. Data shown here represent mean +/- standard error of the mean (SEM). * $p< 0.05$, ** $p<0.01$

2.5 Summary

We developed a model of obesity-driven breast cancer using E0771 breast cancer cells. This model has been previously established but never used to study the adipose tissue in the tumor microenvironment. We used RNA sequencing to examine the transcriptome of adipose tissue near the tumor and on the contralateral side. The PCA plot showed clear separation between all six groups which showed that there were large differences in adipose tissue near the tumor compared to the contralateral adipose tissue.

Determining which differentially regulated genes are functionally involved in linking obesity to tumor progression required further analysis. We began by examining differentially regulated genes between each of the six groups. We wanted to examine genes which were specifically changed in peritumoral adipose tissue in obese mice. We also considered genes which similarly changed in the peritumoral adipose tissue in chow fed mice. Then we began to examine pathway analysis among all six groups. Arginine and Proline Metabolism was upregulated in HFD peritumoral adipose compared to HFD contralateral adipose (Figure 2.2C). When we looked deeper, we saw that this pathway included both Gatm and Odc1. The subsequent chapters describe studies examining the functional significance of these expression changes.

CHAPTER 3

CREATINE BIOSYNTHESIS IN ADIPOSE TISSUE AND ITS EFFECT ON BREAST CANCER PROGRESSION

3.1 Introduction

Chapter 2 showed that Glycine amidinotransferase (Gatm) was increased in HFD peritumoral adipose tissue (Figure 2.3 and 2.5A), and specifically in the adipocytes (Figure 2.5D). Gatm is the rate limiting step in creatine synthesis (Figure 2.3D) and has a role in energy expenditure, diet induced thermogenesis and defense against diet-induced obesity (Kazak et al. 2015). Gatm floxed mice were crossed to adiponectin cre to generate an adipocyte-specific knockout of Gatm (Adipo-Gatm KO). Male adipo-Gatm KO mice have reduced core body temperature during cold exposure, and when housed at thermoneutrality, gain more weight on a chow diet and have impaired glucose tolerance, as compared to Gatm floxed littermate controls (Kazak et al. 2015).

Solute carrier family 6 membrane 8 (Slc6a8), also known as the creatine transporter (CrT), which functions to transport creatine across the cell membrane. Adipocyte specific knockout of Slc6a8 (Adipo-Slc6a8 KO) results in reduced whole-body energy expenditure, cold intolerance, and obesity when fed a HFD at thermoneutrality (Kazak et al. 2019).

Gatm has not previously been linked to breast tumor growth. However, creatine has been shown to promote colorectal cancer metastasis (Loo et al. 2015). Loo et al. demonstrated that in a hypoxic environment creatine is phosphorylated by creatine kinase B (CKB), which can then be imported into cancer cells via Slc6a8 to provide a source of ATP which fuels tumor metastasis (Loo et al. 2015). HER2 signaling in breast cancer cells has been shown to phosphorylate mitochondrial creatine kinase (MtCK1) which increases the amount of ATP to support breast

tumor growth (Kurmi et al. 2018). Additionally, in myeloid leukemia, a proto-oncogene MtCK1 is necessary for survival of EV1-expressing leukemia cells (Fenouille et al. 2017).

Creatine metabolism has also been shown to be upregulated in an *in vitro* spheroid model of colorectal cancer under hypoxic conditions when HIF1a is blocked (Valli et al. 2019). The investigators propose that upregulating creatine metabolism is a response to the hypoxic tumor environment. This is of particular relevance to our work because obese adipose tissue as well as large tumors contribute to a hypoxic microenvironment.

3.2 Obese Adipo-Gatm KO mice show decreased tumor progression

3.2.1 Adipo-Gatm KO

Deletion of Gatm in mammary adipocytes was tested using fractionated mature adipocytes, *in vitro* differentiated adipocytes and whole mammary adipose tissue. Gatm levels were reduced 81% in mature adipocytes from Adipo-Gatm KO mice compared to littermate control (Ct) mice (Figure 3.1A), though this was not statistically significant ($p=0.2$). Gatm levels were also reduced 98.1% ($p<0.05$) in *in vitro* differentiated adipocytes (Figure 3.1B). The lack of significance in the mature adipocytes was most likely due to imperfect fractionation of the whole adipose tissue. Interestingly, there was no reduction in Gatm within whole adipose tissue (Figure 3.1A). Kazak et al. showed that Gatm deletion in Adipo-Gatm KO mice is only visible in mature adipocytes or *in vitro* differentiated adipocytes (Kazak et al. 2015). There was no change in adiponectin between Ct and Adipo-Gatm KO in whole adipose tissue, mature adipocytes or *in vitro* differentiated adipocytes (Figure 3.1A and B).

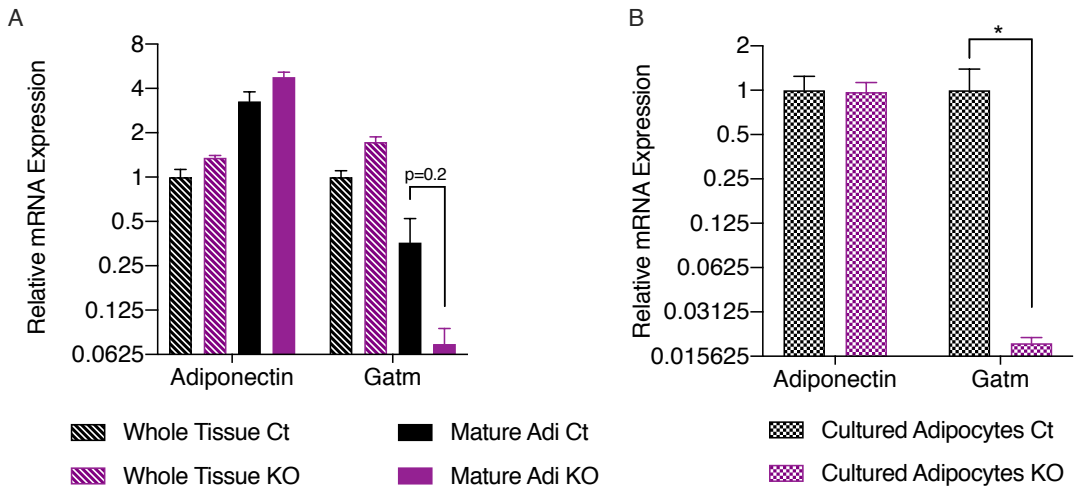

Figure 3.1 mRNA levels of Adiponectin and Gatm in Adipo-Gatm KO mice

A. mRNA levels of adiponectin and Gatm in whole mammary adipose tissue and mature adipocytes from Ct and Adipo-Gatm KO mice. B. mRNA levels of adiponectin and Gatm in *in vitro* cultured and differentiated adipocytes from Ct and Adipo-Gatm KO mice. Data shown here represent mean +/- standard error of the mean (SEM). * $p < 0.05$.

3.2.2 Obese Adipo-Gatm KO mice show decreased E0771 tumor progression

Adipo-Gatm KO and Ct mice were used to test how the deletion of Gatm in adipocytes affects E0771 breast tumor progression. We performed this experiment twice: Figure 3.2 is the combined data, Figure 3.3 is from Cohort 1 and Figure 3.4 is from Cohort 2. Mice were treated identically in each cohort, fed the same diet for the same length of time, measured on the same days and sacrificed after the same number of days.

Mice were placed on a HFD at six weeks of age, and their weight was measured every two weeks (Figure 3.2A, 3.3A and 3.4A). At endpoint, while both Adipo-Gatm KO and Ct mice weighed 60% more on a HFD compared to chow fed mice, Adipo-Gatm KO mice weighed 8% ($p<0.05$) less than Ct mice in the combined data set, trending similarly in each individual cohort (Figure 3.2A, 3.3A and 3.4A). Fat mass between Adipo-Gatm KO and Ct was not different in

mice on the same diet and both HFD Adipo-Gatm KO and Ct mice had 300% more fat mass than chow mice of either genotype (Figure 3.2B, 3.3B, 3.4B). There was no difference in lean mass between diet or genotype (Figure 3.2B, 3.3B, 3.4B).

Adipo-Gatm and Ct mice were injected with 50,000 E0771 breast cancer cells after 9 weeks on a HFD or chow diet, and tumor growth was monitored twice a week for three weeks. In the combined data, tumors in HFD Ct mice grew to be 236% ($p<0.0001$) greater in volume compared to tumors in chow Ct mice, as we saw in our original experiment from Chapter 2. However, tumors in HFD Adipo-Gatm KO mice showed markedly decreased progression compared to tumors in HFD Ct mice ($p<0.001$) (Figure 3.2C). At endpoint, the combined data showed tumors in HFD Adipo-Gatm KO mice were 42% ($p<0.05$) smaller in volume than tumors in HFD Ct mice (Figure 3.2C). Regression analysis found that the difference in mouse body weight was not a predictor of the difference in tumor volume. There was no difference in tumor progression between chow Adipo-Gatm KO and Ct mice (Figure 3.2C). At endpoint, tumors weighed 25% ($p<0.01$) less in HFD Adipo-Gatm KO mice compared to tumors in HFD Ct mice in the combined data (Figure 3.2D). There was no difference in final weight between tumors in chow Adipo-Gatm KO and Ct mice.

Each individual cohort showed the same decreased progression in HFD Adipo-Gatm KO mice compared to tumors in HFD Ct mice (Cohort1: $p<0.05$ and Cohort 2: $p<0.01$). At endpoint, Cohort 1 showed tumors in HFD Adipo-Gatm KO mice were 33.5% ($p=0.72$) smaller in volume and Cohort 2 showed tumors in HFD Adipo-Gatm KO mice were 52% ($p<0.05$) smaller in volume than tumors in HFD Ct mice (Figure 3.3C and 3.4C). Cohort 1 trended towards a 27% ($p=0.2$) decrease in final weight in tumors from HFD Adipo-Gatm KO mice compared to tumors from HFD Ct mice, and cohort 2 showed a 44% ($p<0.05$) decrease (Figure 3.3D and 3.4D). Overall

these experiments showed that deleting Gatm specifically in adipocytes reduced E0771 breast tumor progression. A summary of the statistics for both cohorts and the combined data is seen in Table 3.1A.

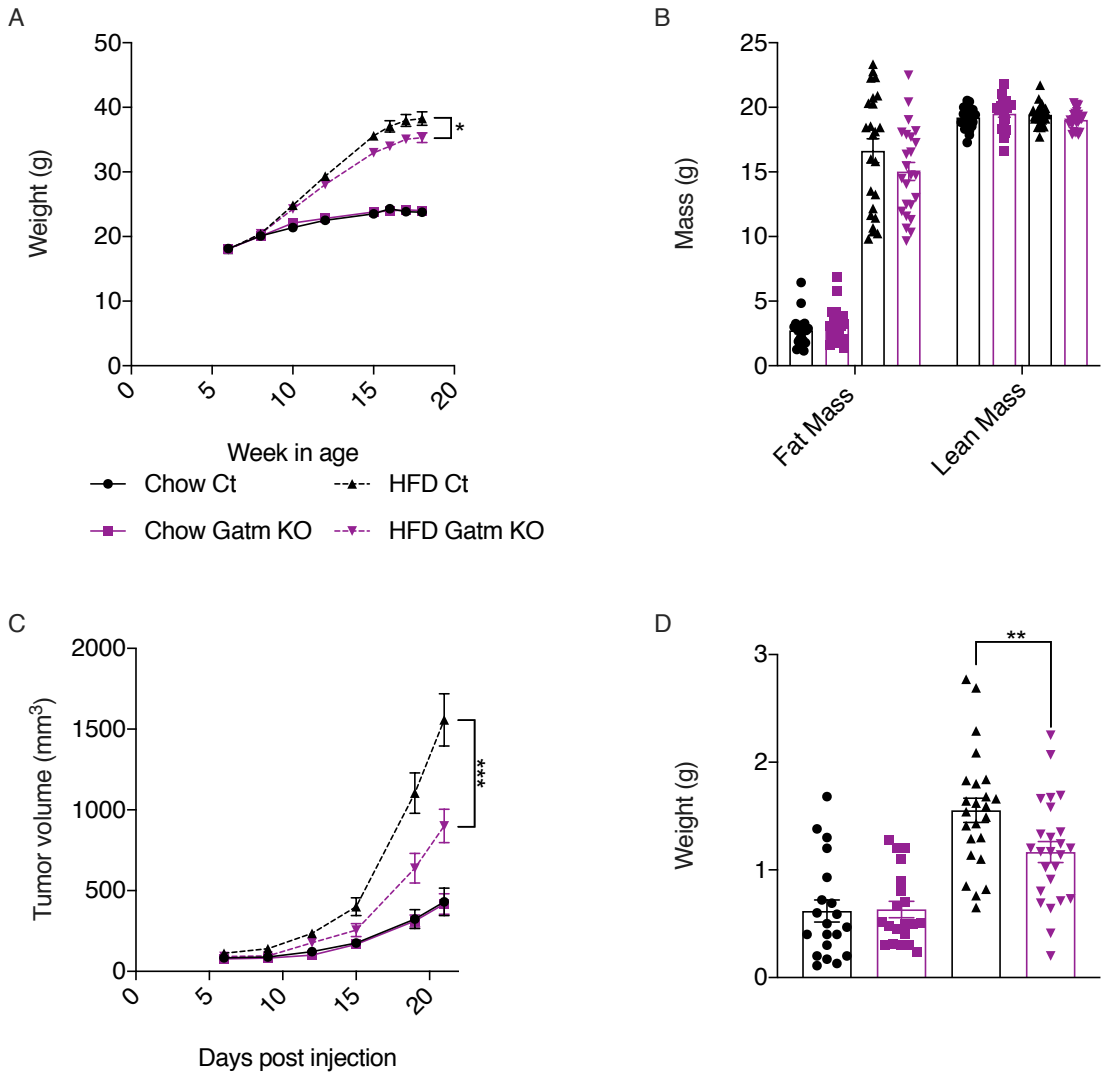

Figure 3.2 Combined data: E0771 breast tumor progression was decreased in Adipo-Gatm KO mice on a HFD

A. Weight of Adipo-Gatm KO and littermate controls on a chow and a HFD. B. Fat and lean mass of Adipo-Gatm KO and littermate controls on a chow and a HFD. C. E0771 tumor progression in Adipo-Gatm KO and littermate controls on a chow and a HFD. D. Weights of tumors from Adipo-Gatm KO and littermate controls on a chow and a HFD at endpoint. Data shown here represent mean +/- standard error of the mean (SEM). * $p < 0.05$, ** $p<0.01$, *** $p<0.001$.

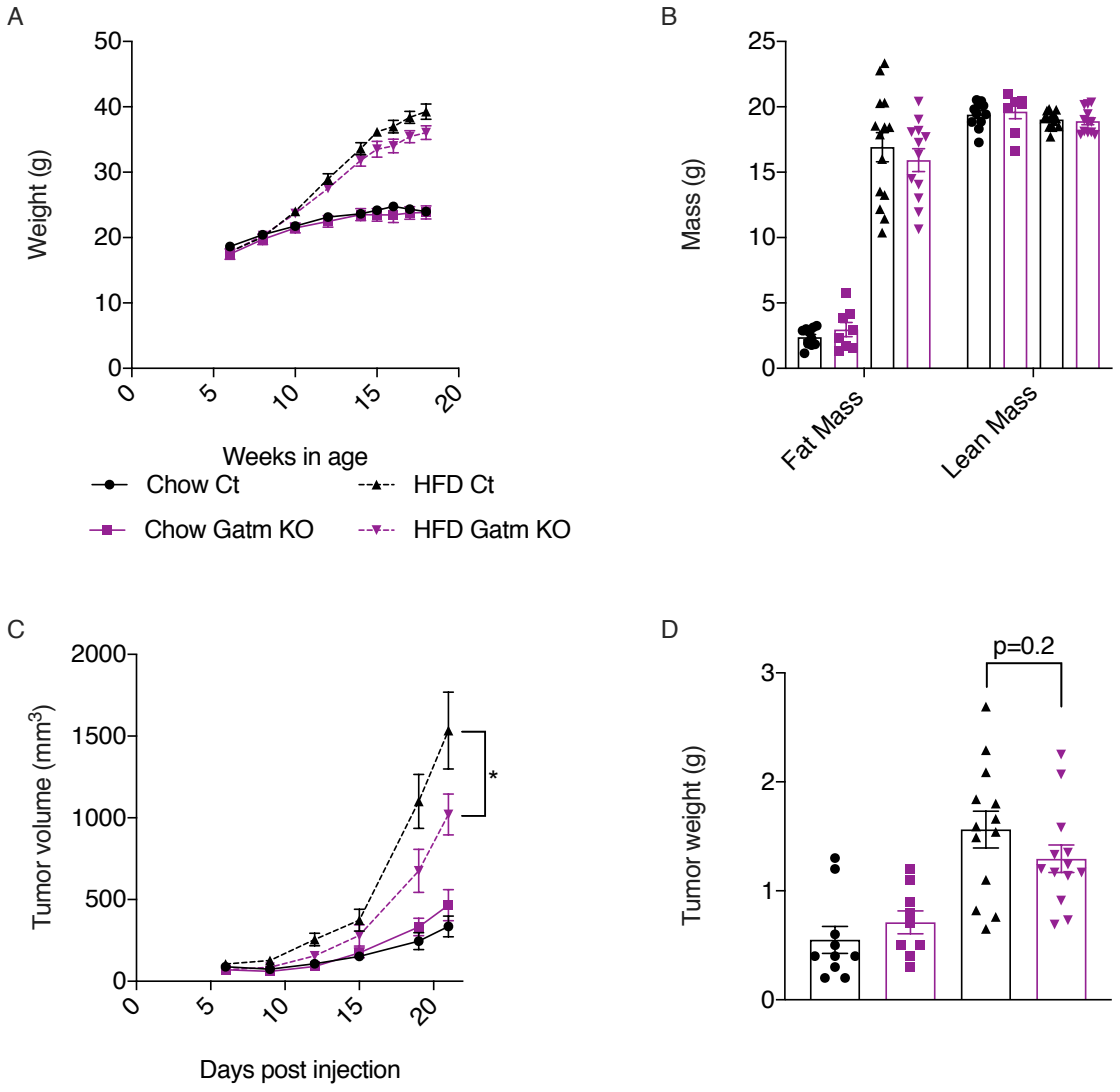

Figure 3.3 Cohort 1: E0771 breast tumor progression was decreased in Adipo-Gatm KO mice on a HFD

A. Weight of Adipo-Gatm KO and littermate controls on a chow and a HFD. B. Fat and lean mass of Adipo-Gatm KO and littermate controls on a chow and a HFD. C. E0771 tumor progression in Adipo-Gatm KO and littermate controls on a chow and a HFD. D. Weights of tumors from Adipo-Gatm KO and littermate controls on a chow and a HFD at endpoint. Data shown here represent mean +/- standard error of the mean (SEM). * $p < 0.05$

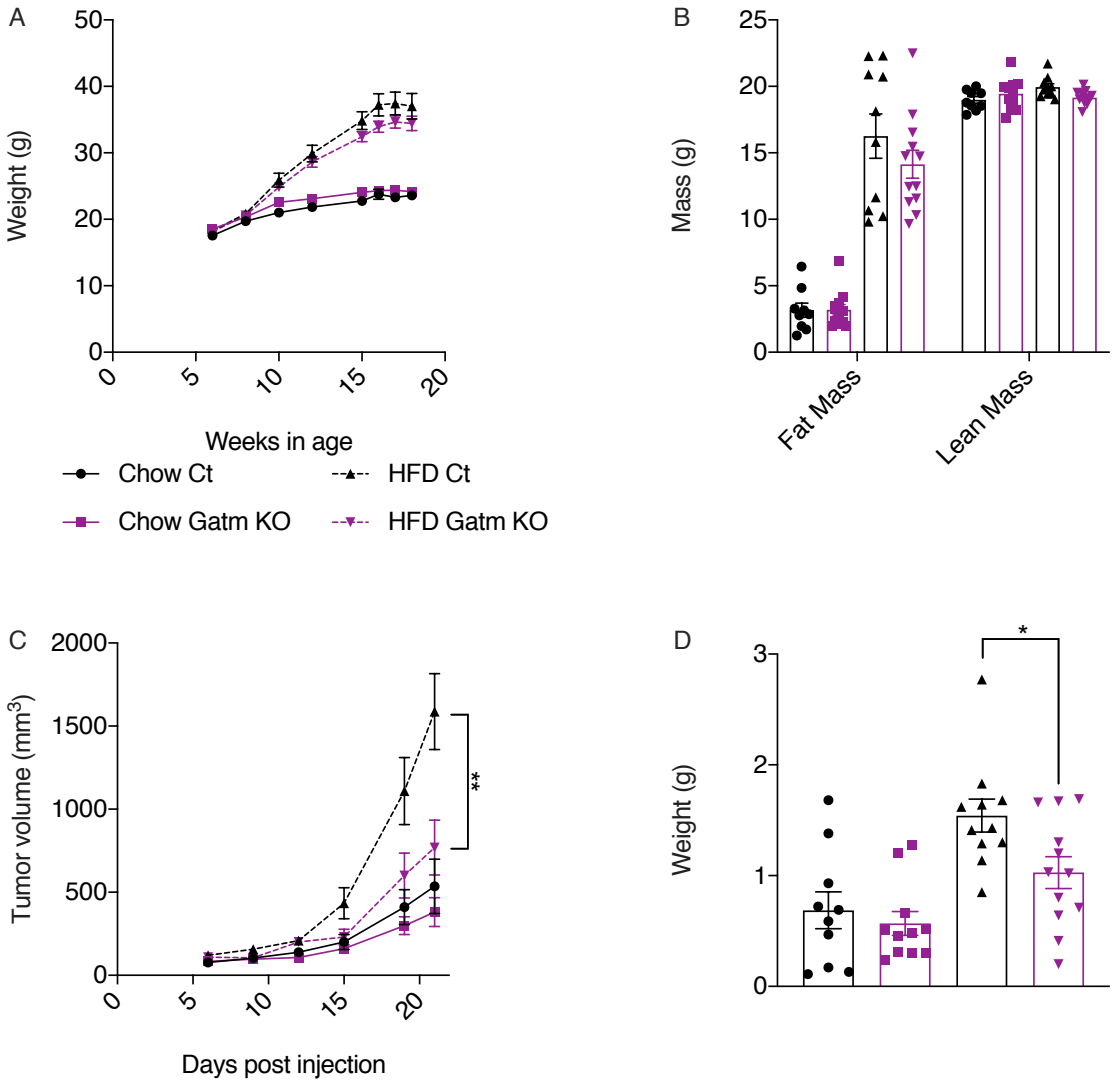

Figure 3.4 Cohort 2: E0771 breast tumor progression was decreased in Adipo-Gatm KO mice on a HFD

A. Weight of Adipo-Gatm KO and littermate controls on a chow and a HFD. B. Fat and lean mass of Adipo-Gatm KO and littermate controls on a chow and a HFD. C. E0771 tumor progression in Adipo-Gatm KO and littermate controls on a chow and a HFD. D. Weights of tumors from Adipo-Gatm KO and littermate controls on a chow and a HFD at endpoint. Data shown here represent mean +/- standard error of the mean (SEM). * $p< 0.05$, ** $p<0.01$

3.3 Slc6a8 knockdown in E0771 cells

3.3.1 Confirming Slc6a8 knockdown in cells and tumors

To determine whether tumor growth is dependent on creatine, we knocked down Slc6a8 (Slc6a8 KD) in mCherry positive E0771 cells. We created a knockdown instead of a knockout because E0771 is not a clonal cell line and other experiments in the lab have shown that clonal selection of E0771 cells changes tumor growth rate. Thus, E0771 cells were transduced with a lentivirus containing an shRNA against Slc6a8 or a scrambled control. E0771 cells which expressed mCherry were used to facilitate FACS sorting of E0771 cells only from the *in vivo* tumor microenvironment in animal studies.

After infecting E0771 cells and selecting with puromycin, Slc6a8 RNA levels were reduced 91% ($p<0.001$) in Slc6a8 KD compared to Ct cells (Figure 3.5A). There was also a 50% reduction in protein level in membrane fractions isolated using differential centrifugation (Figure 3.5B and C). *In vivo,* tumors at endpoint (see section 3.2.2) retained the Slc6a8 KD. Tumors were dissociated into a single cell suspension and cancer cells were FACS sorted using mCherry. There was a significant 90% ($p<0.05$) reduction in Slc6a8 RNA levels in Slc6a8 KD tumor cells compared with Ct tumor cells from HFD mice (Figure 3.5D). There was also a 50% reduction ($p<0.01$) in the final creatine level, as measured by LC-MS, in bulk Slc6a8 KD tumors compared to bulk Ct tumors from HFD mice (Figure 3.5E).

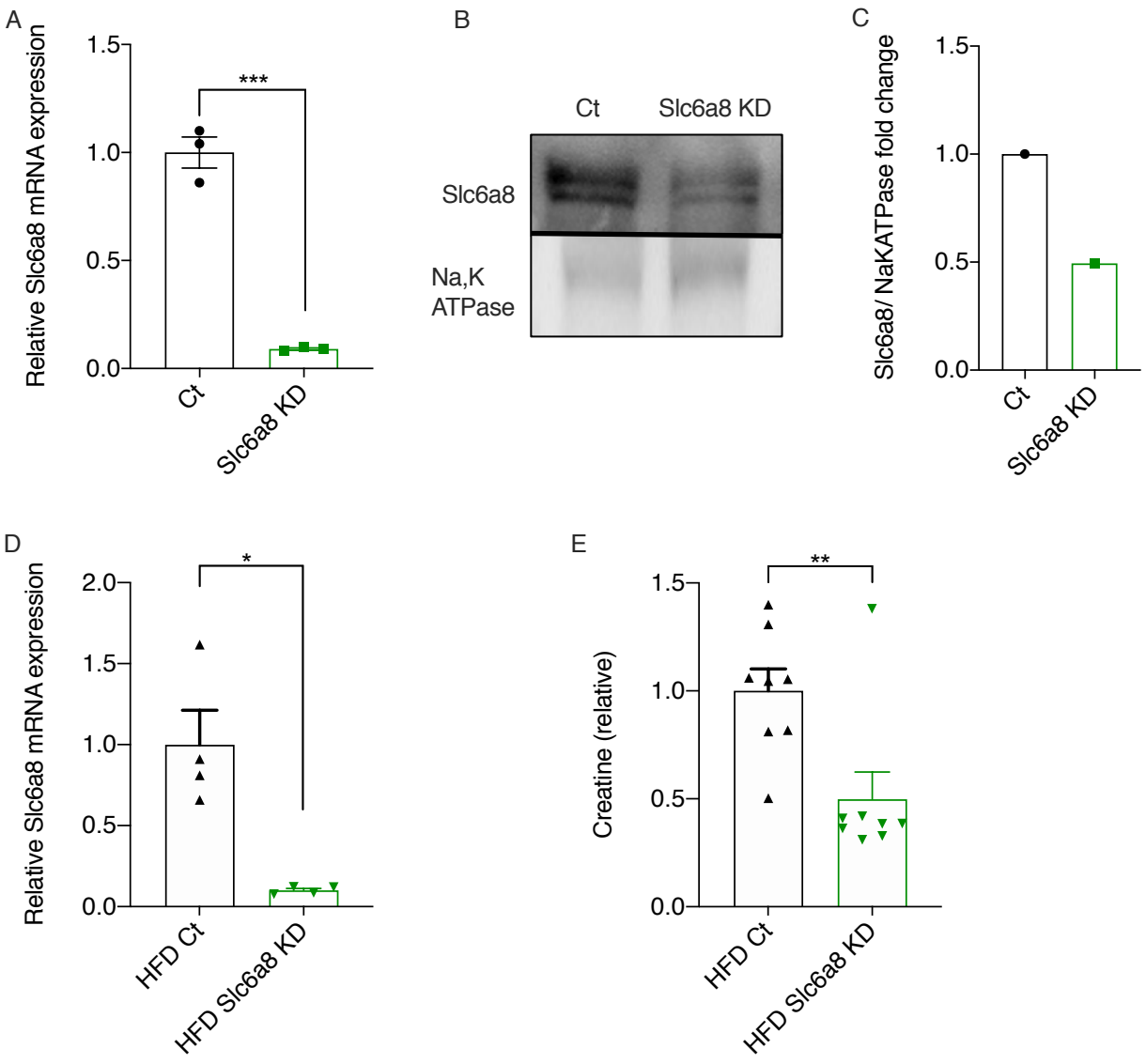

Figure 3.5 Slc6a8 was knocked down in both E0771 cells and tumors

A. mRNA level of Slc6a8 in Ct and Slc6a8 KD E0771 cells (technical replicates). B. Western blot of cellular membrane fraction for Slc6a8 in Ct and Slc6a8 KD E0771 cells. Na/K ATPase was used as a loading control for membrane proteins. C. Quantification of western bands from B. D. mRNA levels of Slc6a8 in FACS sorted tumors from HFD Ct and HFD Slc6a8 KD. E. Creatine levels measured my LC-MS, in bulk tumors from HFD Ct and HFD Slc6a8 KD. Data shown here represent mean +/- standard error of the mean (SEM). * $p< 0.05$, ** $p<0.01$, *** $p<0.001$.

3.3.2 Slc6a8 knockdown in E0771 cells results in decreased tumor progression in obese mice

We injected Ct and Slc6a8 KD cell lines separately into the 4th mammary fat pads of wild-type B6 chow and HFD fed mice. We repeated this experiment in two separate cohorts which were treated in exactly the same manner. Figure 3.6 shows the combined data, Figure 3.7 shows Cohort 1 which only had HFD groups, and Figure 3.8 shows Cohort 2 which had both chow and HFD groups. As expected, at endpoint wild-type B6 mice on a HFD weighed 77% more than chow controls (Figure 3.6A and 3.8A) and had 350% increased fat mass (Figure 3.6B and 3.8B). There was no difference in lean mass between diets (Figure 3.6B and 3.8B). Before tumor injection, the HFD and chow groups were divided into two different (4 total) weight matched groups to ensure that differences in mouse weight among each diet did not contribute to tumor growth (Figure 3.6A, 3.7A, 3.8A).

In the combined cohort, Slc6a8 KD tumors showed decreased progression compared to Ct tumors in HFD mice ($p<0.05$) (Figure 3.6C). At endpoint, Slc6a8 KD tumors were 54% ($p<0.05$) smaller in volume than Ct tumors in HFD mice (Figure 3.6C). In fact, Slc6a8 KD tumors in obese mice were equivalent in size to tumors in non-obese chow fed controls. There was no difference in tumor progression in the chow fed mice (Figure 3.6C). Corresponding to the reduction in tumor volume, Slc6a8 KD tumors weighed 33% ($p<0.01$) less than Ct tumors in HFD mice (Figure 3.6D). There was no difference in the final weight in tumors from the chow fed mice.

Each individual cohort showed the same trend of decreased progression in Slc6a8 KD tumors in HFD mice compared Ct tumors in HFD mice (Cohort1: $p<0.05$ and Cohort 2: $p=0.076$). The same patterns were seen in each individual cohort. At endpoint, Slc6a8 KD tumors were 55% ($p=0.2$) smaller in volume in Cohort 1 and 51% ($p<0.01$) smaller in Cohort 2 compared to Ct tumors in HFD mice (Figure 3.7B and Figure 3.8C). Similarly, in Cohort 1 Slc6a8 KD tumors

weighed 67% (p=0.08) less, and in Cohort 2 Slc6a8 KD tumors weighed 32% (p<0.01) less than Ct tumors in HFD mice (Figure 3.7C and Figure 3.8D). A summary of the statistics for both experiments and the combined data is shown in Table 3.1B.

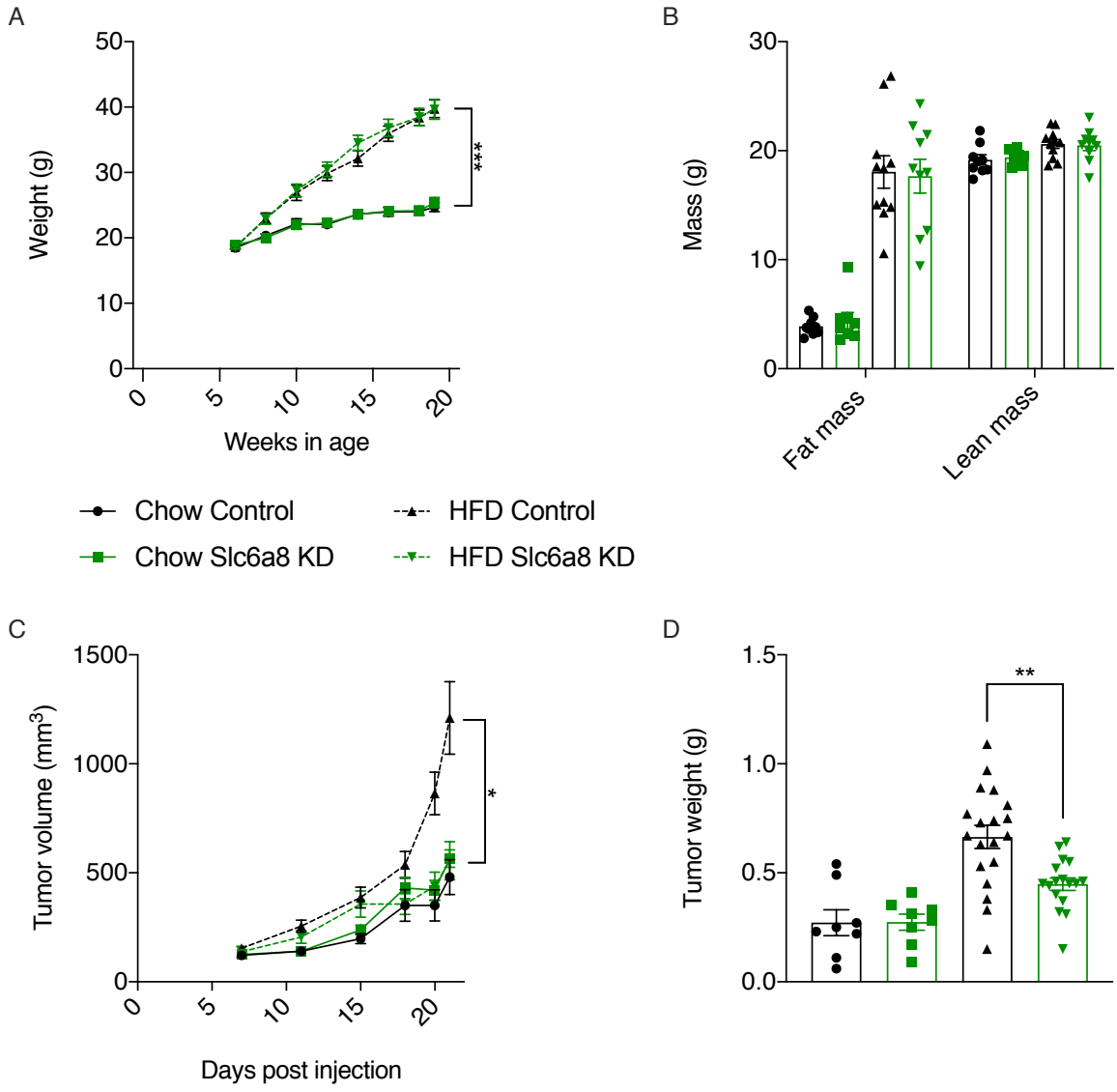

Figure 3.6 Combined data: Slc6a8 knockdown E0771 breast tumor cells showed decreased growth in mice on a HFD

A. Weight of Wt C57 Bl6 mice on chow and HFD. B. Fat and lean mass of Wt C57 Bl6 mice on chow and HFD. C. Slc6a8 KD E0771 and scrambled control E0771 tumor progression in Wt C57 Bl6 mice on chow and HFD. D. Weights of tumors from Slc6a8 KD E0771 and scrambled control E0771 in Wt C57 Bl6 mice on chow and HFD at endpoint. Data shown here represent mean +/- standard error of the mean (SEM). * p< 0.05 , ** p<0.01 , *** p<0.001.

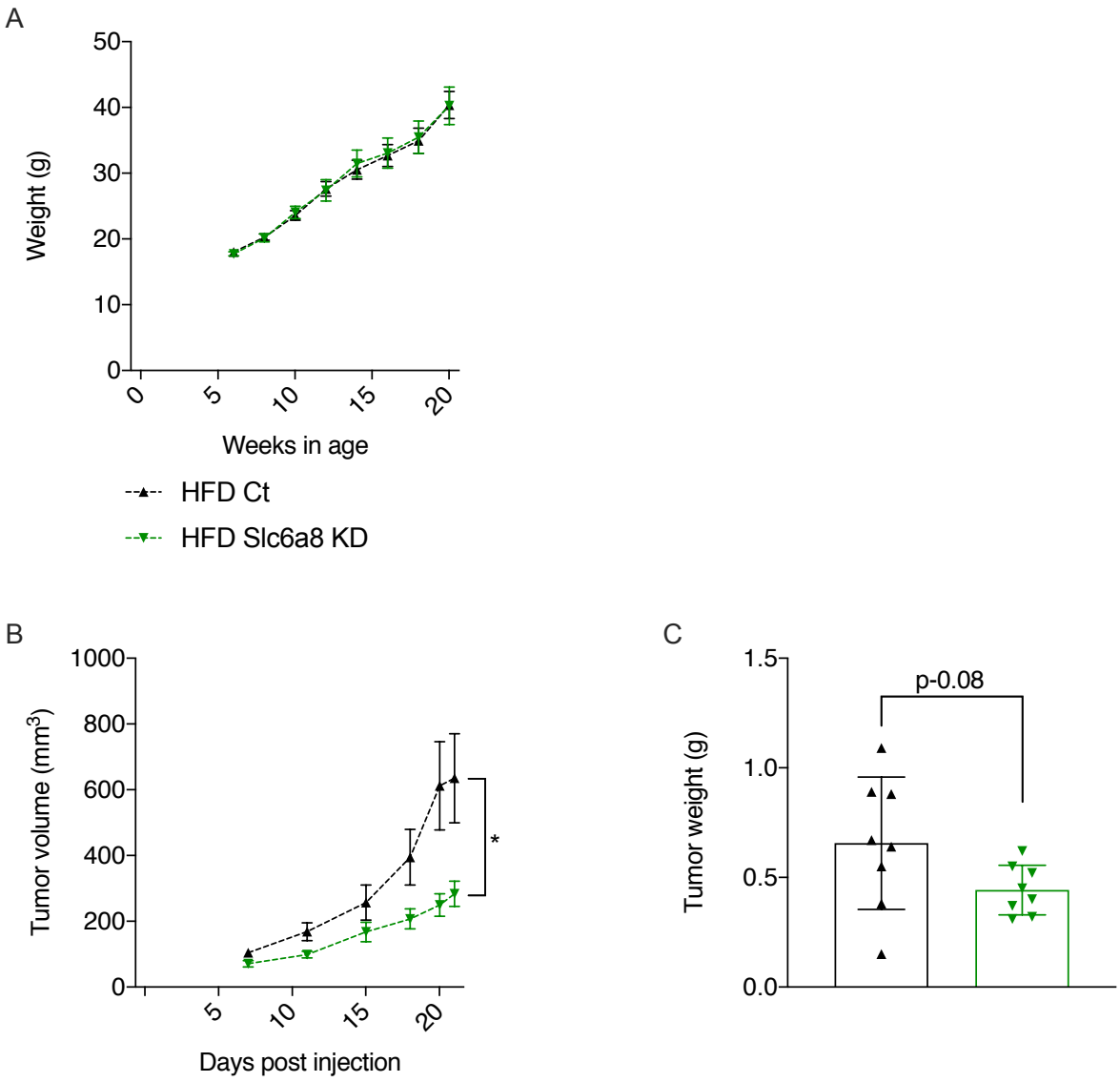

Figure 3.7 Cohort 1: Slc6a8 knockdown E0771 breast tumor cells showed decreased growth on HFD

A. Weight of Wt C57 Bl6 mice on HFD. B. Slc6a8 KD E0771 and scrambled control E0771 tumor progression in Wt C57 Bl6 mice on a HFD. C. Weights of tumors from Slc6a8 KD E0771 and scrambled control E0771 in Wt C57 Bl6 mice on HFD at endpoint. Data shown here represent mean +/- standard error of the mean (SEM). * $p < 0.05$.

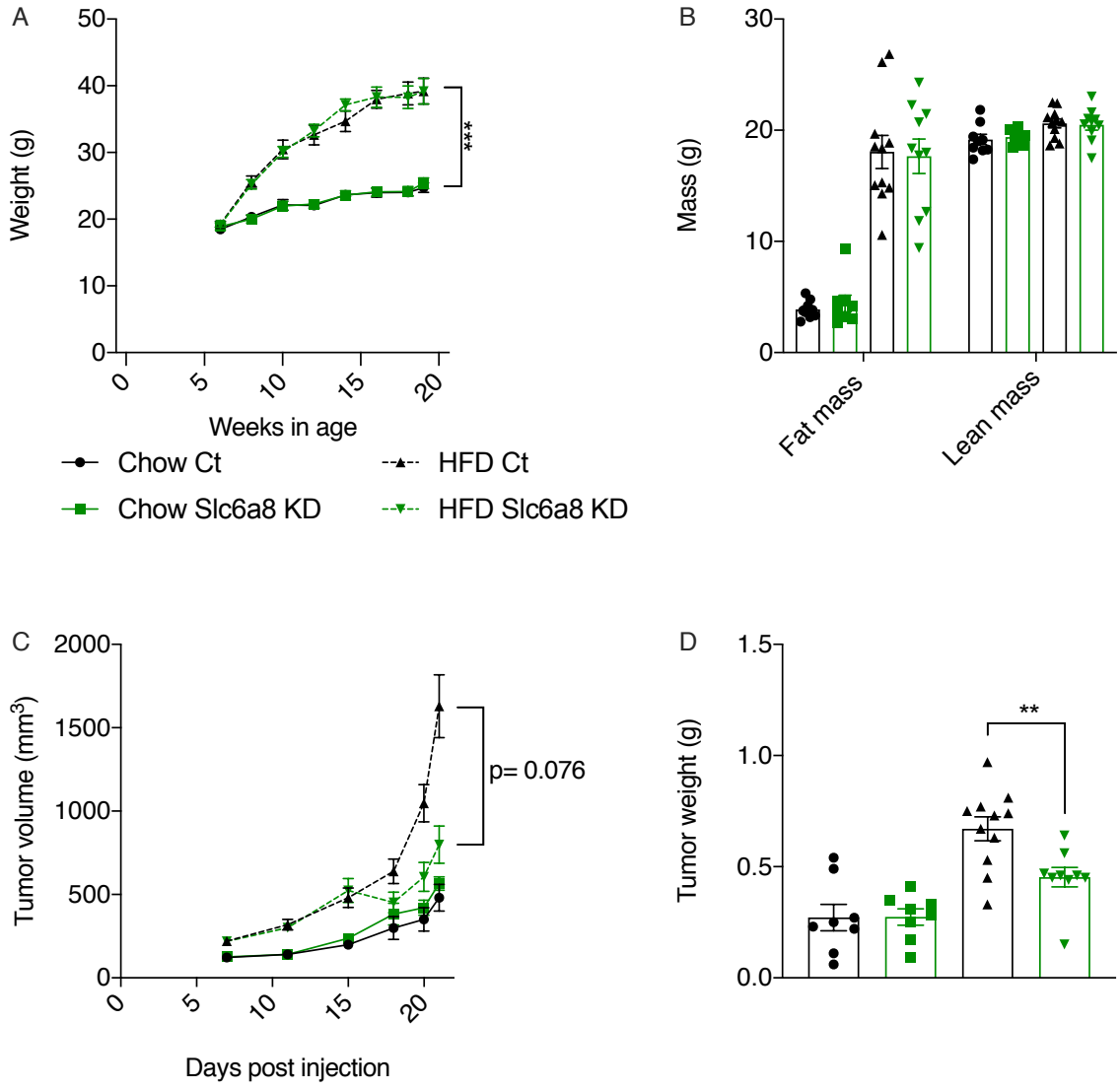

Figure 3.8 Cohort 2: Slc6a8 knockdown E0771 breast tumor cells showed decreased growth on a HFD

A. Weight of Wt C57 Bl6 mice on chow and HFD. B. Fat and lean mass of Wt C57 Bl6 mice on chow and HFD. C. Slc6a8 KD E0771 and scrambled control E0771 tumor progression in Wt C57 Bl6 mice on chow and HFD. D. Weights of tumors from Slc6a8 KD E0771 and scrambled control E0771 in Wt C57 Bl6 mice on chow and HFD at endpoint. Data shown here represent mean +/- standard error of the mean (SEM). ** $p<0.01$, *** $p<0.001$.

3.4 Review of statistics from Adipo-Gatm KO and Slc6a8 experiments

We performed statistical analysis using a mix-effects model with repeated measurements for our datasets from Adipo-Gatm KO and Slc6a8 knockdown experiments. All data were natural log normalized to ensure data were normally distributed. Three comparisons are shown here. In all comparisons the same patterns were seen between both cohorts.

First, we analyzed growth of Adipo-Gatm KO or Slc6a8 KD tumors in mice on a HFD, relative to their respective controls. For the Gatm experiment, both individual cohorts and the combined data showed significant differences in tumor progression. For the Slc6a8 experiment, Cohort 1 and the combined data showed a significant difference in tumor progression and Cohort 2 trended significant with a p value of $p=0.07$.

The second analysis examined tumor size as a function of time. For all experiments, this comparison was significant, which is not surprising as the tumors grow exponentially.

The third analysis examined the interaction between group and time among the HFD groups. An interaction indicates that the growth of the tumor is dependent on time. For the Gatm experiments, Cohort 1 was not significant while Cohort 2 and the combined data were significant. This was also true for the Slc6a8 experiment. This analysis suggests that sometimes the Adipo-Gatm KO or Slc6a8 KD tumors are smaller but with a parallel growth rate to controls, and sometimes there is a time component indicating that at certain times the tumors in the Slc6a8 KD or Adipo-Gatm KO exhibit altered growth rates relative to their respective controls.

While statistics are very important for our analysis of these experiments, these tumors are difficult to measure at the beginning of each study, when they are still very small in size. We believe that the most meaningful comparison is made over the last week and a half of tumor measurements. We also believe that the final tumor weight at endpoint is a key measurement.

Table 3.1 Overview of statistics from Adipo-Gatm KO and Slc6a8 knockdown experiments

A. Statistical analysis of Adipo-Gatm KO cohorts. B. Statistical analysis of Slc6a8 KD cohorts.

A

Gatm KO Cohorts	Groups	Ct HFD vs. KO HFD	Time	Group*Time
Cohort 1	4	0.0157	<0.0001	0.095
Cohort 2	4	0.0075	<0.0001	0.0025
Combined	4	0.0002	<0.0001	0.3382

B

Slc6a8 KD Cohorts	Groups	Ct HFD vs. KD HFD	Time	Group*Time
Cohort 1	2	0.0257	<0.0001	0.5491
Cohort 2	4	0.0763	<0.0001	<0.0001
Combined	4	0.0347	<0.0001	0.0001

3.5 Levels of creatine, phosphocreatine and ATP/ADP

Creatine, phosphocreatine (PCr), ATP and ADP were all measured using LC/MS. The sample preparation and mass spec were completed in collaboration with Dr. Lawrence Kazak's lab at McGill University. Levels of creatine and PCr were not different within tumors from HFD Adipo-Gatm KO and Ct mice (Figure 3.9A and B). Furthermore, there was no difference in creatine or PCr in the peritumoral or contralateral adipose tissue from HFD Adipo-Gatm KO relative to Ct (Figure 3.9C and D). Tissues analyzed here were from Gatm Cohort 1.

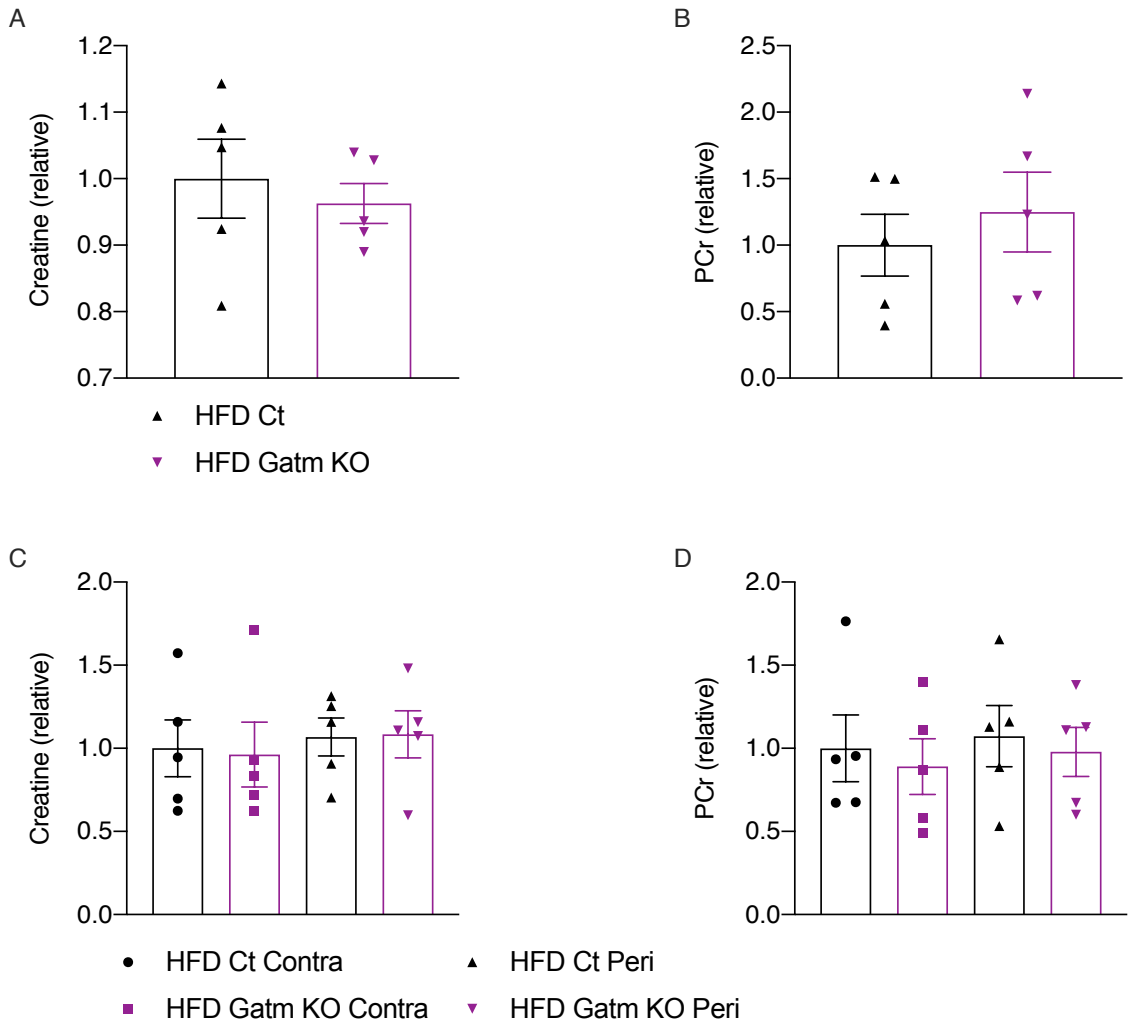

Figure 3.9 Creatine and Phosphocreatine levels in Adipo-Gatm KO vs. control tumors and adipose tissue

A. Creatine levels in tumors from HFD Ct and Adipo-Gatm KO mice. B. Phosphocreatine levels in tumors from HFD Ct and Adipo-Gatm KO mice. C. Creatine levels in peritumoral and contralateral adipose tissue from HFD Ct and Adipo-Gatm KO mice. D. Phosphocreatine levels in peritumoral and contralateral adipose tissue from HFD Ct and Adipo-Gatm KO mice. Data shown here represent mean +/- standard error of the mean (SEM).

We have already shown that bulk Slc6a8 KD tumors from HFD mice have reduced creatine levels compared to Ct tumors from HFD mice (Figure 3.5D). We show this data again in Figure 3.10A for comparison. Interestingly, PCr and ATP/ADP levels were not changed between Slc6a8

KD tumors compared to Ct tumors in HFD mice (Figure 3.10B and C). These tissues were from Slc6a8 Cohort 1.

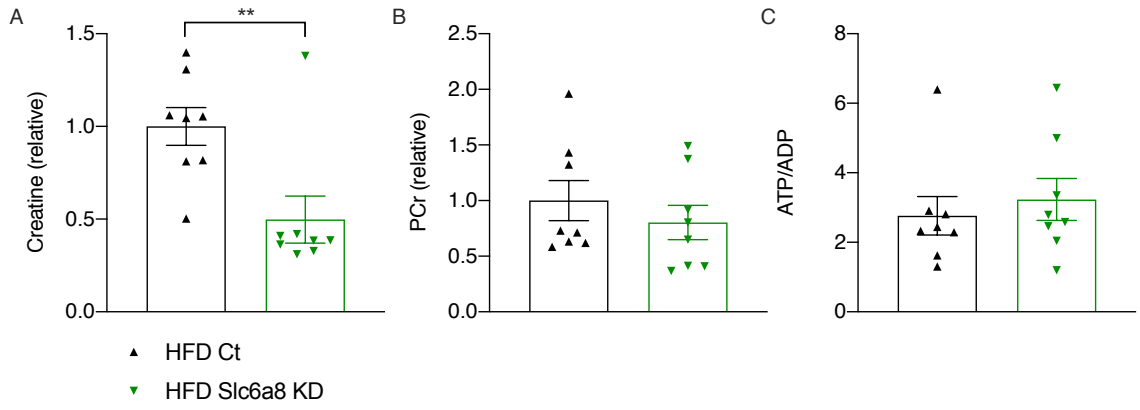

Figure 3.10 Creatine, Phosphocreatine, ATP/ADP levels in Slc6a8 knockdown and control tumors in HFD mice

A. Creatine levels in Slc6a8 KD and Ct tumors from HFD mice. Repeated from Figure 3.5E. B. Phosphocreatine levels in Slc6a8 KD and Ct tumors from HFD mice. C. ATP/ADP levels in Slc6a8 KD and Ct tumors from HFD mice. Data shown here represent mean +/- standard error of the mean (SEM). ** $p<0.01$

3.6 Role of hypoxia and current *in vitro* studies

As obese adipose tissue expands as the breast tumor grows, the microenvironment becomes hypoxic. Many of the studies involving creatine and cancer (see 3.1 Introduction) show that hypoxia is a key condition affecting creatine metabolism. We found that hypoxia inducible factor 1 subunit alpha (Hif1a), the master regulator of the cellular response to hypoxia, was increased at the protein level in bulk E0771 tumors from HFD mice compared to bulk tumors from chow fed mice (Figure 3.11A).

We then tested the proliferation of scrambled Ct and Slc6a8 KD E0771 cells in a high O_2 condition (21%) and in hypoxia (0.5%). Using the Cell Titer Glo proliferation assay we found that

the Slc6a8 KD cells proliferated less than Ct cells in both 21% and 0.5% O_2 (Figure 3.11B). Interestingly, when we added 1mM creatine (Cr) to the cells, we saw the same pattern of slower Slc6a8 KD cell proliferation, but no increase in Ct cells compared to non-creatine treated cells (Figure 3.11B). We also saw a reduction in overall proliferation in the 0.5% O_2 state compared to the 21% O_2 state (Figure 3.11B).

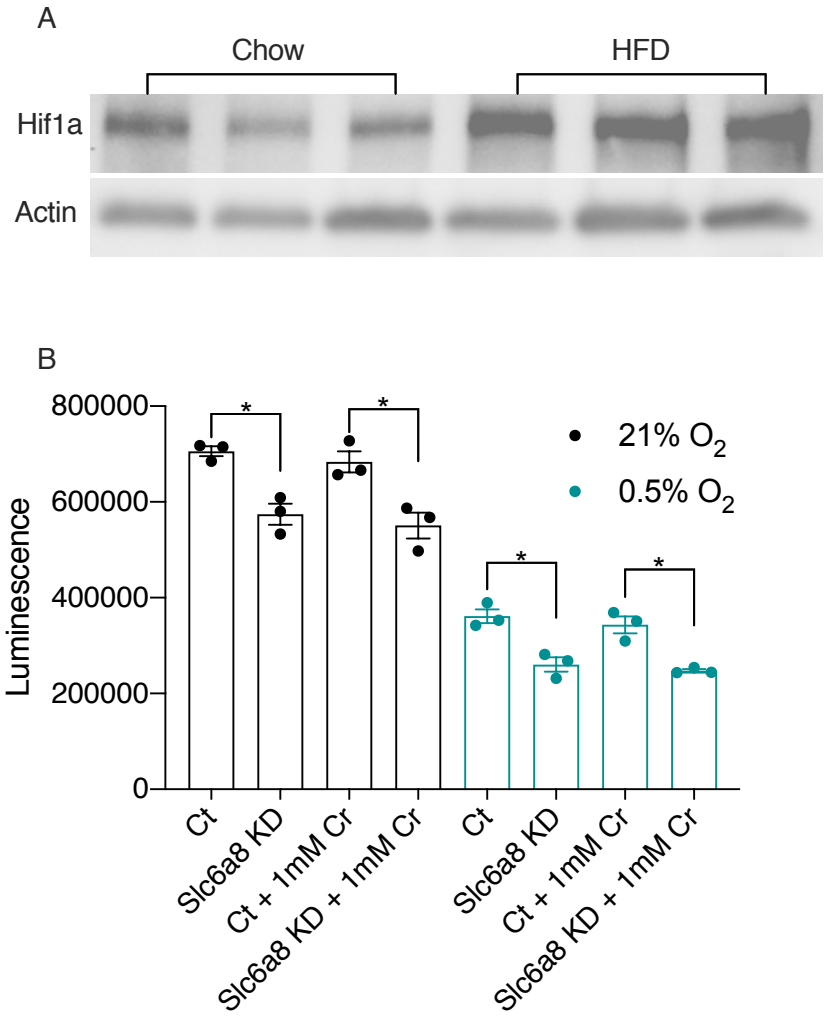

Figure 3.11 Hif1a was increased in obese tumors and *in vitro* studies showed decreased proliferation in Slc6a8 knockdown E0771 cells

A. Western blot of Hif1a of E0771 tumors from chow fed and HFD fed B6 mice. B. Cell glo proliferation assay of scrambled Ct and Slc6a8 KD E0771 cells in 21% O_2 and 0.5% O_2 with or without 1mM creatine (Cr). Data shown here represent mean +/- standard error of the mean (SEM). * $p < 0.05$

3.7 Summary

We identified a candidate from transcriptomic analysis: Gatm. We then tested the role of adipocyte Gatm in an adipocyte-specific knockout model and found that obese Adipo-Gatm KO mice have decreased breast tumor progression compared to obese floxed controls. Since Gatm is the rate limiting step in creatine synthesis, this suggests that creatine metabolism is important for breast tumor growth. To further investigate we knocked down the creatine transporter (Slc6a8) in E0771 breast cancer cells. We found that Slc6a8 KD E0771 tumors progressed more slowly than scrambled control E0771 tumors in HFD mice. This further suggests that creatine metabolism is key in obese breast tumor progression.

Our current hypothesis is that increased Gatm in obese peritumoral adipose tissue produces more creatine which then is used by the tumor to support increased size. We saw that in tumors and adipose tissue from Adipo-Gatm KO vs. Ct mice there was no difference in creatine or PCr. This was unexpected, as we had anticipated that Adipo-Gatm KO adipose would have lower creatine levels and that correspondingly tumors from Adipo-Gatm KO mice would have less creatine. It is possible that the heterogeneity of the adipose tumor microenvironment is masking differences in creatine levels. It is also possible that adipocyte specific deletion of Gatm results in changes beyond creatine biosynthesis.

Interestingly, when studied Slc6a8 KD tumors in obese mice, we saw a reduction in creatine in the tumor. Yet when we looked at PCr and ATP/ADP ratios there was no change. This suggests that the difference in tumor size in Slc6a8 KD tumors is not due to changed energetics (ATP). We believe that creatine may instead be taken up by tumor cells, broken down into glycine and arginine, and that these amino acids are then used by the tumor as building blocks to support cell proliferation.

We have seen *in vivo* that there is an increase in Hif1a in tumors from HFD fed mice compared to chow fed mice. From a literature review, we believe that a hypoxic condition is key for the tumor relying on creatine metabolism instead of other sources for growth. Thus far, we have not been able to show that hypoxia is affecting tumor cell proliferation with relation to creatine metabolism. We have seen that Slc6a8 KD E0771 cells proliferate more slowly compared to Ct cells in both normoxia and hypoxia. Future *in vitro* experiments will examine varying concentrations of creatine and how hypoxia can affect cell proliferation in these conditions.

Although the *in vivo* studies described here are key, they do not prove without a doubt that creatine is coming from adipocytes and affecting breast tumor progression. We are currently working on two *in vivo* projects to further answer this question. The first makes use of Adipo-Slc6a8 KO mice. In these mice, creatine cannot be exported from adipocytes, and therefore, cannot be transported to the tumor. Therefore, when we inject these mice with E0771 cells, we expect that tumors will be smaller in HFD Adipo-Slc6a8 KO mice compared to HFD littermate controls.

We are also developing approaches using isotope-labeled arginine, a precursor to creatine, to trace creatine from the obese adipocytes to the tumor. We anticipate that metabolic tracing of arginine into creatine will be elevated in peritumoral but not contralateral adipocytes in obese mice, resulting in greater labeling in the adjacent tumor. These *in vivo* experiments will provide further proof that creatine metabolism is important in our model of obesity-driven breast cancer.

CHAPTER 4

POLYAMINE SYNTHESIS IN ADIPOSE TISSUE AND ITS EFFECTS ON BREAST CANCER PROGRESSION

4.1 Introduction

Chapter 2 showed that Ornithine decarboxylase 1 (Odc1) was upregulated in HFD peritumoral adipose tissue (Figure 2.5A). Odc1 converts ornithine into putrescine. Further downstream reactions convert putrescine into the polyamines spermidine and spermine. We found many of the genes involved in polyamine synthesis to be increased in HFD peritumoral adipose tissue (Figure 4.1). Specifically, we saw significant increases in Odc1 (359%), arginase 1 (Arg1) (443%), spermidine synthase (SRM) (203%), spermine synthase (SMS) (87%), spermidine/spermine acetyl transferase (Sat1) (32%) and spermine oxidase (Smox) (203%) and Myc (200%), the transcriptional regulator of Odc1, in HFD peritumoral adipose compared to HFD contralateral adipose.

Putrescine, spermidine and spermine are all polyamines, which are small positively charged molecules containing amine groups. Odc1 encodes the rate limiting enzyme in polyamine synthesis. Polyamines are known to induce proliferation of cancer cells, and Odc1 is overexpressed in several cancer types including endometrial (Kim et al. 2017), prostate (Gamat et al. 2015; Zabala-Letona et al. 2017) and colorectal cancer (Witherspoon et al. 2013). Odc1 is also a transcriptional target gene of Myc. Thus, polyamines have also been studied in neuroblastoma, where Myc drives tumor progression (Bassiri et al. 2015). The polyamine spermidine can also be converted into hypusine which is essential for eIF5A activity. Inactivation of eif5A is lethal to mammalian cells and hypusine modification of eif5A promotes translation by binding to and

stabilizing mRNA providing another mechanism by which polyamines can affect cell proliferation (M. H. Park and Wolff 2018).

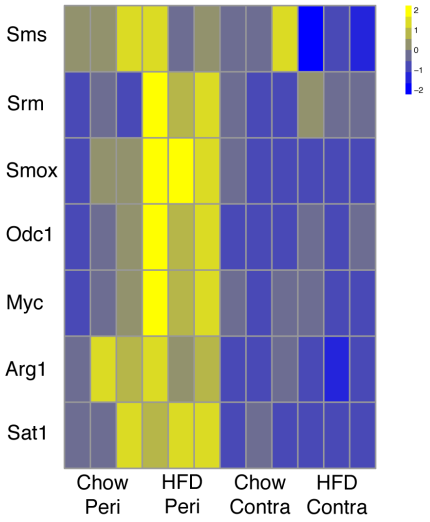

Figure 4.1 RNA sequencing showed upregulation of polyamine synthesis genes in HFD peritumoral adipose

Heat map of significantly ($p<0.05$) regulated genes involved in polyamine synthesis.

4.2 Pharmacologic inhibition of Odc1 using DFMO reduced tumor size in obese mice

Difluoromethylornithine (DFMO) (Figure 4.2C) is an irreversible chemical inhibitor of Odc1. DFMO is approved for the treatment of *Trypanosoma brucei gambinese encephalitis* ("African sleeping sickness") and is in clinical trials for the treatment of neuroblastoma in children (Bassiri et al. 2015). We administered DFMO (2% in the drinking water) for one week before E0771 tumor cell injection and throughout tumor progression. At endpoint, mice on a HFD weighed 65% ($p<0.0001$) more and had 400% more fat mass than mice on a chow diet (Figure 4.2A and 4.2B). Importantly, we observed no difference in body weight or body composition between vehicle H_2O and DFMO treated groups on the same diet (Figure 4.2A and 4.2B). Mice drank a similar amount of water in both vehicle and treatment groups (Figure 4.2D). Interestingly,

HFD mice drank about half the amount of water compared to chow mice. We believe this was due to the moist nature of the HFD food pellets.

Mice were injected with E0771 cells into the 4th mammary fat pad and growth of orthotopic tumors was monitored twice a week. Tumors in HFD DFMO treated mice showed decreased progression compared to tumors in HFD H_2O treated mice (<0.001) (Figure 4.2E). At endpoint, tumors in the HFD DFMO treated mice were 69% (p=0.07) smaller than tumors in the HFD vehicle control mice (Figure 4.2E). There was no difference in the chow fed groups, even as the tumor volume was measured beyond the usual three-week mark (Figure 4.2E). Tumor weight was measured after three weeks for the HFD groups and after four weeks for the chow groups (Figure 4.2F), which is why the chow tumors had similar final weights to the HFD groups in Figure 4.2F. The final weight of the tumors in HFD DFMO treated mice was 50% (p=0.055) less than the tumors in the HFD H_2O treated mice, though this was not quite statistically significant (Figure 4.2F). There was no difference in final tumor weight between tumors in chow fed DFMO treated or vehicle control mice.

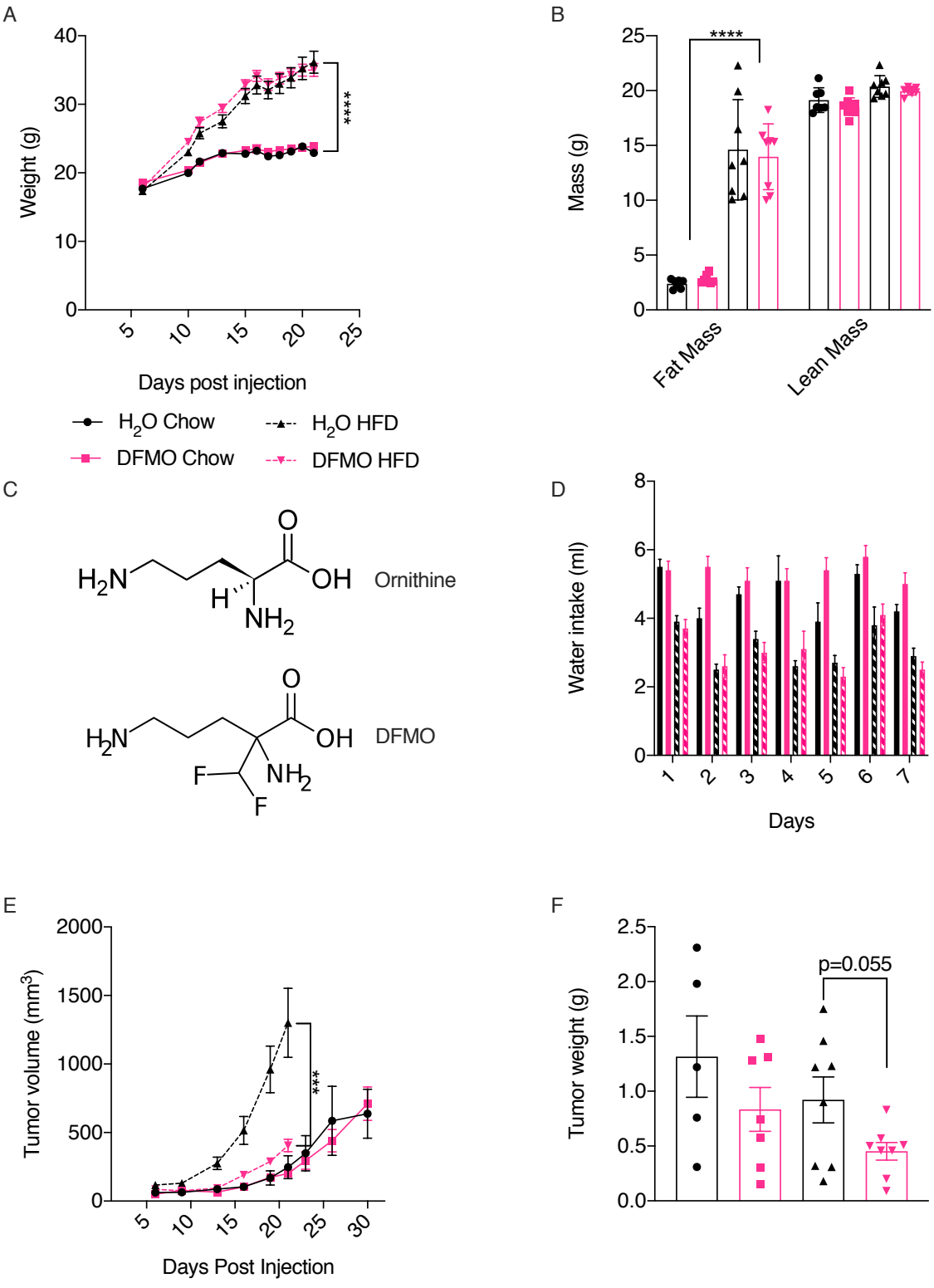

Figure 4.2 DFMO inhibited Odc1 and reduced tumor growth in mice on a HFD

A. Weight of C57 Bl6 mice on chow or HFD treated with DFMO or vehicle control. B. Fat and lean mass of mice on chow or HFD treated with DFMO or vehicle control. C. Chemical structure of ornithine and DFMO. D. Water intake for mice on chow or HFD treated with DFMO or vehicle control. E. E0771 tumor growth in chow or HFD mice treated with DFMO or vehicle control. F. Final tumor weight at necropsy of chow or HFD mice treated with DFMO or vehicle control. Data shown here represent mean +/- standard error of the mean (SEM). *** $p<0.001$, **** $p<0.0001$.

4.3 *In vitro* studies using polyamines

In vitro, we studied the effects of exogenous polyamines (spermine, spermidine and putrescine) on the viability of E0771 cells (Figure 4.3). We used a CellTiter-Glo assay, which measures ATP levels. 24 hours after treating E0771 cells with increasing amounts of either spermidine, spermine or putrescine, we found a dose-dependent increase in ATP levels (Figure 4.3). In particular, it appears that 0.01μM was the optimal concentration of polyamine to ensure maximal cell viability. These data are consistent with a model in which polyamines derived from peritumoral adipose tissue can be used by the tumor to support cancer cell proliferation.

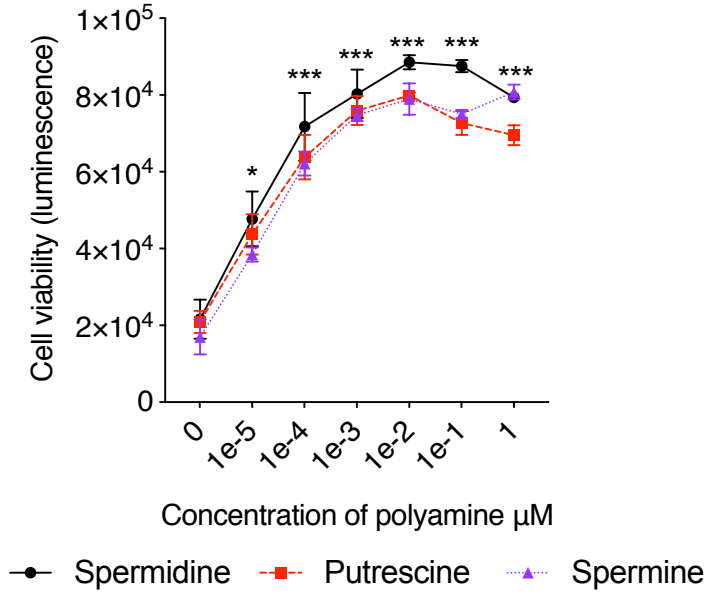

Figure 4.3 Treating E0771 cancer cells with polyamines increased cell viability

Increasing concentrations of polyamines were added to E0771 cells and cell viability was assayed using CellTiterGlo (measure of ATP). Data shown here represent mean +/- standard error of the mean (SEM). * $p< 0.05$, *** $p<0.001$.

4.4 Overexpressing Odc1 did not alter tumor growth

Inhibiting Odc1 using DFMO attenuated tumor progression. However, DFMO acts throughout the body, so it is not clear that these effects are specifically due to Odc1 inhibition in adipose tissue. We therefore examined a gain of function model in which we overexpressed Odc1 in mammary adipocytes using AAV8. Although this AAV serotype is not completely specific for adipocytes, it does show relative tropism for fat cells. We anticipated that mice with adipocyte over-expression (OE) of Odc1 would have increased tumor progression. Mice were placed on either chow or HFD (Figure 4.4A), and at 8 weeks on their respective diets, were injected with either AAV8 Odc1 or AAV8 GFP as a control. Injections were done locally into the mammary adipose to ensure the best possible uptake by adipocytes. The virus contained a CB7 promoter driving either GFP as a control or Odc1 with a 3x flag tag.

We tested our plasmid by transfecting 293T cells (Figure 4.4B). We found that we could detect overexpression of Odc1 *in vitro* using both an Odc1 as well as an anti-flag antibody (Figure 4.4B). We also found that the virus was effective at overexpressing Odc1 in mammary adipose tissue one week after injecting the AAV directly into the fat pad. At the RNA level, there was an increase, though not statistically significant, for both chow fed (430%, $p=0.08$) and HFD fed Odc1 injected mice (500%, $p=0.06$) as compared to GFP injected controls (Figure 4.4C). Western blotting also clearly showed that Odc1 overexpression was successful within the mammary adipose tissue (Figure 4.4D).

A week after the viral injections, when we had shown that Odc1 was overexpressed, all mice were injected with 50,000 E0771 cancer cells. Tumors in HFD mice with either GFP or Odc1 overexpression showed increased progression compared to tumors in chow fed mice ($p<0.0001$). However, tumor progression was not different between mice injected with GFP or Odc1 on either diet (Figure 4.4E). This was mirrored in the final tumor weights (Figure 4.4F). While it could be that overexpression of Odc1 does not promote increased E0771 tumor growth, it could also be that the level of Odc1 increase by the AAV viral injection was not sufficient to increase E0771 tumor growth. There are many caveats to using an adeno-associated viral approach, but we believe it was a valuable experiment because there is not currently an Odc1 transgenic mouse line.

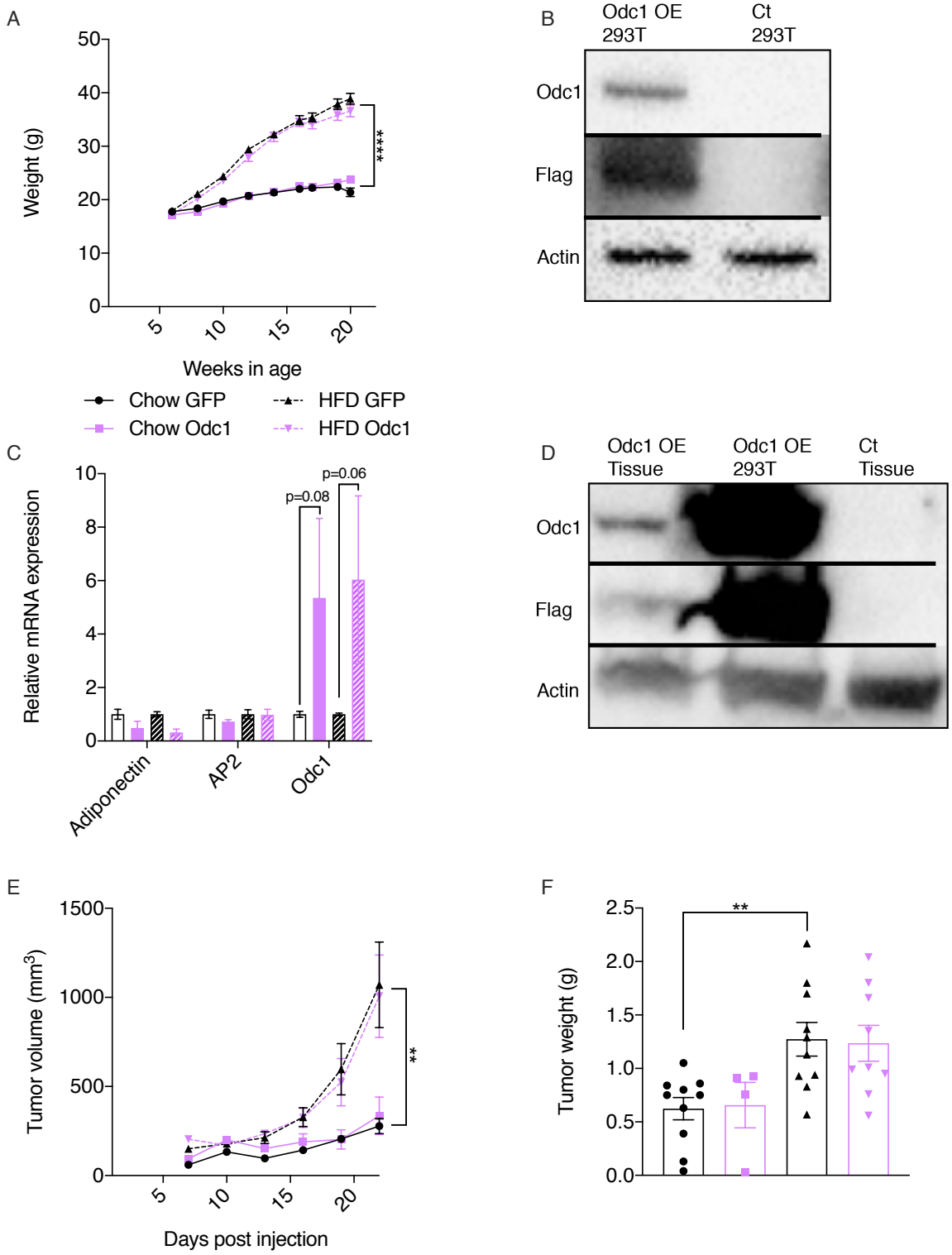

Figure 4.4 Overexpressing Odc1 in adipose tissue did not alter E0771 tumor progression

A. Weight of C57 Bl6 chow and HFD fed mice. B. Western blot showing Odc1 overexpression via transfection *in vitro*. C. qPCR of subcutaneous adipose from mice injected with AAVs driving overexpression of Odc1 or GFP. D. Western showing Odc1 overexpression via AAV transduction *in vivo* in subcutaneous adipose tissue of HFD mice. E. E0771 tumor progression in chow and HFD mice with Odc1 or GFP overexpression. Data shown here represent mean +/- standard error of the mean (SEM). ** $p<0.01$, **** $p<0.0001$.

4.5 Generation of an adipose-specific Odc1 knockout mouse

Inhibiting Odc1 with DFMO decreased tumor growth, specifically in HFD mice. However, when we overexpressed Odc1 in mammary adipocytes using AAV, we did not see an increase in tumor growth. Both of these experiments likely had off target effects. Systemically administered DFMO can affect all tissue types and AAVs can also target other tissue types and may have varied effects, even within individual adipocytes. To more rigorously ascertain the role of Odc1 in this biology, we obtained Odc1 floxed mice (kindly provided by Dr. Raghu Mirmira, Indiana University School of Medicine) and crossed them to Adiponectin-Cre mice. Adipo-Odc1 KO mice had substantially decreased Odc1, with a 72% ($p<0.01$) reduction at the mRNA level (Figure 4.5). Interestingly, Adipo-Odc1 KO mice also show a reduction in adiponectin (50%) and aP2 (20%), though these values are not statistically significant.

Odc1 floxed mouse was generated on an FVB background, so we have been backcrossing this line to B6. We have now backcrossed these mice sufficiently that the E0771 tumors can grow without rejection. We have created our first cohort of Adipo-Odc1 KO and littermate controls on the B6 background. The mice are now being monitored on a chow and a HFD. They will be ready for E0771 injections in November 2019. We will monitor mouse weight and tumor progression. We expect that HFD fed Adipo-Odc1 KO mice will develop smaller tumors compared to HFD littermate controls.

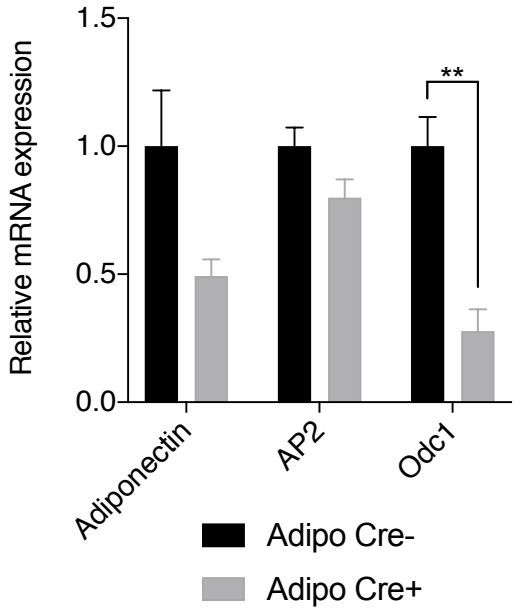

Figure 4.5 Adipo-Odc1 KO mammary adipose showed reduced Odc1 expression level via qPCR

mRNA levels of adipose related genes and Odc1 from mammary adipose of Adipo-Odc1 KO and littermate controls as measured via qPCR. Data shown here represent mean +/- standard error of the mean (SEM). ** $p<0.01$.

4.6 Summary

We have seen that Odc1 and many other key genes in the polyamine pathway are upregulated in HFD peritumoral adipose tissue. Treating mice with DFMO, an Odc1 inhibitor, decreased tumor progression, specifically in obese mice. Conversely, overexpressing Odc1 using AAV vectors did not change tumor progression in obese or lean mice. Both experiments had unavoidable off-target effects, but we remain encouraged that Odc1 may play an important role in the link between breast cancer and obesity.

Odc1 and polyamines have been shown to affect tumor growth by affecting the cell cycle and by generating hypusine which in turn activates eIF1A. Yet, Odc1 and polyamines have not been studied in adipocytes or in the context of obesity. Since breast cancer develops in a

microenvironment surrounded by adipocytes, if polyamines can be transported from adipose tissue to the tumor and used to support increase tumor size, this would represent a novel connection between adipocytes and breast cancer. The Adipo-Odc1 KO mouse will be an important step in determining whether such a connection exists. If we see decreased tumor size in Adipo-Odc1 KO mice we will then move to *in vivo* tracing of polyamines.

CHAPTER 5

HUMAN BREAST CANCER PATIENTS

5.1 Introduction

We have found that Gatm induction in peritumoral fat is important for obesity-driven breast cancer in a mouse model. We are also continuing to investigate the role of Odc1 and polyamine synthesis in mouse models. To assess the translational relevance of these findings, we studied Gatm and Odc1 in human samples, in collaboration with colleagues at Memorial Sloan Kettering Cancer Center (MSKCC) and Weill Cornell.

We have an IRB approved protocol to collect mammary adipose tissue from female MSKCC patients with breast cancer undergoing mastectomy. Mammary adipose tissue is collected from a region near the tumor and from a distal location (minimum of 5 cm away from the tumor) in an uninvolved quadrant of the breast. Patients with BRCA mutations or those undergoing lumpectomy were excluded. We refer to this protocol as "Peritumoral and distal human mammary adipose tissue collection".

In parallel, we have worked with our collaborators to examine other previously established human mammary adipose tissue data sets for regulation of Gatm. We analyzed Gatm expression in a cohort of 100 female breast cancer patients (96 patients analyzed here) known as the Prevent Cohort (Iyengar, Zhou, et al. 2016). The purpose of the original Prevent Cohort study was to examine whether WAT inflammation has prognostic importance for breast cancer. Interestingly, this study did not focus on BMI and only examined patients for WAT inflammation, which is defined as the presence of crown like structure in breast adipose tissue (CLS-B). Crown like structures are macrophages which encircle dead or dying adipocytes and are known to appear in correlation with an inflammatory signature in WAT. This study found that patients with breast

WAT inflammation had elevated insulin, glucose, leptin, triglycerides, C-reactive protein, IL-6, lower HDL cholesterol and adiponectin. Patients with breast WAT inflammation (positive for CLS-B) had a hazard ratio of 1.83 for worse clinical course in patients that develop metastatic breast cancer compared to patients negative for WAT inflammation (Iyengar, Zhou, et al. 2016).

5.2 Peritumoral and distal human mammary adipose tissue collection

The peritumoral and distal human mammary adipose tissue collection protocol is designed to mimic our *in vivo* mouse model, where we analyzed peritumoral and contralateral adipose tissue in the E0771 obesity-driven breast cancer model. Collection of tissues is ongoing. As of August 2019, we have collected samples from 28 patients. These include 11 normal weight patients (BMI<25) and 17 overweight/obese patients (BMI≥25) (Table 5.1). Within the normal weight cohort, patients are between 38 to 81 years old, with tumor diameters between 0.5 - 7.2 cm and predominately histologic grade III/III (Table 5.1). The obese/overweight cohort contains patients between 24 to 72 years old, with tumor diameters between 0.2 - 8.5 cm and are predominately histologic grade III/III (Table 5.1). The obese/overweight patients have a significant increase in BMI ($p<0.0001$) compared to normal weight patients while all other factors are matched.

Table 5.1 Human peritumoral and distal mammary adipose tissue collection

Characterization of MSKCC breast cancer patients whose peritumoral and contralateral adipose were collected as part of the peritumoral and distal mammary adipose tissue protocol. BMI is increased in the obese/overweight patients compared to the normal weight patients. All other factors are matched.

Peritumoral and Distal Adipose Collection

Variables	Normal Weight 11/28 (39.3%)	Obese/Overweight 17/28 (60.7%)
Age (years)		
Median (range)	46 (38 to 81)	54 (24 to 72)
BMI		
Median (range)	22.76 (19.3-24.9)	32.2 (25-44.9)
Tumor Diameter (cm)		
Median (range)	2 (0.5 to 7.2)	2 (0.2 to 8.4)
Histologic Grade		
II/III	3 (27.3%)	3 (17.6%)
III/III	6 (54.5%)	12 (70.6%)
N/A	2 (18.2%)	2 (11.8%)

While subject accrual for this study is ongoing, we isolated RNA from a subset of the patients and synthesized cDNA for qPCR analysis. Thus far, there was no significant differences in Gatm or Odc1 expression between distal or peritumoral adipose in normal weight or obese/overweight patients (Figure 5.1). Figure 5.1A and C show results from normal weight patients, and 5.1B and D show results from overweight/obese patients. We anticipated that we would observe increased Gatm and Odc1 in peritumoral mammary adipose tissue from overweight/obese patients. While our data do not support such a relationship, this analysis is preliminary and statistically underpowered. Moreover, as reflected in Table 5.1, there is a wide range of patient ages and thus variable menopausal status, as well as substantial variation in histologic grade of the tumors. As we collect more patient samples, we will be powered to analyze gene expression data as a function of important predictive variable such as BMI, age, menopausal status, histologic grade, and hormone receptor subtype (Her2, PR, ER).

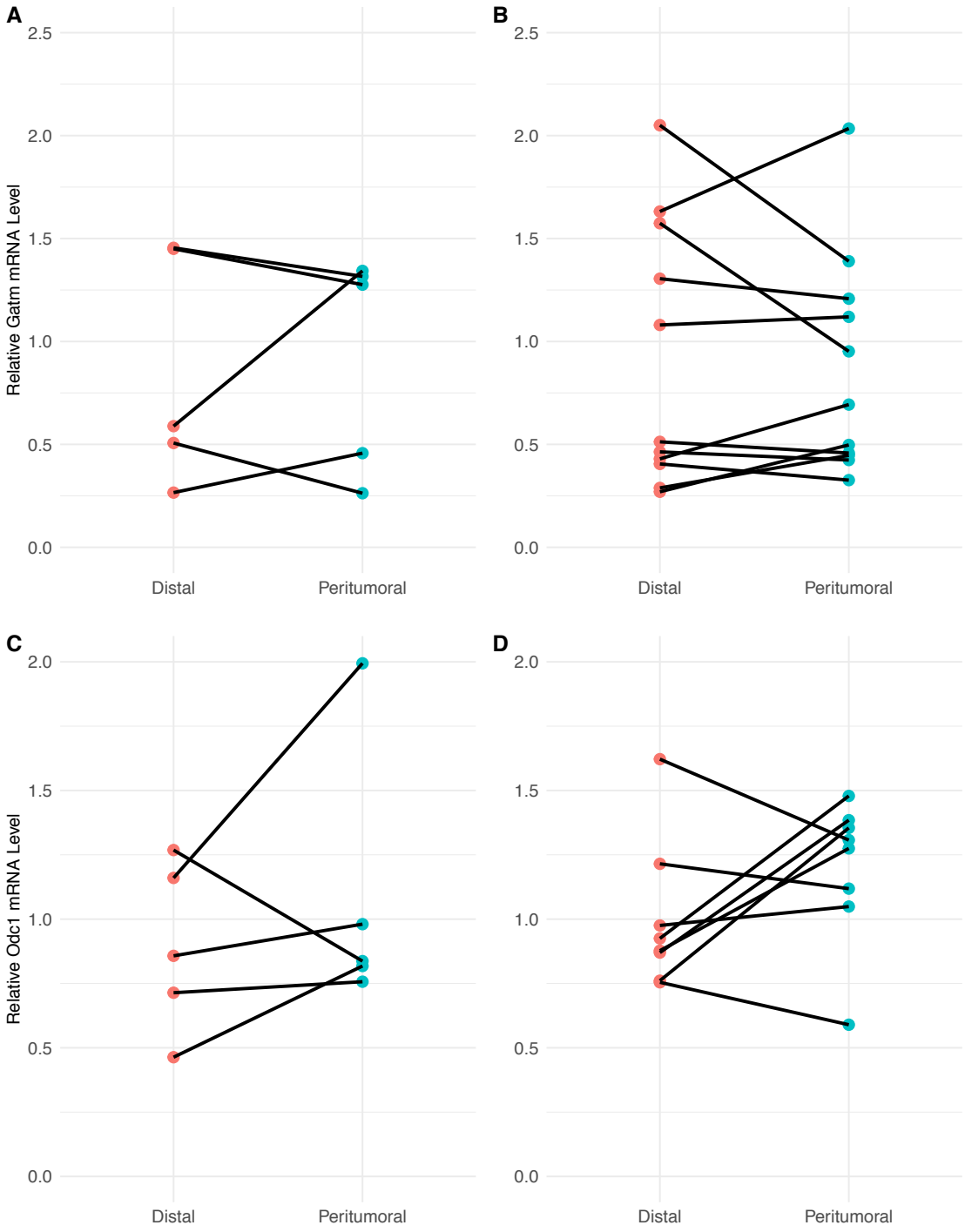

Figure 5.1 Odc1 and Gatm expression in peritumoral and distal human mammary adipose tissue

A. Gatm mRNA levels in normal weight patients. B. Gatm mRNA levels in obese and overweight patients. C. Odc1 mRNA levels in normal weight patients. D. Odc1 mRNA levels in obese and overweight patients.

5.3 Prevent Cohort

We used the Prevent Cohort, a much larger and previously published study (Iyengar, Zhou, et al. 2016), to examine whether Gatm is increased in mammary adipose tissue of obese/overweight patients compared to normal weight patients with breast cancer. This study is different from our peritumoral and distal collection in that only one mammary adipose tissue sample was collected per patient. The sample was collected from an uninvolved quadrant of the breast. In this cohort, patient age ranged from 27 to 70 years old; 50 patients were obese/overweight (BMI≥25) patients and 46 were normal weight (BMI<25) (Table 5.2). The obese/overweight patients had an increased average BMI compared to the normal weight patients ($p<0.0001$) while other factors were matched.

Gatm expression was increased 67% ($p<0.05$) in breast adipose tissue from obese/overweight patients compared to normal weight patients (Figure 5.2). We did not find that Gatm expression was related to the presence of CLS-B or any of the other factors examined in the original Prevent Cohort study. We also found that Gatm levels were increased in mammary adipose tissue from patients with invasive tumors as compared to those with ductal carcinoma in situ (DCIS). This increase was not statistically significant ($p=0.31$), though we were likely underpowered due to the small number of DCIS patients (n=13).

Table 5.2 Prevent Cohort

Characterization of patients whose mammary adipose tissue was collected as part of the Prevent Cohort (Iyengar, Zhou, et al. 2016). The obese/overweight patients had an increased average BMI compared to the normal weight patients ($p<0.0001$) while other factors were matched.

Prevent Cohort

Variables	Normal Weight 46/96 (48%)	Obese/Overweight 50/96 (52%)
BMI		
Median (range)	21.8 (17.5 to 24.9)	28.4 (25.3 to 50)
Pathology		
Benign	2 (2.1%)	8 (8.3%)
DCIS	9 (9.3%)	4 (4.2%)
LCIS	1 (1.1%)	0 (0%)
Invasive	34 (35.4%)	38 (39.6%)

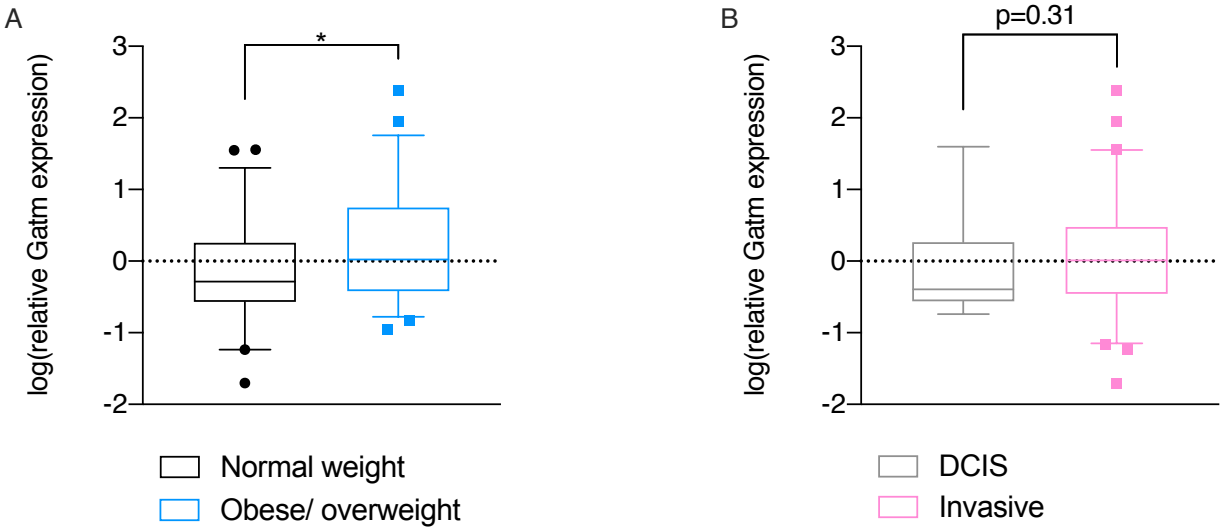

Figure 5.2 Gatm mRNA expression was increased in mammary adipose tissue from overweight/obese breast cancer patients and in patients with invasive tumors vs. DCIS

A. mRNA levels of Gatm in mammary adipose tissue of overweight/obese compared to normal weight breast cancer patients. B. mRNA levels of Gatm in mammary adipose tissue of patients with invasive breast cancer vs. DCIS. Data represent median, interquartile range, 5th-95th percentile and outliers. * $p< 0.05$ (Iyengar, Zhou, et al. 2016).

5.4 Summary of Chapter 5

This project focuses on the links between obesity and breast cancer. This work has predominantly been done in mice but extending our findings to human patients brings a translational element to this project. We have established our own human mammary adipose tissue collection protocol and have examined a previously established patient cohort. Our protocol is continuing to collect peritumoral and distal adipose from female patients undergoing at MSKCC. Preliminary analysis does not show increased Gatm or Odc1 levels in peritumoral mammary adipose tissue of overweight/obese patients relative to distal mammary adipose tissue. However, our cohort thus far is very small and heterogeneous. We will continue to collect patient samples and will examine Odc1 and Gatm mRNA levels once we are powered to control for other key predictive variables. We also plan to measure levels of polyamines and creatine in these samples.

We also analyzed Gatm mRNA expression in mammary adipose tissue from the Prevent Cohort, which collected samples from an uninvolved quadrant of the breast from 96 female breast cancer patients. Gatm was significantly increased in mammary adipose tissue of overweight/obese patients, suggesting that our findings in mouse models may extend to humans.

CHAPTER 6

BEIGE ADIPOSE AND ITS ROLE IN OBESITY AND BREAST CANCER

6.1 Introduction

We also examined the role of mammary adipose tissue health in the tumor microenvironment. Beige adipocytes are embedded within white mammary adipose tissue and express a thermogenic gene program in response to stimuli such as cold exposure, aerobic exercise and PPARγ agonists like rosiglitazone and pioglitazone (Ohno et al. 2012). Stimulation of beige adipocytes is commonly referred to as "beiging". Rosiglitazone and pioglitazone are both thiazolidinediones and have been used for the treatment of type 2 diabetes.

PPARγ ligands can induce beiging, and this process is dependent on the transcriptional coregulator Prdm16 (Ohno et al. 2012). Prdm16 is expressed in subcutaneous adipose and is the key regulator of beige adipocytes (Seale et al. 2011). When Prdm16 is over expressed in adipose tissue using an aP2 promoter (aP2-Prdm16 Tg), mice display increased energy expenditure, limited weight gain and improved glucose tolerance on a HFD (Seale et al. 2011). When Prdm16 is deleted (KO) in adipocytes (Adipo-Prdm16 KO), beige fat function is ablated. Adipo-Prdm16 KO mice show increased weight gain, severe insulin resistance and hepatic steatosis on a HFD (Cohen et al. 2014). We hypothesized that changes in adipose tissue phenotype would affect breast cancer growth in models of obesity-driven breast cancer. Therefore, we examined the role of beige adipocytes, which are associated with favorable metabolic health. Our studies utilized pharmacologic agents (rosiglitazone) and genetic models (aP2-Prdm16 Tg and Adipo-Prdm16 KO) in mice with orthotopic E0771 breast tumors.

6.2 Pharmacologic activation of beige adipose tissue

In an initial pilot study, we used the PPARγ agonist rosiglitazone to beige the subcutaneous adipose tissue of male DIO mice. As a cancer model, we used the Moc1 head and neck tumor line, which has been shown to be obesity dependent. Mice were given intraperitoneal (i.p.) injections with 10mg/kg/day of rosiglitazone or vehicle control, starting one week prior to Moc1 cancer cell injection.

The subcutaneous adipose tissue of mice treated with rosiglitazone had an increase in thermogenic gene expression and a decrease in inflammatory gene expression in both chow and HFD fed mice (Figure 6.1A and Figure 6.1B). We then injected 250,000 Moc1 cancer cells into the flank and continued to administer daily i.p. rosiglitazone. We measured tumor volume over time using calipers and found that HFD fed mice treated with rosiglitazone had significantly decreased tumor progression compared to HFD mice treated with vehicle ($p<0.05$) (Figure 6.1C). At endpoint, the average tumor volume in the HFD mice treated with rosiglitazone was 62% ($p<0.05$) smaller than in HFD vehicle treated mice. The final weight of tumors in the HFD rosiglitazone treated mice was half the weight of the tumors in the HFD vehicle treated mice, though this was not statistically significant ($p=0.07$) (Figure 6.1D). Interestingly, there was no difference in tumor growth or final tumor weight between the chow fed rosiglitazone and vehicle treated groups (Figure 6.1C and D).

This experiment indicated that activation of beige adipose with rosiglitazone treatment could attenuate tumor progression in HFD mice. However, rosiglitazone treatment has systemic effects and could also act directly on the tumor as well as other organs. Thus, our next studies used genetic models (aP2-Prdm16 Tg and Adipo-Prdm16 KO mice) to further study the role of beige adipose tissue in the tumor microenvironment.

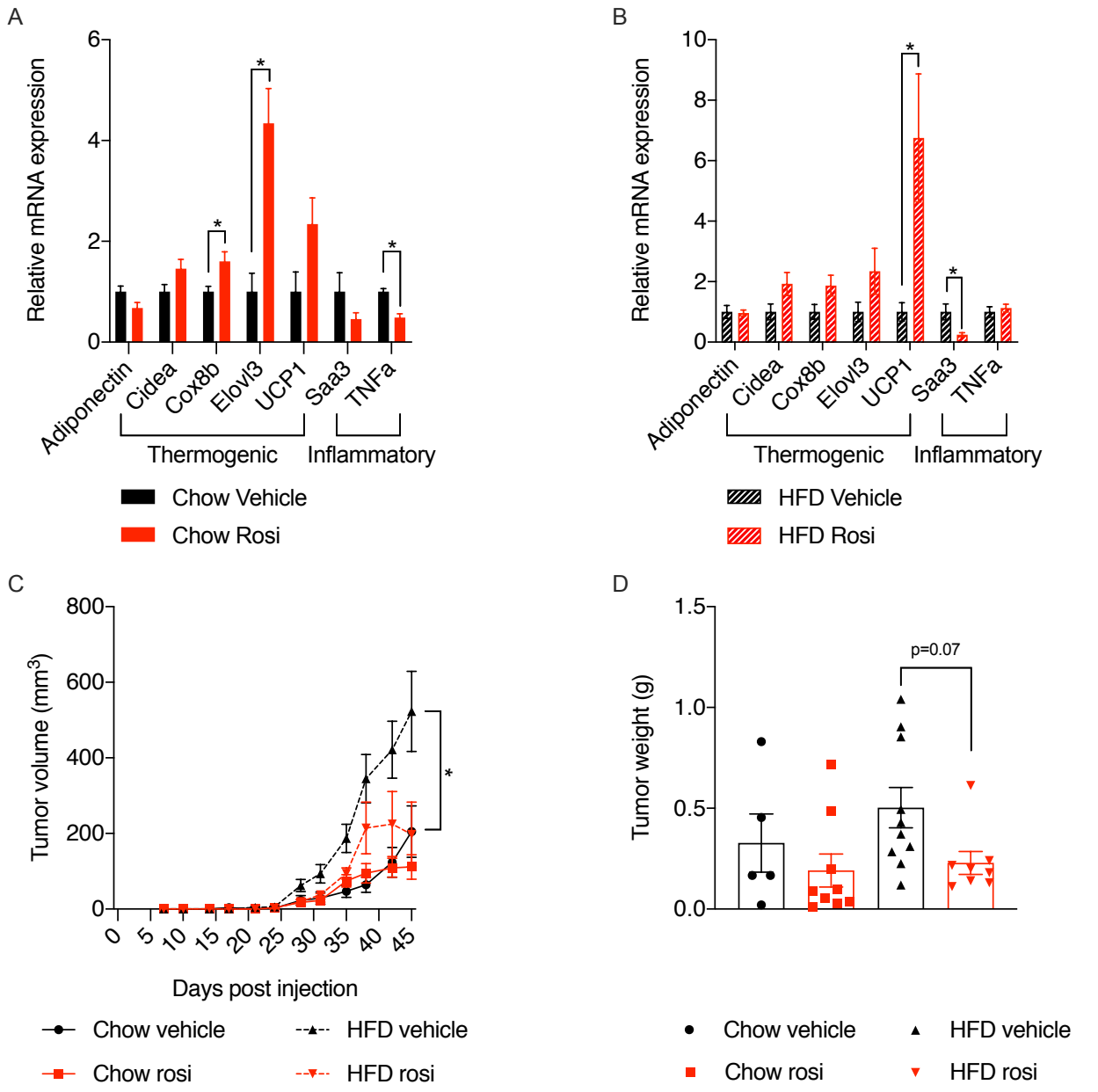

Figure 6.1. Rosiglitazone treatment promoted beiging of subcutaneous adipose tissue and attenuates Moc1 tumor growth in HFD mice

A. mRNA expression of thermogenic and inflammatory genes in chow fed mice treated with 10mg/kg/day rosiglitazone or vehicle control. B. mRNA expression of thermogenic and inflammatory genes in HFD fed mice treated with 10mg/kg/day rosiglitazone or vehicle control. C. Moc1 tumor progression in HFD and chow fed mice treated with 10mg/kg/day rosiglitazone or vehicle control. D. Final weights of Moc1 tumors at necropsy. Data shown here represent mean +/- standard error of the mean (SEM). * $p < 0.05$

6.3 Room temperature Adipo-Prdm16 transgenic and knockout cohorts

We generated two cohorts: one of aP2-Prdm16 Tg female mice and littermate controls and another of Adipo-Prdm16 KO female mice and littermate controls. Both sets of mice were placed on a HFD at 6 weeks of age. Adipo-Prdm16 KO became slightly heavier than littermate controls, though there was not a statistical difference (Figure 6.2A). There was no difference in weight between the aP2-Prdm16 Tg and littermate controls (Figure 6.2C).

We injected both cohorts of mice with E0771 cancer into the 4^{th} mammary fat pad after 10 weeks on a HFD. Tumor progression was monitored using calipers twice a week. There was no difference in tumor volume between Adipo-Prdm16 KO and littermate controls (Figure 6.2B) nor between aP2-Prdm16 Tg and littermate controls (Figure 6.2D).

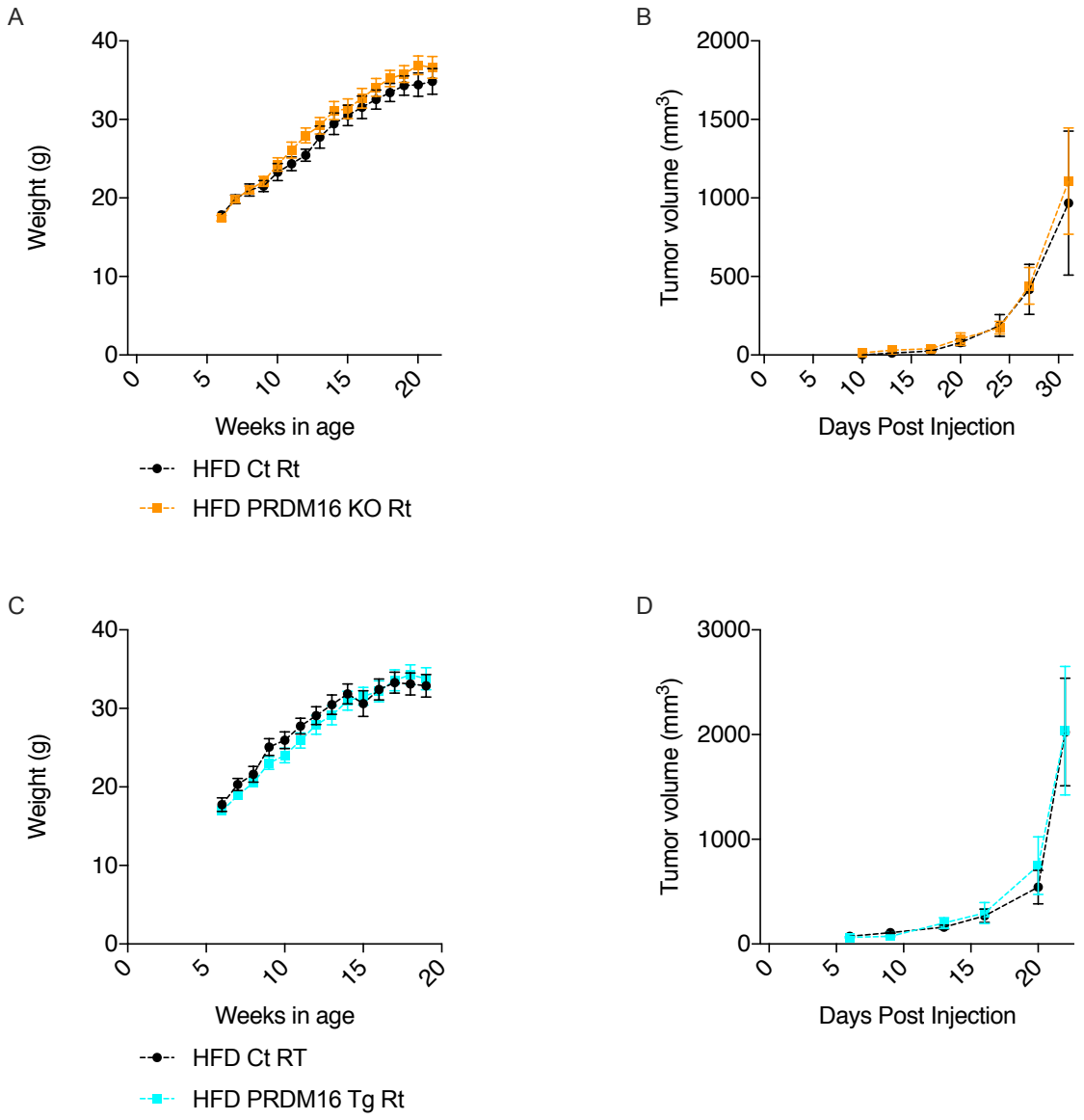

Figure 6.2. Adipo-Prdm16 KO and aP2-Prdm16 Tg mice have similar weights to littermate controls and no difference in E0771 tumor growth

A. Weight of Adipo-Prdm16 KO and littermate controls on a HFD. B. Volume of E0771 tumors in Adipo-Prdm16 KO and littermate controls over time. C. Weight of aP2-Prdm16 Tg and littermate controls on a HFD. D. Volume of E0771 tumors in aP2-Prdm16 Tg and littermate controls over time. Data shown here represent mean +/- standard error of the mean (SEM).

We confirmed that Adipo-Prdm16 KO mice had a reduction in thermogenic genes compared to HFD littermate controls, in both peritumoral and contralateral mammary adipose tissue (Figure 6.3A). HFD aP2-Prdm16 Tg mice had an increase in thermogenic genes compared to HFD littermate controls in both peritumoral and contralateral mammary adipose tissue (Figure 6.3B). There was not a statistically significant increase in thermogenic gene expression in the aP2-Prdm16 Tg mice, though there was a clear trend. Overall, these data show that mammary adipose tissue in Adipo-Prdm16 KO and aP2-Prdm16 Tg mice exhibited distinct phenotypes, though there was no difference in E0771 tumor growth.

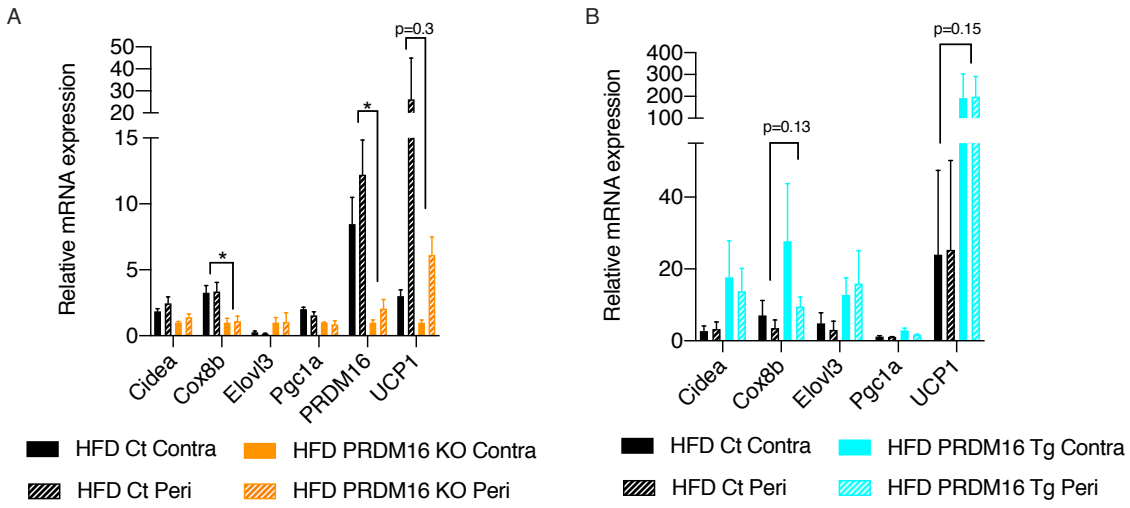

Figure 6.3 Adipo-Prdm16 KO and aP2-Prdm16 Tg mice have altered thermogenic gene expression in mammary adipose tissue

A. mRNA levels of thermogenic genes from peritumoral and contralateral mammary adipose tissue in HFD Adipo-Prdm16KO and Ct mice. B. mRNA levels of thermogenic genes from peritumoral and contralateral mammary adipose in HFD aP2-Prdm16 Tg and Ct mice. Data shown here represent mean +/- standard error of the mean (SEM). * $p < 0.05$,

6.4 Cold exposed Adipo-Prdm16 KO cohorts

We saw that rosiglitazone treatment increased beige fat activation and reduced tumor size in mice on a HFD. Yet, when we used Adipo-Prdm16 KO (beigeless mice) and aP2-Prdm16 Tg (enhanced beige) mice on a HFD, we did not see a difference in tumor growth. This could have been because we used different models of cancer in these two experiments, though both Moc 1 and E0771 obesity dependent. We hypothesized that the phenotypes in these genetic models were too subtle to modulate tumor growth. The initial studies were conducted at room temperature, and stimulation, with cold exposure for example, is known to activate beige fat. We therefore decided to study tumor progression in cold-exposed (6.5°C) Adipo-Prdm16 KO mice and littermate controls.

Cold exposure resulted in the activation of beige adipose tissue in Ct mice, while beige fat function was completely ablated in beige Adipo-Prdm16 KO mice. HFD Ct mice exposed to cold showed increased thermogenic gene expression in peritumoral and contralateral mammary adipose tissue compared to cold exposed HFD Adipo-Prdm16 KO (Figure 6.4A). There was no change in adipose marker genes. The HFD Ct mice also showed decreased inflammatory gene expression compared to HFD Adipo-Prdm16 KO mice (Figure 6.4B). Similar results were seen in chow fed mice (data not shown).

Before mice were cold exposed, HFD fed mice weighed 50% more than chow fed mice for both genotypes (KO and Ct). After mice were placed in the cold chamber (14 weeks of age), the HFD mice began to lose weight, weighing only a few grams more than the chow controls by endpoint (Figure 6.4C). After one week of cold exposure, we injected all mice with E0771 breast cancer cells into the 4th mammary fat pad. We found that tumor progression in cold exposed HFD littermate controls was reduced compared to cold exposed Adipo-Prdm16 KO mice, room temp

controls and room temp Adipo-Prdm16 KO mice, though this was not statistically significant (p=0.06) (Figure 6.4C). At endpoint, tumor volume in the HFD cold exposed Ct mice was 71.8% (p=0.32) less than tumor volume in HFD cold exposed Adipo-Prdm16 KO mice (Figure 6.4C). This pattern was not seen in chow fed mice. This suggested that activated beige fat from cold exposure reduced tumor progression in HFD Ct mice compared to Adipo-Prdm16 KO mice, which are unable to activate beige fat.

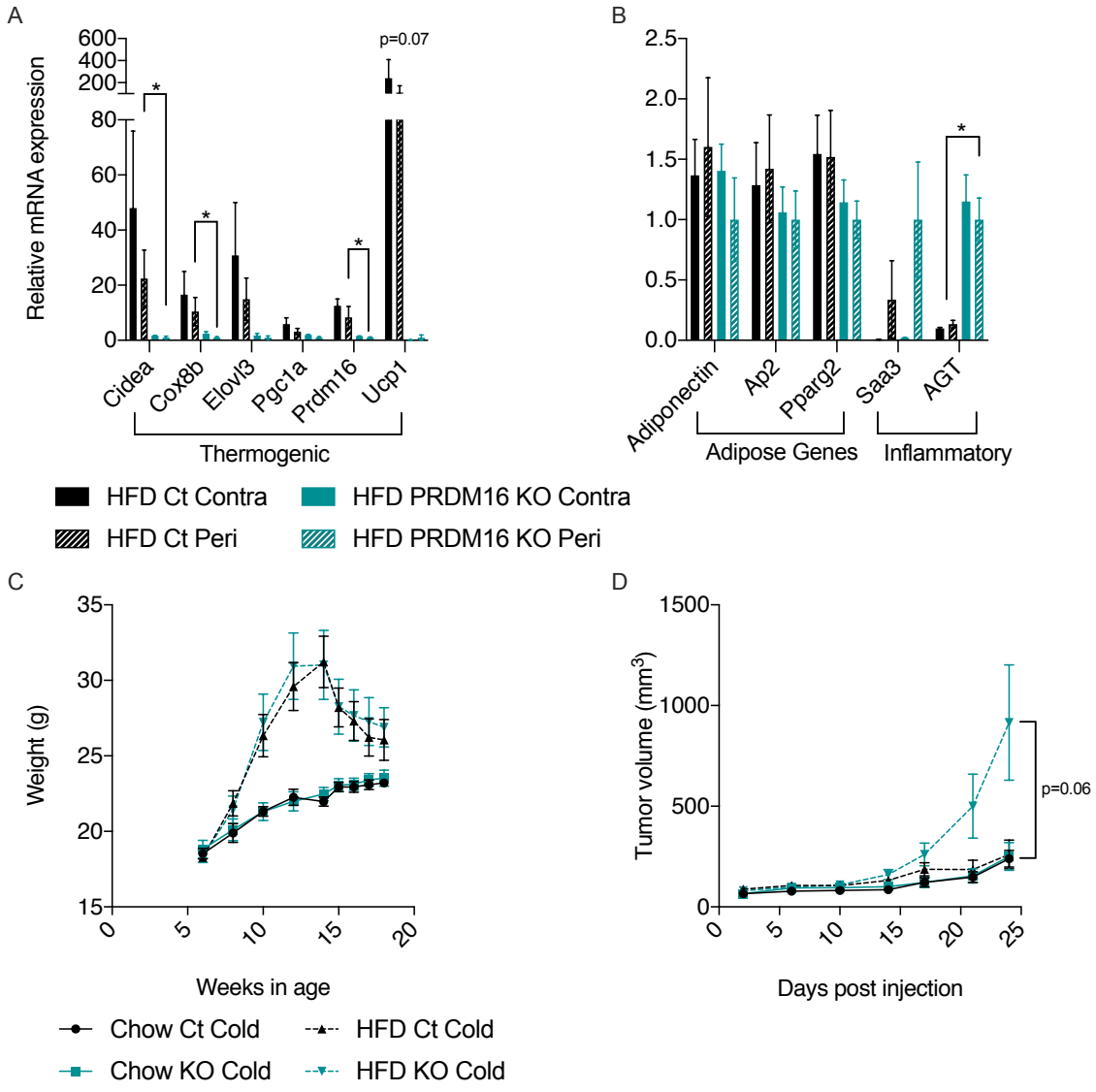

Figure 6.4 Cold exposed HFD Adipo-Prdm16 KO mice show increased breast tumor progression compared to HFD littermate controls with activated beige fat.

A. mRNA levels of thermogenic genes from peritumoral and contralateral mammary adipose tissue from cold exposed HFD Adipo-Prdm16 KO and littermate controls. B. mRNA levels of general adipose markers and inflammatory genes from peritumoral and contralateral mammary adipose tissue from cold exposed HFD Adipo-Prdm16 KO and littermate controls. C. Weights of chow and HFD fed Adipo-Prdm16 KO and littermate controls housed in a cold incubator at 14 weeks of age. D. Progression of E0771 tumors in chow and HFD fed Adipo-Prdm16 KO and littermate controls housed in a cold incubator. Data shown here represent mean +/- standard error of the mean (SEM). * $p< 0.05$

Since this experiment showed a trend towards differential breast tumor progression between cold exposed Adipo-Prdm16 KO and littermate controls, we repeated the experiment with all appropriate controls. Figure 6.5 separates chow and HFD mice for simplicity, but all mice were monitored as one large cohort. Room temp and cold exposed chow fed Adipo-Prdm16 KO and Ct mice had similar weights (Figure 6.5A), and no difference in progression of E0771 tumors (Figure 6.5B). In the HFD setting, mice began to lose weight after being placed in the cold chamber (6.5°C) at 14 weeks of age (8 weeks on a HFD) (Figure 6.5C). Adipo-Prdm16 KO mice lost less weight than littermate controls, but this difference was not significant. We again found that tumor progression in cold exposed HFD littermate controls was reduced compared to cold exposed Adipo-Prdm16 KO mice, room temperature controls and room temperature Adipo-Prdm16 KO mice ($p<0.05$) (Figure 6.5D). At endpoint, tumor volume in HFD cold exposed Ct mice was 51.8% ($p<0.0001$) less than in HFD cold exposed Adipo-Prdm16 KO mice (Figure 6.5D). This was the second time that beige fat activation (cold exposed controls) was associated with reduced tumor progression, compared to mice with an ablation of beige fat (Adipo-Prdm16 KO cold exposed mice).

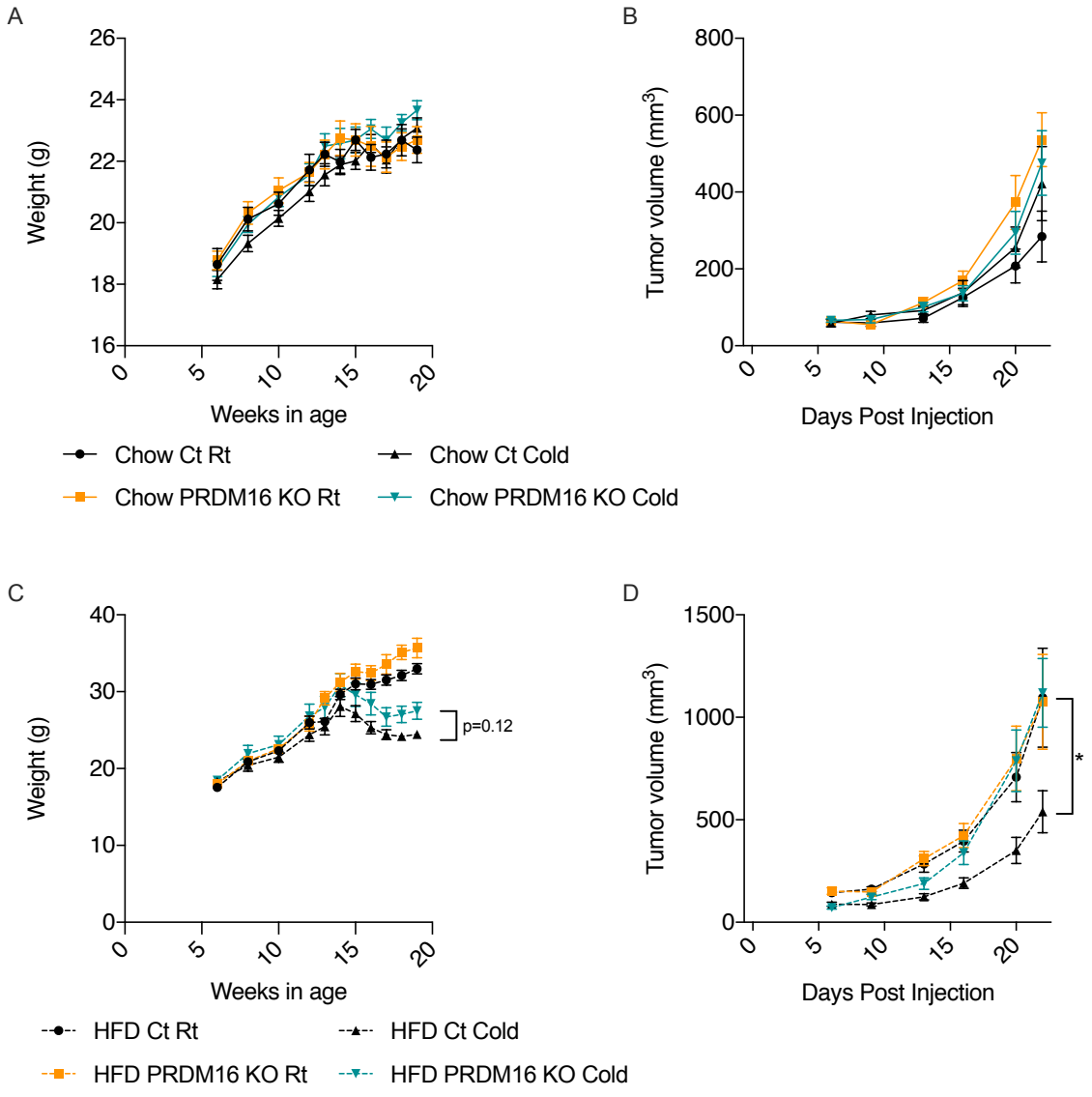

Figure 6.5. Cold exposed HFD Adipo-Prdm16 KO mice show increased breast tumor progression compared to HFD littermate controls with activated beige fat.

A. Weight of chow fed Adipo-Prdm16 KO and littermate controls at room temperature and with cold exposure. B. E0771 tumor growth in chow fed Adipo-Prdm16 KO and littermate controls at room temperature and with cold exposure. C. Weight of HFD fed AdipoPrdm16 KO and littermate controls at room temperature and with cold exposure. D. E0771 tumor growth in HFD fed Adipo-Prdm16 KO and littermate controls at room temperature and with cold exposure. Data shown here represent mean +/- standard error of the mean (SEM). * $p < 0.05$

We have seen twice that HFD littermate controls exposed to cold have attenuated progression of breast tumors compared to HFD Adipo-Prdm16 KO cold exposed mice. We decided to test another cohort to be sure that the phenotype was consistent. We saw again that HFD Adipo-Prdm16 KO and littermate controls lost weight after they were placed in the cold incubator after 7 weeks on a chow or HFD diet (Figure 6.6A). Yet when we tracked E0771 breast tumors over time, in this study, we did not see a decrease in tumor size in HFD cold exposed littermate controls (Figure 6.6B). This was in contrast to our other two experiments, and thus the role of beige adipose tissue activation in breast tumor progression remains to be fully clarified.

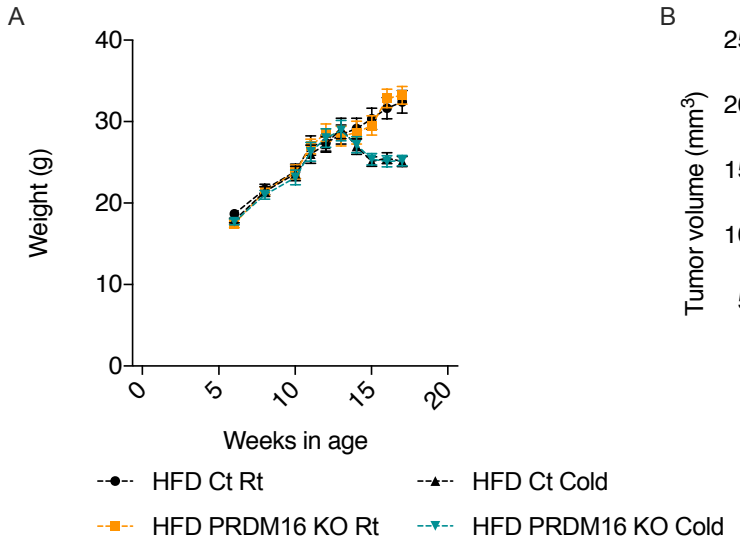

Figure 6.6. Cold exposed HFD Adipo-Prdm16 KO mice do not show increased breast tumor progression compared to HFD littermate controls with activated beige fat.

A. Weight of HFD Adipo-Prdm16 KO and littermate controls at room temperature and with cold exposure. B. E0771 tumor progression in HFD Adipo-Prdm16 KO and littermate controls at room temperature and with cold exposure. Data shown here represent mean +/- standard error of the mean (SEM).

6.5 Summary

This project was based on the well-established concept that beige adipose tissue is associated with favorable metabolic health. Heathier beige adipose is more thermogenic and less inflamed. We have seen that rosiglitazone can induce beiging in subcutaneous adipose tissue. We further confirmed that Adipo-Prdm16 KO mice could not undergo beiging of mammary adipose tissue, while aP2-Prdm16 Tg mice had enhanced beige mammary adipose tissue. Since completing the studies shown here, we have learned that the aP2 promoter is not adipocytes specific and that PRDM16 is increased in other tissues apart from adipocytes.

Our initial pilot showed that the activation of beige subcutaneous adipose tissue slowed the progression of Moc1 head and neck tumors. Our results were encouraging, but in addition to promoting beiging, rosiglitazone may have actions on the tumor as well as other tissues in the mice.

We then turned to the aP2-Prdm16 Tg (increased beige fat) and Adipo-Prdm16 KO (ablated beige fat) mouse models. At room temperature, E0771 breast tumors did not progress at different rates. We hypothesized that this was because there was not a large enough difference in the phenotype of mammary adipose of Tg or KO mice compared to littermate controls. Therefore, we used cold exposure to induce beiging in the mammary adipose tissue of control mice, while the mammary adipose tissue in Adipo-Prdm16 KO mice could not undergo beiging. We found that two of three experiments showed that cold exposed HFD control mice had slower tumor progression compared to cold exposed Adipo-Prdm16 KO mice.

Interestingly, we did not see the same results in cold exposed chow fed mice. This could be because there was increased adiposity in the HFD mice which could affect tumor growth. However, HFD mice rapidly lost weight upon cold exposure, complicating our model of obesity-

driven breast cancer. We believe that adipose tissue in the tumor microenvironment plays a key role in the link between obesity and breast cancer. We believe that beige fat may play a role, but our current models each have confounding factors. Future studies may involve efforts to expose mice to more modest cold, such that the tissue is prompted to beige, but with minimal weight loss on a HFD. If such experiments show that beige fat activation is associated with attenuated tumor progression, these data would suggest that beige adipose in the breast tumor microenvironment is key for obesity dependent breast cancer progression.

CHAPTER 7

DISCUSSION

This study aimed to elucidate how transcriptional changes in obese peritumoral adipocytes affect breast tumor progression. We developed multiple models of obesity dependent breast tumor progression in B6 mice, sequenced the mammary adipose tissue from peritumoral and contralateral locations, investigated key candidates, and examined how the health of adipose tissue can affect breast tumor progression. Examining obesity-driven breast cancer from an adipocyte-centric view is unique in the field. Our findings provide novel pathways which may provide molecular targets for therapeutic intervention.

Here we show that we have successfully developed orthotopic models of obesity-driven breast cancer (E0771 and Py8119). Importantly, we also determined that it is obesity itself and not the diet (HFD) which is affecting tumor progression. RNA sequencing of peritumoral and contralateral adipose in chow and HFD fed mice provided gene expression data to identify key genetic pathways in our model of obesity accelerated breast tumor growth.

From this RNA sequencing data, we identified two gene candidates: Odc1 and Gatm. We have shown that the absence of Gatm in adipocytes of obese mice reduced tumor progression compared to obese controls. Since Gatm is the rate limiting step in creatine synthesis, this suggests that adipocyte-derived creatine may support tumor growth.

To test if creatine was playing a role in our model, we deleted the creatine transporter (Slc6a8) from E0771 cancer cells. In this model, tumor progression was reduced in HFD mice with Slc6a8 KD compared to scrambled Ct. This further showed that creatine can affect breast tumor growth in obese mice. Interestingly, in all of our creatine studies, the chow fed mice did not show the same phenotype as HFD fed mice suggesting an obesity-specific mechanism.

We are currently working on a survival study using chow and HFD Adipo-Gatm KO and littermate controls with E0771 tumors. We will continue to monitor the tumors in each group until they have reached a humane endpoint (2000mm^3). This experiment will determine if tumors in chow fed Adipo-Gatm mice will eventually diverge in size compared to tumors in Ct mice. A divergence in tumor growth will suggest that creatine metabolism is accelerated in the obese state but still important for breast cancer growth in lean mice. If there is no divergence in tumor growth in the chow groups, this would suggest that changes in creatine metabolism are strictly driven by obesity in the tumor microenvironment.

We have shown that removing Gatm from adipocytes and deleting Slc6a8 from tumor cells mitigates obesity dependent tumor progression. Yet, we have not shown that it is specifically creatine which moves from adipocytes to the tumor in order to affect breast tumor progression. In order to answer this question, we are currently working with collaborators to perform the same E0771 tumor progression experiment in Adipo-Slc6a8 KO mice. If the creatine is in fact coming from the adipocytes and trafficking to the tumor to enhance growth, then we should see a decrease in tumor progression in HFD fed Adipo-Slc6a8 KO mice compared to HFD Ct mice. We are also working with a collaborator to use stable isotope labeling to trace creatine from adipocytes to the tumor, using labeled arginine. These projects are ongoing and will further elucidate the role of creatine in the tumor microenvironment.

From a literature review, we believe that hypoxia could be a key condition of the tumor microenvironment prompting the tumor to rely on creatine metabolism rather than other methods for cell proliferation. We determined that tumors in obese mice had increased Hif1α expression compared to tumors from chow mice. However, exogenous creatine did not affect E0771 cell

viability in 21% O_2 or 0.5% O_2 (hypoxic) conditions. We are continuing to perform *in vitro* studies using increasing levels of creatine within a hypoxic chamber.

Creatine is known to be phosphorylated by creatine kinases into phosphocreatine which can in turn produce ATP for energy. This pathway has been implicated in cancer progression which made it a promising pathway for our model. However, phosphocreatine and ATP/ADP levels were not reduced in Slc6a8 KD tumors compared to Ct tumors. This suggests that energetics are not necessarily driving the difference in tumor size.

We did see a reduction in creatine in the Slc6a8 KD compared to Ct tumors in HFD mice. This suggests that creatine itself is affecting tumor progression. Creatine is generated from glycine and arginine by Gatm. We hypothesize that this pathway can also operate in reverse, which would allow creatine to be used by the cancer cell to produce glycine and arginine. These amino acids can then be recycled or further broken down into nucleotides for DNA replication and cell proliferation.

Importantly, we also showed that Gatm levels are increased in adipose tissue of overweight/obese breast cancer patients compared to normal weight patients. This suggests that changes in creatine metabolism may be relevant in humans and could be a target for human therapeutics. As we continue to parse out creatine's mechanism of action in the mouse breast tumor model, we may also be able to extend these mechanistic findings to human patients.

Overall, we have shown that creatine metabolism is key in our model of obesity-driven breast cancer. We are also examining another gene candidate, Odc1, and have promising initial results suggesting that Odc1 and polyamine synthesis may play an important role. An exciting possibility is that Odc1 and Gatm, which are linked through arginine and ornithine, work together

to affect breast tumor progression. Future experiments with the Adipo-Odc1 KO model will determine if Odc1 and polyamine synthesis are relevant in our model.

This project began with a phenotype of obesity accelerated E0771 breast tumor growth. We determined that creatine metabolism is a key, novel pathway connecting obese adipocytes to breast tumor progression. We have extended our findings to human breast cancer patients and continue to investigate the mechanism by which creatine regulates breast tumor growth.

FUTURE DIRECTIONS

Obesity is overtaking smoking as the leading preventable cause of breast cancer. As the prevalence of obesity in the U.S. increases dramatically, investigating the links between obesity and cancer has emerged as an important and urgent area of research. Studying the mechanisms through which excessive adipose tissue enhances the progression of breast cancer will ultimately contribute to novel therapeutic strategies for treating breast cancer. In this respect, we have found novel mechanisms connecting obesity and breast cancer and investigated the mechanisms of action on tumor cells. Here, we will describe future projects which can expand upon the data presented above.

This project involved RNA sequencing of adipose tissue in six distinct groups (see Chapter 2). One comparison we have not yet examined, is the difference in gene expression between contralateral adipose tissue and adipose tissue from non-tumor bearing mice. This would provide data on genes which are dysregulated systemically in the adipose tissue. It is possible that there are circulating factors or systemic changes to adipose tissue which occur in all mammary adipose tissues that affect breast tumor progression.

Since we know that the tumor microenvironment contains multiple cell types, we used the TRAP method to determine if the differentially regulated genes from our RNA sequencing results were specifically changed in adipocytes. The TRAP data set itself, however, has yet to be examined. TRAP also provides the added benefit of examining transcripts which are being actively translated within adipocytes. This data set would provide an adipocyte specific profile of actively translated genes in the peritumoral and contralateral adipose of lean and obese mice. Pathway analysis and confirmation of genes found in this data set may identify other novel pathways connecting obesity and breast cancer.

The studies described here focused on Gatm and Odc1 in peritumoral adipocytes. Deletion of Gatm in adipocytes has clearly shown effects on tumor progression. There is still much to be done to elucidate the mechanism by which creatine enters the cancer cell and affects cancer cell growth. While many of these Gatm related experiments are already underway (see Chapter 3: Summary and Chapter 7: Discussion), the Adipo-Odc1 KO mouse line is now back crossed to B6 and can be used to test E0771 progression. If we see a difference in tumor progression between obese Adipo-Odc1 KO and Ct mice, this could become an entirely new direction of this project. Interestingly, Odc1 and polyamine synthesis are connected to creatine metabolism through arginine and ornithine and thus Gatm could work together with Odc1 to modulate tumor progression.

MATERIALS AND METHODS

Mice

C57Bl/6J wild-type mice were from Jackson Labs. Gatm floxed mice crossed to adiponectin cre (strain # 028020, Jackson Labs) were provided by Dr. Bruce Spiegelman (Dana-Farber Cancer Institute) (Kazak et al. 2019). Rosa26^{fsTRAP} (strain # 022367) were from Jackson Labs. Odc1 floxed mice were provided by Dr. Raghu Mirmira (Indiana University School of Medicine). These mice will be crossed to adiponectin cre (028020) and will be used to study Odc1. All mice were weaned at 3 weeks of age and placed on Purina 5053 diet. At 6 weeks of age, low fat diet (LFD 10%) mice were fed D12450J from Research Diets and high fat diet (HFD 60%) mice were fed D12492. Chow fed controls remained on Purina 5053 diet. Mice were weighed every two weeks and experiments were started after 8-9 weeks of diet.

Genotyping

Mice were weaned at 3 weeks of age. Tail clips were collected (IACUC approved) and boiled in NaOH for 45 minutes. The solution was neutralized with Tris-HCl. Genotyping 2x mastermix (Denville) was used along with specific primers (see genotyping primers). Genotyping protocol was run in a PCR machine (Bio-rad) (see genotyping protocols) and samples were then run on a 1% agarose gel with EtBr. Gels were imaged in a Bio-rad Gel Doc System.

In vitro subcutaneous adipocyte isolation and differentiation

Subcutaneous adipose was dissected and the lymph node was kept in the tissue. Adipose was minced with spring scissors and placed in 50ml Eppendorf's with 10mls of digestion buffer. Digestion buffer contained Collagenase D (10mg/ml, Roche), Dispase II (2.4mg/ml, Roche) and

$CaCl_2$ (10mM). Adipose was digested in a shaking water bath for 45 minutes. Complete medium was added to quench the digestion buffer and then the tubes were spun down at 500g for 10 minutes. Mature adipocytes and liquid were removed by aspiration. Pellet was resuspended and passed through 100μm filter. Tubes were spun again, supernatant was removed, pellet was resuspended and passed through a 70μm filter and spun down again. Final pellet was resuspended in the desired amount of F-12 Glutamax medium (Thermo Fisher Scientific) containing 10% Fetal Bovine Serum (Gemini Bioproducts) and 1% PenStrep (Thermo Fisher Scientific) and plated into collagen coated plates (most often 12 well plates) (Corning). Cells were kept in 37°C incubators with 10% CO_2.

Pre-adipocytes were differentiated after the cells reached 100% confluence. On that day, differentiation medium was added which contained IBMX (0.5mM), dexamethasone (1μM), insulin (850nM), and rosiglitazone (1μM). On day two medium was switched to insulin and rosiglitazone only. On day 4 medium was switched to insulin only. Day 6, insulin was continued. Finally, on day 7 adipocytes were fully differentiated.

AAV production and injections

AAV serotype 8 was generated by the UPenn Vector Core. Two viruses AAV8-GFP and AAV8-Odc1 (mouse Odc1 was tagged with 3xFlag peptide) were generated. Both plasmids were designed using pENN.AAV.CB7.Cl.Null.IRES.eGFP.WPRE.RBG (p4189) backbone from UPenn. Boluses of 100ul with $1x10^{11}$ GC/ml were injected into the subcutaneous mammary adipose tissue to generate Odc1 over expression (OE) or control (GFP). After AAV injection, mice were housed in a biosafety level 2 (BSL2) facility in the Comparative Biosciences Center (CBC). Mice with the same injections were placed in one cage to prevent cross contamination. Three days

later these mice were transferred from the BSL2 facility back into the non-hazard mouse facility room. One week later these mice injected with 50,000 E0771 cells and tumors were monitored.

Adipose Fractionation

Subcutaneous adipose was dissected and lymph node was removed. Adipose was minced with spring scissors and placed in 5ml Eppendorf's with digestion buffer. Digestion buffer contained Collagenase D (10mg/ml, Roche), dispase II (2.4mg/ml, Roche) and $CaCl_2$ (10mM). Adipose was digested in a shaking water bath for 45 minutes. The digested tissue was spun down at 500g for 10 minutes, resulting in a pellet containing the stromal vascular fraction and a layer of mature adipocytes floating at the top of the supernatant. Pellet was removed using a 25g needle. Mature fraction was washed again with PBS, spun down and any remaining supernatant/pellet was removed with a 27g needle. Mature adipose was frozen at -80°C. Needles containing the pellet were ejected into a separate tube and spun down. Pellet was also frozen at -80°C. Frozen samples were correspondingly used for RNA extraction and cDNA synthesis (see RNA isolation, cDNA synthesis and qPCR).

Body Composition Analysis

Body composition analysis was performed using an EchoMRI on the day mice were sacrificed. Calibration was run using canola oil which has a fat mass of 35.3. Ideal temperature range is 21-22°C for the machine. Each mouse was then restrained and placed into the MRI machine. Fat mass, lean mass and free water were measured.

Cell Lines and Injections

All cancer cells were cultured in 1640 RPMI medium (Thermo fisher scientific) with 10% FBS (Gemini Bioproducts) and 1% PenStrep (Thermo Fisher Scientific). Cells were kept in a 37°C incubator at 5% CO_2.

The E0771 (CH3 BioSystems) cell line was derived from a spontaneous mammary tumor in a C57Bl/6 mouse (Sugiura and Stock 1952) and is negative for progesterone receptor and Erb-b2/Neu and expresses a non-functional estrogen receptor (Johnstone et al. 2015). E0771 cells were injected into the 4th mammary fat pad of female mice. The mCherry plasmid (derived from pHIV-Luc-ZsGreen #39196 Addgene) was provided by Ben Ostendorf from the Tavazoie lab at The Rockefeller University. Lentivirus was produced using this plasmid and used to infect E0771 cells. E0771 cell lines positive for mCherry were generated and cells were FACS sorted for high expressing mCherry.

The Py8119 cell line (ATCC) was derived from MMTV-PyMT transgenic mice, which express the Polyoma virus middle T antigen under the control of a mouse mammary tumor virus promoter/enhancer. Py8119 cells are negative for the estrogen receptor, progesterone receptor and Erb-b2/Neu (Gibby et al. 2012). Py8119 cells were injected into the 4th mammary fat pad of female mice.

Moc1 cells (ATCC) are a model of head and neck cancer and were injected into the flank of male C57 Bl6 mice. They were developed from primary tumors in C57 Bl6 mice (Judd et al. 2012).

Cells were injected into mice at 15 weeks of age (9 weeks on a high fat diet). 50,000 Py8119, 50,000 E0771, or 250,000 Moc1 cells were mixed 1:1 with serum free RPMI 1640 medium (Thermo Fisher Scientific) and growth factor reduced (GFR) basement membrane matrix,

phenol red-free (Matrigel Corning) and injected into the left 4th mammary fat pad using a 27g needle (except for Moc1, flank injection). The needle was loaded from the back to prevent cell shearing. All material was kept on ice prior to injections to prevent the Matrigel from solidifying. Mice were anesthetized using isoflurane gas to ensure accuracy of the injections.

Creatine, phosphocreatine and ATP/ADP measurements

Creatine, phosphocreatine, ATP and ADP were all measured using LC/MS from snap frozen tissue. Relative amounts were determined among groups described in Chapter 3. All processing and mass spec was performed in Dr. Lawrence Kazak's laboratory by Janane Rahbani at McGill University.

DFMO and Roziglitazone treatment

DFMO was obtained by the generous donation of Dr. Patrick Woster from the Medical University of South Carolina. DFMO was administered at 2% in the drinking water in sippers attached to 50ml conical tubes. No palatable additive was used. Water was changed every two days and fresh DFMO was mixed. Mice treated with rosiglitazone (Sigma) were given daily intraperitoneal (i.p.) injections at 10mg/kg/day. Mice were injected with rosiglitazone or vehicle every day for one week before tumor injection and then every day during the tumor progression. Vehicle consisted of 75% PBS, 15% Koliphor (Sigma) and 10% DMSO (with or without rosiglitazone).

Subcellular fractionation

Subcellular fractionation was achieved using differential centrifugation. Frozen samples were minced into small pieces and homogenized in fractionation buffer using a KONTES dounce tissue grinder 20 times with piston A and 20 times with piston B on ice. Fractionation buffer included 20mM Hepes pH 7.4, 10mM KCl, 2mM $MgCl_2$, 1mM EDTA, 1mM EGTA, 1mM DTT, 1x protease inhibitor (Roche), 1x phosphostop (Roche). Homogenate was incubated on ice for 20 minutes and strained through a 100um filter. Tubes were then centrifuged at 720xg for 5 minutes, at 4°C, following which, the supernatant was spun again at 10,000xg for 5 minutes to isolate the mitochondrial pellet. Supernatant was transferred to a fresh tube and spun in an ultracentrifuge at 40,000rpm for 1 hour at 4°C, to isolate the membrane fraction. The resulting pellet containing the membrane fraction was resuspended in one pellet volume of Tris Buffered Saline buffer containing 0.1% SDS. Samples were then run for protein quantification (see Westerns).

FACS Sorting

FACS sorting was performed by The Rockefeller Flow Cytometry Core facility. Tumors were harvested and digested using the Miltenyi tumor dissociation kit. Cell suspension from a tumor was spun down and treated with red cell lysis buffer. Cells were stained with DAPI and resuspended in FACS buffer for sorting. mCherry negative and mCherry positive live cells were separately collected and then processed to isolate RNA or protein.

RNA isolation, cDNA synthesis and qPCR

RNA was isolated from fresh or frozen tissue using Trizol and chloroform extraction. Tissue was homogenized in trizol with a Tissue Lyser (Qiagen) using two metal beads. Samples

were then transferred to a fresh tube and chloroform was added. Samples were chilled at 20°C for 15 minutes and then spun at top speed for 15 minutes at 4°C. The aqueous supernatant was mixed with 70% EtOH and purified using RNAeasy (Qiagen) columns. RNA was eluted in water. cDNA was synthesized using 1-2ug of RNA and the High Capacity cDNA Reverse Transcription Kit (Applied Biosciences). qPCR was performed using a QuantStudio 6 Flex Real-Time PCR System (Thermo Fisher Scientific) and Power Sybr Green mastermix (Life Technologies). TBP was used as a loading control. Relative gene expression differences were determined using the delta CT method.

RNA-Sequencing

RNA was isolated with the RNeasy kit (Qiagen). RNA was pooled from two mice per sample. RNA integrity number (RIN) was measured with an Agilent Bioanalyzer. Samples with RIN over 8.5 was used for library preparation by the Rockefeller Genomics Resource Center. Samples were sequenced using the Illumina HiSeq 2500. Data were generated as fastq files and reads were mapped to the mm10 genome using TopHat. DESeq was then used to make binary comparisons between each of the groups. GSEA KEGG metabolic pathway analysis was performed using the GAGE method (Luo et al. 2009) to compare samples.

Human Sample Handling

Patient samples were collected in surgery at MSKCC and placed in 15ml conical tubes in RNAlater (Thermo Fisher Scientific). Samples were then delivered to Weill Cornell to Dr. Andrew Dannenberg's lab, where the tissue was removed from RNAlater using forceps, spun down at 8,000g for 10 minutes and stored at -80°C in the Dannenberg lab. All samples were then processed

for RNA using Trizol and the RNAeasy kit (Qiagen). cDNA was created using the Quantabio cDNA kit (different from mouse tissue processing) and qPCR was run using Sybr green.

Hypoxic Chamber

Cells were plated and left to sit overnight in regular 5% CO_2, 21% O_2 incubator. The next day samples were transferred into an InvivoO_2 400 (Baker) incubator at 0.5% O_2 in the Birsoy Lab. Samples remained in 0.5% O_2 for 24hours and then were removed and assessed for cell viability, using an *in vitro* cell viability assay, CellTiter Glo (Promega).

In vitro cell viability assay

Viability assays were completed in 96 well plates using 10K E0771 cells / well. Cells were plated and allowed to sit down overnight. Medium was then changed to the desired treatment and left for 24 hours in a 5% CO2 37C incubator. Dialyzed FBS or no FBS at all was used to prevent polyamine or creatine contamination in the culture. Cell viability was then measured using CellTiter Glo (Promega) which measures ATP. Luminescence was read in a plate reader.

Necropsy

Mice were sacrificed at the time points indicated or at humane endpoint (tumor>1.5cm in diameter) as defined by IACUC. Blood was collected by cardiac puncture or decapitation. 4th mammary fat pads were then dissected. Tumors were carefully dissected away from the surrounding adipose tissue. The tumor was weighed and then dissected with one-half for histology (10% formalin) and one-half flash frozen. In addition, 4th mammary fat pads (without the lymph node), and other tissues including visceral white adipose tissue, brown adipose tissue, and kidney

were collected. Blood samples were spun at 2,000g for 15 minutes and serum was collected and stored at -80°C. All tissue samples were flash frozen in liquid nitrogen and stored at -80°C. Following overnight fixation, fixed tissues (10% formalin) were washed with PBS and placed in 70% EtOH.

Slc6a8 Knockdown E0771 cells

A lentivirus plasmid was built using the pLKO.1 TRC cloning vector with a U6 promoter from Addgene. Two plasmids were created, one with an shRNA against Slc6a8 (CTCAAGCCTGACTGGTCAAAG) and another with scrambled control (SCH016 Sigma: GGCGCGATAGCGCTAATAATTT). Lentivirus was produced using 293T cells and used to infect mCherry positive E0771 cells. Puromycin was then used to select shRNA expressing cells. These cells were then tested for Slc6a8 knockdown using qPCR and western.

GFP-Translating ribosome affinity purification (TRAP)

Flash frozen mammary adipose tissue from Rosa26^{fsTRAP} mice crossed to adiponectin cre with E0771 tumors was used. Tissue was minced in 3ml of homogenization buffer (50mM Tris (pH 7.5), 100mM KCl, 12mM MgCl2, 1% NP40, 100ug/ml CHX, 1mg/ml heparin, 2mM DTT, 0.1u/ul RNAsin (Promega), 0.1u/ul Superase (Thermo Fisher Scientific), 1x Roche protease inhibitor. Tissue was dounced with a KONTES dounce tissue grinder (VWR) 20 times with piston A and 20 times with piston B. Samples were then spun at 13k rpm for 10 minutes at 4C. The lipid layer was removed and 3ml of supernatant was transferred to a 5 ml tube. Supernatant was incubated with 4ul (5mg/ml) of ab290 (GFP) for 1 hour at 4C. 5% of the input was saved and frozen at 80°C. 200ul (30mg/ml) of protein G Dynabeads beads (Themo Fisher Scientific) were

prepared by washing twice in low salt buffer (50mM Tris (pH 7.5), 100mM KCl, 12mM MgCl2, 1% NP40, 100ug/ml CHX, 2mM DTT). Antibody containing supernatant was added to dry beads for 30min on a rotator at 4°C. Beads were washed with high salt buffer three times (50mM Tris (pH 7.5), 300mM KCl, 12mM MgCl2, 1% NP40, 100ug/ml CHX, 2mM DTT). RLT buffer (RNAeasy Qiagen) was used to elute RNA from the beads. RNA was isolated using an RNAeasy micro kit (Qiagen) and eluted in 14ul of water. cDNA was synthesized using high capacity the cDNA reverse transcription kit (Applied Biosciences).

Tumor measurements

Tumors were measured twice weekly starting at 6-7 days post tumor injection. Endpoint of tumor>1.5cm was reached at ~21days for E0771, ~28 days for Py8119, ~145 days for MMTV-PyMT and ~45 days for Moc 1. Tumor length and width was measured using digital calipers. The formula length x ($width^2$) was used to generate volume (mm^3). For the MMTV-PyMT model, the largest tumor on each mouse was measured over time.

Immunoblot Assays

Similar to RNA extraction, the Tissue Lyser (Qiagen) was used to homogenize fat and tumor tissue, with RIPA lysis buffer (150mM NaCl, 1% NP40, 0.5% Sodium deoxycholate (DOC), 0.1% SDS, 25mM Tris (pH 7.4)). Samples, containing 30ug of cellular lysate protein, were boiled with laemmli buffer and were resolved on 4-20% BisTris gels (Bio-rad). The samples were then transferred onto a PVDF membrane (Immobilion-P, Millipore) using transfer buffer (Bio-Rad) prepared according to manufacturer's instructions. Transfers were completed on ice for 1hr at 100V. Blots were washed in TBST and blocked using SuperBlock (Thermofisher) for 1hr at room

temperature. After blocking, blots were exposed to primary antibody (refer to Antibody list below) overnight at 4°C. The following day, membranes were washed 3 times with TBS-Tween 20 (0.1%) for 5 minutes each and exposed to secondary HRP-tagged antibodies (Jackson ImmunoResearch) for 1hr at room temperature. The blot was developed using Western Lightning Plus-ECL (PerkinElmer) and imaged in a Bio-rad Gel Doc System. Quantification was done using the Bio-rad Image Lab Software.

Antibody List

Antigen	Company	Product Number	Dilution
GFP	Abcam	ab290	6.6ug/ml
Odc1	Thermofisher	PA1-36025	1-400
Flag	Sigma	f3165	1-1000
Actin	Gene tex	109639	1-10000
Hif1a	Cell Signaling	36169T	1-1000
Slc6a8	Thermofisher	PA5-37060	1-1000
NaK ATPase	Cell Signaling	3010S	1-1000

Genotyping Primers

Mouse Line	Primer
Odc1_lox1_F	AATGCTAGTACTGCATGAAAGTTCC
Odc1_lox1_R	AAGTAGCCAGTACAGGAAGAACTG
Odc1_lox2_F	CTGAGGAGCCCAGAGAGGACATC
Odc1_lox2_R	GAAGCACCCATACAAGCATACAC
Gatm C_F	GAGCCATGCGTGATAAGACAT
Gatm Wt_R	AGCTAGCCCATCTTCGCATAG
Gatm Mut_R	CAACGGGTTCTTCTGTTAGTCC
ROSA Trap Mut_R	CGGGCCATTTACCGTAAGTTAT
ROSA TRAP WT_R	CCGAAAATCTGTGGGAAGTC
ROSA TRAP C_F	AAGGGAGCTGCAGTGGAGTA
AP2-PRDM16_F	TGTCTCCTCCACAATGAGGCA
AP2-PRDM16_R	TTCGGTCTCCTCCTCGGCACT
PRDM16 LOX/LOX_F	GAGCTAGGCAAGGACACTGCT
PRDM16 LOX/LOX_R	CCAGTATCAGAGAGGCAAGAA
UCRE_F	ACCTGAAGATGTTCGCGATTATCT
UCRE_R	ACCGTCAGTACGTGAGATATCTT
MMTV-Pymt_F	GGAAGCAAGTACTTCACAAGGG
MMTV-Pymt_R	GGAAAGTCACTAGGAGCAGGG

Genotyping Protocols

Gatm

	Degrees	Time	
1	95	5 min	
2	94	30 sec	39 cycles
3	65	45 sec	
4	72	45 sec	
5	72	10 min	
6	4	hold	

ROSA TRAP

	Degrees	Time	
1	95	3 min	
2	95	5 sec	40 cycles
3	60	30 sec	
4	4	pause	

Odc1 lox1

	Degrees	Time	
1	94	2 min	
2	94	30 sec	30 cycles
3	55	45 sec	
4	72	1 min	
5	4	hold	

Odc1 lox2

	Degrees	Time	
1	94	2 min	
2	94	30 sec	30 cycles
3	60	45 sec	
4	72	1 min	
5	4	hold	

MMTV-Pymt

	Degrees	Time	
1	94	2 min	
2	94	20 sec	-0.5C per cycle decrease repeat setps 2-4 10x
3	65	15 sec	
4	68	10 sec	
5	94	15 sec	repeat steps 5-7 28x
6	60	15 sec	
7	72	10 sec	
8	72	2 min	
9	4	pause	

AP2-PRDM16 Tg, PRDM16 lox/lox, Ucre

	Degrees	Time	
1	95	5 min	
2	95	45 sec	34 cycles
3	56	45 sec	
4	72	1 min	
5	72	5 min	
6	4	hold	

qPCR Primers

Species	Gene	Forward	Reverse
Mouse	Odc1	GACGAGTTTGACTGCCACATC	CGCAACATAGAACGCATCCTT
Mouse	Slc6a8	GTGTGGAGATCTTCCGCCAT	CCCGTGGAGAGCCTCAATAC
Mouse	Gatm	GCTTCCTCCCGAAATTCCTGT	CCTCTAAAGGGTCCCATTCGT
Mouse	Adiponectin	GCACTGGCAAGTTCTACTGCAA	GTAGGTGAAGAGAACGGCCTTGT
Mouse	aP2	ACACCGAGATTTCCTTCAAACTG	CCATCTAGGGGTTATGATGCTCTTCA
Mouse	Cidea	TGCTCTTCTGTATCGCCCAGT	GCCGTGTTAAGGAATCTGCTG
Mouse	Cox8b	GAACCATGAAGCCAACGACT	GCGAAGTTCACAGTGGTTCC
Mouse	Elovl3	TCCGCGTTCTCATGTAGGTCT	GGACCTGATGCAACCCTATGA
Mouse	Ucp1	ACTGCCACACCTCCAGTCATT	CTTTGCCTCACTCAGGATTGG
Mouse	Saa3	GAAAGAAGCTGGTCAAGGGTC	TCCGGGCAGCATCATAGTTC
Mouse	Tnfa	CCACCACGCTCTTCTGTCTA	AGGGTCTGGGCCATAGAACT
Mouse	Prdm16	CAGCACGGTGAAGCCATTC	GCGTGCATCCGCTTGTG
Mouse	Ppary	GTGCCAGTTTCGATCCGTAGA	GGCCAGCATCGTGTAGATGA
Mouse	TBP	GGGTATCTGCTGGCGGTTT	TGAAATAGTGATGCTGGGCACT
Human	Odc1_H	GCCATCGTGAAGACCCTTG	GGCAATCCGCAAAACCAACTT
Human	Gatm_H	ACGAATGGGACCCCTTAGAGG	CCTTACTGTCACTCCTTCCGTT
Human	TBP_H	CCCGAAACGCCGAATATAATCC	AATCAGTGCCGTGGTTCGTG

Statistics

Graphs display mean values with standard error of the mean (SEM) except for human data in Chapter 5: Figure 5.2 which displayed median, interquartile range, 5th-95th percentile and outliers. Data from tumor progression studies were log transformed and analyzed using a mixed-effects model with repeated measurements. Post hoc testing was used to determine significance between specific groups and at specific time points. The same method was used to analyze mouse body weights. For the Gatm study, mouse weight was also entered into the model to determine if mouse weight contributed to tumor volume. Final tumor weight and qPCR data was analyzed via two-way ANOVA (two-factors four groups), one-way ANOVA (one-factor three or more groups), or t-test (one-factor two groups). * $p< 0.05$, ** $p<0.01$, *** $p<0.001$, **** $p<0.0001$. Statistical analyses were performed in collaboration with the Rockefeller hospital biostatistics group.

REFERENCES

Ackerman, Sarah E., Olivia A. Blackburn, François Marchildon, and Paul Cohen. 2017. "Insights into the Link Between Obesity and Cancer." *Current Obesity Reports* 6 (2): 195–203. https://doi.org/10.1007/s13679-017-0263-x.

Alcalá, Martín, María Calderon-Dominguez, Dolors Serra, Laura Herrero, and Marta Viana. 2019. "Mechanisms of Impaired Brown Adipose Tissue Recruitment in Obesity." *Frontiers in Physiology* 10. https://doi.org/10.3389/fphys.2019.00094.

An, Wei, Yu Bai, Shang-Xin Deng, Jie Gao, Qi-Wen Ben, Quan-Cai Cai, Hua-Gao Zhang, and Zhao-Shen Li. 2012. "Adiponectin Levels in Patients with Colorectal Cancer and Adenoma: A Meta-Analysis." *European Journal of Cancer Prevention: The Official Journal of the European Cancer Prevention Organisation (ECP)* 21 (2): 126–33. https://doi.org/10.1097/CEJ.0b013e32834c9b55.

Arnold, Melina, Nirmala Pandeya, Graham Byrnes, Prof Andrew G. Renehan, Gretchen A. Stevens, Prof Majid Ezzati, Jacques Ferlay, et al. 2015. "Global Burden of Cancer Attributable to High Body-Mass Index in 2012: A Population-Based Study." *The Lancet. Oncology* 16 (1): 36–46. https://doi.org/10.1016/S1470-2045(14)71123-4.

Barone, Bethany B., Hsin-Chieh Yeh, Claire F. Snyder, Kimberly S. Peairs, Kelly B. Stein, Rachel L. Derr, Antonio C. Wolff, and Frederick L. Brancati. 2008. "Long-Term All-Cause Mortality in Cancer Patients with Preexisting Diabetes Mellitus: A Systematic Review and Meta-Analysis." *JAMA* 300 (23): 2754–64. https://doi.org/10.1001/jama.2008.824.

Bassiri, Hamid, Adriana Benavides, Michelle Haber, Susan K. Gilmour, Murray D. Norris, and Michael D. Hogarty. 2015. "Translational Development of Difluoromethylornithine (DFMO) for the Treatment of Neuroblastoma." *Translational Pediatrics* 4 (3): 226–38. https://doi.org/10.3978/j.issn.2224-4336.2015.04.06.

Berg, A. H., T. P. Combs, X. Du, M. Brownlee, and P. E. Scherer. 2001. "The Adipocyte-Secreted Protein Acrp30 Enhances Hepatic Insulin Action." *Nature Medicine* 7 (8): 947–53. https://doi.org/10.1038/90992.

Bhaskaran, Krishnan, Ian Douglas, Harriet Forbes, Isabel dos-Santos-Silva, David A Leon, and Liam Smeeth. 2014. "Body-Mass Index and Risk of 22 Specific Cancers: A Population-Based Cohort Study of 5·24 Million UK Adults." *Lancet* 384 (9945): 755–65. https://doi.org/10.1016/S0140-6736(14)60892-8.

Biswas, Tanuka, Xiang Gu, Junhua Yang, Lesley G. Ellies, and Lu-Zhe Sun. 2014. "Attenuation of TGF-β Signaling Supports Tumor Progression of a Mesenchymal-like Mammary Tumor Cell Line in a Syngeneic Murine Model." *Cancer Letters* 346 (1): 129–38. https://doi.org/10.1016/j.canlet.2013.12.018.

Boden, Guenther. 2008. “Obesity and Free Fatty Acids (FFA).” *Endocrinology and Metabolism Clinics of North America* 37 (3): 635–ix. https://doi.org/10.1016/j.ecl.2008.06.007.

Bol, D K, K Kiguchi, I Gimenez-Conti, T Rupp, and J DiGiovanni. 1997. “Overexpression of Insulin-like Growth Factor-1 Induces Hyperplasia, Dermal Abnormalities, and Spontaneous Tumor Formation in Transgenic Mice.” *Oncogene* 14 (14): 1725–34. https://doi.org/10.1038/sj.onc.1201011.

Bråkenhielm, Ebba, Niina Veitonmäki, Renhai Cao, Shinji Kihara, Yuji Matsuzawa, Boris Zhivotovsky, Tohru Funahashi, and Yihai Cao. 2004. “Adiponectin-Induced Antiangiogenesis and Antitumor Activity Involve Caspase-Mediated Endothelial Cell Apoptosis.” *Proceedings of the National Academy of Sciences of the United States of America* 101 (8): 2476–81. https://doi.org/10.1073/pnas.0308671100.

“Breast Cancer Statistics | CDC.” 2019. July 29, 2019. https://www.cdc.gov/cancer/breast/statistics/index.htm.

Bredel, Markus, Denise M. Scholtens, Ajay K. Yadav, Angel A. Alvarez, Jaclyn J. Renfrow, James P. Chandler, Irene L. Y. Yu, et al. 2011. “NFKBIA Deletion in Glioblastomas.” *The New England Journal of Medicine* 364 (7): 627–37. https://doi.org/10.1056/NEJMoa1006312.

Bu, Dawei, Clair Crewe, Christine M. Kusminski, Ruth Gordillo, Alexandra L. Ghaben, Min Kim, Jiyoung Park, et al. 2019. “Human Endotrophin as a Driver of Malignant Tumor Growth.” *JCI Insight* 5 (March). https://doi.org/10.1172/jci.insight.125094.

Burkitt, Michael D., Abdalla F. Hanedi, Carrie A. Duckworth, Jonathan M. Williams, Joseph M. Tang, Lorraine A. O’Reilly, Tracy L. Putoczki, et al. 2015. “NF-KB1, NF-KB2 and c-Rel Differentially Regulate Susceptibility to Colitis-Associated Adenoma Development in C57BL/6 Mice.” *The Journal of Pathology* 236 (3): 326–36. https://doi.org/10.1002/path.4527.

Calle, Eugenia E., Carmen Rodriguez, Kimberly Walker-Thurmond, and Michael J. Thun. 2003. “Overweight, Obesity, and Mortality from Cancer in a Prospectively Studied Cohort of U.S. Adults.” *New England Journal of Medicine* 348 (17): 1625–38. https://doi.org/10.1056/NEJMoa021423.

Cao, Yihai. 2018. “Obesity Protects Cancer from Drugs Targeting Blood Vessels.” *Cell Metabolism* 27 (6): 1163–65. https://doi.org/10.1016/j.cmet.2018.05.014.

Chang, Chao-Ching, Meng-Ju Wu, Jer-Yen Yang, Ignacio G. Camarillo, and Chun-Ju Chang. 2015. “Leptin-STAT3-G9a Signaling Promotes Obesity-Mediated Breast Cancer Progression.” *Cancer Research* 75 (11): 2375–86. https://doi.org/10.1158/0008-5472.CAN-14-3076.

Chen, Chun-Te, Yi Du, Hirohito Yamaguchi, Jung-Mao Hsu, Hsu-Ping Kuo, Gabriel N. Hortobagyi, and Mien-Chie Hung. 2012. "Targeting the IKKβ/MTOR/VEGF Signaling Pathway as a Potential Therapeutic Strategy for Obesity-Related Breast Cancer." *Molecular Cancer Therapeutics* 11 (10): 2212–21. https://doi.org/10.1158/1535-7163.MCT-12-0180.

Cleary, Margot P., and Michael E. Grossmann. 2009. "Obesity and Breast Cancer: The Estrogen Connection." *Endocrinology* 150 (6): 2537–42. https://doi.org/10.1210/en.2009-0070.

Coelho, Marisa, Teresa Oliveira, and Ruben Fernandes. 2013. "Biochemistry of Adipose Tissue: An Endocrine Organ." *Archives of Medical Science : AMS* 9 (2): 191–200. https://doi.org/10.5114/aoms.2013.33181.

Cohen, Paul, Julia D. Levy, Yingying Zhang, Andrea Frontini, Dmitriy P. Kolodin, Katrin J. Svensson, James C. Lo, et al. 2014. "Ablation of PRDM16 and Beige Adipose Causes Metabolic Dysfunction and a Subcutaneous to Visceral Fat Switch." *Cell* 156 (1–2): 304–16. https://doi.org/10.1016/j.cell.2013.12.021.

Cohen, Paul, and Bruce M. Spiegelman. 2015. "Brown and Beige Fat: Molecular Parts of a Thermogenic Machine." *Diabetes* 64 (7): 2346–51. https://doi.org/10.2337/db15-0318.

Couto, Joana Pinto, Laura Daly, Ana Almeida, Jeffrey A. Knauf, James A. Fagin, Manuel Sobrinho-Simões, Jorge Lima, et al. 2012. "STAT3 Negatively Regulates Thyroid Tumorigenesis." *Proceedings of the National Academy of Sciences of the United States of America* 109 (35): E2361-2370. https://doi.org/10.1073/pnas.1201232109.

Cowen, Sarah, Sarah L. McLaughlin, Gerald Hobbs, James Coad, Karen H. Martin, I. Mark Olfert, and Linda Vona-Davis. 2015. "High-Fat, High-Calorie Diet Enhances Mammary Carcinogenesis and Local Inflammation in MMTV-PyMT Mouse Model of Breast Cancer." *Cancers* 7 (3): 1125–42. https://doi.org/10.3390/cancers7030828.

Cui, F. Z., W. M. Tian, S. P. Hou, Q. Y. Xu, and I.-S. Lee. 2006. "Hyaluronic Acid Hydrogel Immobilized with RGD Peptides for Brain Tissue Engineering." *Journal of Materials Science. Materials in Medicine* 17 (12): 1393–1401. https://doi.org/10.1007/s10856-006-0615-7.

De Palma, Michele, and Claire E. Lewis. 2013. "Macrophage Regulation of Tumor Responses to Anticancer Therapies." *Cancer Cell* 23 (3): 277–86. https://doi.org/10.1016/j.ccr.2013.02.013.

Engin, Atilla. 2017. "Adipose Tissue Hypoxia in Obesity and Its Impact on Preadipocytes and Macrophages: Hypoxia Hypothesis." *Advances in Experimental Medicine and Biology* 960: 305–26. https://doi.org/10.1007/978-3-319-48382-5_13.

Fantozzi, Anna, and Gerhard Christofori. 2006. "Mouse Models of Breast Cancer Metastasis." *Breast Cancer Research* 8 (4): 212. https://doi.org/10.1186/bcr1530.

Fenouille, Nina, Christopher F. Bassil, Issam Ben-Sahra, Lina Benajiba, Gabriela Alexe, Azucena Ramos, Yana Pikman, et al. 2017. "The Creatine Kinase Pathway Is a Metabolic Vulnerability in EVI1-Positive Acute Myeloid Leukemia." *Nature Medicine* 23 (3): 301–13. https://doi.org/10.1038/nm.4283.

Ferguson, Rosalyn D, Ruslan Novosyadlyy, Yvonne Fierz, Nyosha Alikhani, Hui Sun, Shoshana Yakar, and Derek Leroith. 2012. "Hyperinsulinemia Enhances C-Myc-Mediated Mammary Tumor Development and Advances Metastatic Progression to the Lung in a Mouse Model of Type 2 Diabetes." *Breast Cancer Research : BCR* 14 (1): R8. https://doi.org/10.1186/bcr3089.

Finkelstein, Eric A., Justin G. Trogdon, Joel W. Cohen, and William Dietz. 2009. "Annual Medical Spending Attributable to Obesity: Payer-and Service-Specific Estimates." *Health Affairs (Project Hope)* 28 (5): w822-831. https://doi.org/10.1377/hlthaff.28.5.w822.

Finucane, Mariel M., Gretchen A. Stevens, Melanie J. Cowan, Goodarz Danaei, John K. Lin, Christopher J. Paciorek, Gitanjali M. Singh, et al. 2011. "National, Regional, and Global Trends in Body-Mass Index since 1980: Systematic Analysis of Health Examination Surveys and Epidemiological Studies with 960 Country-Years and 9·1 Million Participants." *Lancet (London, England)* 377 (9765): 557–67. https://doi.org/10.1016/S0140-6736(10)62037-5.

Gamat, Melissa, Rita L. Malinowski, Linnea J. Parkhurst, Laura M. Steinke, and Paul C. Marker. 2015. "Ornithine Decarboxylase Activity Is Required for Prostatic Budding in the Developing Mouse Prostate." *PLOS ONE* 10 (10): e0139522. https://doi.org/10.1371/journal.pone.0139522.

Gati, Asma, Soumaya Kouidhi, Raja Marrakchi, Amel El Gaaied, Nadia Kourda, Amine Derouiche, Mohamed Chebil, Anne Caignard, and Aurélie Perier. 2014. "Obesity and Renal Cancer." *Oncoimmunology* 3 (January). https://doi.org/10.4161/onci.27810.

Gibby, Krissa, Weon-Kyoo You, Kuniko Kadoya, Hildur Helgadottir, Lawrence Jt Young, Lesley G. Ellies, Yunchao Chang, Robert D. Cardiff, and William B. Stallcup. 2012. "Early Vascular Deficits Are Correlated with Delayed Mammary Tumorigenesis in the MMTV-PyMT Transgenic Mouse Following Genetic Ablation of the NG2 Proteoglycan." *Breast Cancer Research: BCR* 14 (2): R67. https://doi.org/10.1186/bcr3174.

Global BMI Mortality Collaboration, null, Emanuele Di Angelantonio, Shilpa Bhupathiraju, David Wormser, Pei Gao, Stephen Kaptoge, Amy Berrington de Gonzalez, et al. 2016. "Body-Mass Index and All-Cause Mortality: Individual-Participant-Data Meta-Analysis of 239 Prospective Studies in Four Continents." *Lancet (London, England)* 388 (10046): 776–86. https://doi.org/10.1016/S0140-6736(16)30175-1.

Goossens, Gijs H. 2017. “The Metabolic Phenotype in Obesity: Fat Mass, Body Fat Distribution, and Adipose Tissue Function.” *Obesity Facts* 10 (3): 207–15. https://doi.org/10.1159/000471488.

Grote, Verena A., Sabine Rohrmann, Laure Dossus, Alexandra Nieters, Jytte Halkj??r, Anne Tj??nneland, Kim Overvad, et al. 2012. “The Association of Circulating Adiponectin Levels with Pancreatic Cancer Risk: A Study within the Prospective EPIC Cohort.” *International Journal of Cancer* 130 (10): 2428–2437. https://doi.org/10.1002/ijc.26244.

Gu, Jian-Wei, Emily Young, Sharla G. Patterson, Kristina L. Makey, Jeremy Wells, Min Huang, Kevan B. Tucker, and Lucio Miele. 2011. “Postmenopausal Obesity Promotes Tumor Angiogenesis and Breast Cancer Progression in Mice.” *Cancer Biology & Therapy* 11 (10): 910–17.

Gunter, Marc J., Donald R. Hoover, Herbert Yu, Sylvia Wassertheil-Smoller, Thomas E. Rohan, JoAnn E. Manson, Jixin Li, et al. 2009. “Insulin, Insulin-like Growth Factor-I, and Risk of Breast Cancer in Postmenopausal Women.” *Journal of the National Cancer Institute* 101 (1): 48–60. https://doi.org/10.1093/jnci/djn415.

Guy, C T, R D Cardiff, and W J Muller. 1992. “Induction of Mammary Tumors by Expression of Polyomavirus Middle T Oncogene: A Transgenic Mouse Model for Metastatic Disease.” *Molecular and Cellular Biology* 12 (3): 954–61.

Hales, Craig M., Margaret D. Carroll, Cheryl D. Fryar, and Cynthia L. Ogden. 2017. “Prevalence of Obesity Among Adults and Youth: United States, 2015-2016.” *NCHS Data Brief*, no. 288: 1–8.

Harms, Matthew, and Patrick Seale. 2013. “Brown and Beige Fat: Development, Function and Therapeutic Potential.” *Nature Medicine* 19 (10): 1252–63. https://doi.org/10.1038/nm.3361.

Harris, Holly R., Shelley S. Tworoger, Susan E. Hankinson, Bernard A. Rosner, and Karin B. Michels. 2011. “Plasma Leptin Levels and Risk of Breast Cancer in Premenopausal Women.” *Cancer Prevention Research* 4 (9): 1449–56. https://doi.org/10.1158/1940-6207.CAPR-11-0125.

Hosogai, Naomi, Atsunori Fukuhara, Kazuya Oshima, Yugo Miyata, Sachiyo Tanaka, Katsumori Segawa, Shigetada Furukawa, et al. 2007. “Adipose Tissue Hypoxia in Obesity and Its Impact on Adipocytokine Dysregulation.” *Diabetes* 56 (4): 901–11. https://doi.org/10.2337/db06-0911.

Hursting, Stephen D., John Digiovanni, Andrew J. Dannenberg, Maria Azrad, Derek Leroith, Wendy Demark-Wahnefried, Madhuri Kakarala, Angela Brodie, and Nathan A. Berger. 2012. “Obesity, Energy Balance, and Cancer: New Opportunities for Prevention.” *Cancer Prevention Research (Philadelphia, Pa.)* 5 (11): 1260–72. https://doi.org/10.1158/1940-6207.CAPR-12-0140.

Incio, Joao, Jennifer A. Ligibel, Daniel T. McManus, Priya Suboj, Keehoon Jung, Kosuke Kawaguchi, Matthias Pinter, et al. 2018. "Obesity Promotes Resistance to Anti-VEGF Therapy in Breast Cancer by up-Regulating IL-6 and Potentially FGF-2." *Science Translational Medicine* 10 (432): eaag0945. https://doi.org/10.1126/scitranslmed.aag0945.

Iyengar, Neil M., Rhonda Arthur, JoAnn E. Manson, Rowan T. Chlebowski, Candyce H. Kroenke, Lindsay Peterson, Ting-Yuan D. Cheng, et al. 2018. "Association of Body Fat and Risk of Breast Cancer in Postmenopausal Women With Normal Body Mass Index: A Secondary Analysis of a Randomized Clinical Trial and Observational Study." *JAMA Oncology*, December. https://doi.org/10.1001/jamaoncol.2018.5327.

Iyengar, Neil M., Ronald A. Ghossein, Luc G. Morris, Xi K. Zhou, Amit Kochhar, Patrick G. Morris, David G. Pfister, et al. 2016. "White Adipose Tissue Inflammation and Cancer-Specific Survival in Patients with Squamous Cell Carcinoma of the Oral Tongue." *Cancer* 122 (24): 3794–3802. https://doi.org/10.1002/cncr.30251.

Iyengar, Neil M., Ayca Gucalp, Andrew J. Dannenberg, and Clifford A. Hudis. 2016. "Obesity and Cancer Mechanisms: Tumor Microenvironment and Inflammation." *Journal of Clinical Oncology: Official Journal of the American Society of Clinical Oncology* 34 (35): 4270–76.

Iyengar, Neil M., Xi Kathy Zhou, Ayca Gucalp, Patrick G. Morris, Louise R. Howe, Dilip D. Giri, Monica Morrow, et al. 2016. "Systemic Correlates of White Adipose Tissue Inflammation in Early-Stage Breast Cancer." *Clinical Cancer Research: An Official Journal of the American Association for Cancer Research* 22 (9): 2283–89. https://doi.org/10.1158/1078-0432.CCR-15-2239.

Johnstone, Cameron N., Yvonne E. Smith, Yuan Cao, Allan D. Burrows, Ryan S. N. Cross, Xiawei Ling, Richard P. Redvers, et al. 2015. "Functional and Molecular Characterisation of EO771.LMB Tumours, a New C57BL/6-Mouse-Derived Model of Spontaneously Metastatic Mammary Cancer." *Disease Models & Mechanisms* 8 (3): 237–51. https://doi.org/10.1242/dmm.017830.

Judd, Nancy P., Ashley E. Winkler, Oihana Murillo-Sauca, Joshua J. Brotman, Jonathan H. Law, James S. Lewis, Gavin P. Dunn, Jack D. Bui, John B. Sunwoo, and Ravindra Uppaluri. 2012. "ERK1/2 Regulation of CD44 Modulates Oral Cancer Aggressiveness." *Cancer Research* 72 (1): 365–74. https://doi.org/10.1158/0008-5472.CAN-11-1831.

Kadowaki, Takashi, Toshimasa Yamauchi, Naoto Kubota, Kazuo Hara, Kohjiro Ueki, and Kazuyuki Tobe. 2006. "Review Series Adiponectin and Adiponectin Receptors in Insulin Resistance , Diabetes , and the Metabolic Syndrome." *The Journal of Clinical Investigation* 116 (7): 1784–1792. https://doi.org/10.1172/JCI29126.1784.

Kajimura, Shingo, Bruce M. Spiegelman, and Patrick Seale. 2015. “Brown and Beige Fat: Physiological Roles beyond Heat Generation.” *Cell Metabolism* 22 (4): 546–59. https://doi.org/10.1016/j.cmet.2015.09.007.

Kazak, Lawrence, Edward T. Chouchani, Mark P. Jedrychowski, Brian K. Erickson, Kosaku Shinoda, Paul Cohen, Ramalingam Vetrivelan, et al. 2015. “A Creatine-Driven Substrate Cycle Enhances Energy Expenditure and Thermogenesis in Beige Fat.” *Cell* 163 (3): 643–55. https://doi.org/10.1016/j.cell.2015.09.035.

Kazak, Lawrence, Janane F. Rahbani, Bozena Samborska, Gina Z. Lu, Mark P. Jedrychowski, Mathieu Lajoie, Song Zhang, et al. 2019. “Ablation of Adipocyte Creatine Transport Impairs Thermogenesis and Causes Diet-Induced Obesity.” *Nature Metabolism* 1 (3): 360–70. https://doi.org/10.1038/s42255-019-0035-x.

Kern, Lara, Melanie J. Mittenbühler, Anna Juliane Vesting, Anna Lena Ostermann, Claudia Maria Wunderlich, and F. Thomas Wunderlich. 2018. “Obesity-Induced TNFα and IL-6 Signaling: The Missing Link between Obesity and Inflammation—Driven Liver and Colorectal Cancers.” *Cancers* 11 (1). https://doi.org/10.3390/cancers11010024.

Khandekar, Melin J., Paul Cohen, and Bruce M. Spiegelman. 2011. “Molecular Mechanisms of Cancer Development in Obesity.” *Nature Reviews. Cancer* 11 (12): 886–95. https://doi.org/10.1038/nrc3174.

Kim, Hong Im, Chad R. Schultz, Andrea L. Buras, Elizabeth Friedman, Alyssa Fedorko, Leigh Seamon, Gadisetti V. R. Chandramouli, G. Larry Maxwell, André S. Bachmann, and John I. Risinger. 2017. “Ornithine Decarboxylase as a Therapeutic Target for Endometrial Cancer.” *PLOS ONE* 12 (12): e0189044. https://doi.org/10.1371/journal.pone.0189044.

Kolb, Ryan, Liem Phan, Nicholas Borcherding, Yinghong Liu, Fang Yuan, Ann M. Janowski, Qing Xie, et al. 2016. “Obesity-Associated NLRC4 Inflammasome Activation Drives Breast Cancer Progression.” *Nature Communications* 7 (October): 13007. https://doi.org/10.1038/ncomms13007.

Kurmi, Kiran, Sadae Hitosugi, Jia Yu, Felix Boakye-Agyeman, Elizabeth K. Wiese, Thomas R. Larson, Qing Dai, et al. 2018. “Tyrosine Phosphorylation of Mitochondrial Creatine Kinase 1 Enhances a Druggable Tumor Energy Shuttle Pathway.” *Cell Metabolism* 28 (6): 833-847.e8. https://doi.org/10.1016/j.cmet.2018.08.008.

Ladoire, Sylvain, Franck Bonnetain, Mélanie Gauthier, Sylvie Zanetta, Jean Michel Petit, Séverine Guiu, Isabelle Kermarrec, et al. 2011. “Visceral Fat Area as a New Independent Predictive Factor of Survival in Patients with Metastatic Renal Cell Carcinoma Treated with Antiangiogenic Agents.” *The Oncologist* 16 (1): 71–81. https://doi.org/10.1634/theoncologist.2010-0227.

Lazar, Ikame, Emily Clement, Stéphanie Dauvillier, Delphine Milhas, Manuelle Ducoux-Petit, Sophie Le Gonidec, Cédric Moro, et al. 2016. "Adipocyte Exosomes Promote Melanoma Aggressiveness through Fatty Acid Oxidation: A Novel Mechanism Linking Obesity and Cancer." *Cancer Research*, May, canres.0651.2016. https://doi.org/10.1158/0008-5472.CAN-16-0651.

Lee, Yun Sok, Jung-whan Kim, Olivia Osborne, Da Young Oh, Roman Sasik, Simon Schenk, Ai Chen, et al. 2014. "Increased Adipocyte O2 Consumption Triggers HIF-1α, Causing Inflammation and Insulin Resistance in Obesity." *Cell* 157 (6): 1339–52. https://doi.org/10.1016/j.cell.2014.05.012.

Loo, Jia Min, Alexis Scherl, Alexander Nguyen, Fung Ying Man, Ethan Weinberg, Zhaoshi Zeng, Leonard Saltz, Philip B. Paty, and Sohail F. Tavazoie. 2015. "Extracellular Metabolic Energetics Can Promote Cancer Progression." *Cell* 160 (3): 393–406. https://doi.org/10.1016/j.cell.2014.12.018.

Lopez, Theresa, and Douglas Hanahan. 2002. "Elevated Levels of IGF-1 Receptor Convey Invasive and Metastatic Capability in a Mouse Model of Pancreatic Islet Tumorigenesis." *Cancer Cell* 1 (4): 339–353. https://doi.org/10.1016/S1535-6108(02)00055-7.

Luo, Weijun, Michael S. Friedman, Kerby Shedden, Kurt D. Hankenson, and Peter J. Woolf. 2009. "GAGE: Generally Applicable Gene Set Enrichment for Pathway Analysis." *BMC Bioinformatics* 10 (1): 161. https://doi.org/10.1186/1471-2105-10-161.

Ma, Jing, Haojie Li, Ed Giovannucci, Lorelei Mucci, Weiliang Qiu, Paul L. Nguyen, J. Michael Gaziano, Michael Pollak, and Meir J. Stampfer. 2008. "Prediagnostic Body-Mass Index, Plasma C-Peptide Concentration, and Prostate Cancer-Specific Mortality in Men with Prostate Cancer: A Long-Term Survival Analysis." *The Lancet. Oncology* 9 (11): 1039–47. https://doi.org/10.1016/S1470-2045(08)70235-3.

Maffei, M., J. Halaas, E. Ravussin, R. E. Pratley, G. H. Lee, Y. Zhang, H. Fei, et al. 1995. "Leptin Levels in Human and Rodent: Measurement of Plasma Leptin and Ob RNA in Obese and Weight-Reduced Subjects." *Nature Medicine* 1 (11): 1155–61. https://doi.org/10.1038/nm1195-1155.

Martyn, J. A. Jeevendra, Masao Kaneki, and Shingo Yasuhara. 2008. "Obesity-Induced Insulin Resistance and Hyperglycemia: Etiologic Factors and Molecular Mechanisms." *Anesthesiology* 109 (1): 137–48. https://doi.org/10.1097/ALN.0b013e3181799d45.

McCampbell, Adrienne S., Russell R. Broaddus, David S. Loose, and Peter J. A. Davies. 2006. "Overexpression of the Insulin-like Growth Factor I Receptor and Activation of the AKT Pathway in Hyperplastic Endometrium." *Clinical Cancer Research: An Official Journal of the American Association for Cancer Research* 12 (21): 6373–78. https://doi.org/10.1158/1078-0432.CCR-06-0912.

Miyoshi, Yasuo, Tohru Funahashi, Sachiyo Tanaka, Tetsuya Taguchi, Yasuhiro Tamaki, Iichiro Shimomura, and Shinzaburo Noguchi. 2006. “High Expression of Leptin Receptor MRNA in Breast Cancer Tissue Predicts Poor Prognosis for Patients with High, but Not Low, Serum Leptin Levels.” *International Journal of Cancer* 118 (6): 1414–1419. https://doi.org/10.1002/ijc.21543.

Morris, Patrick G., Clifford A. Hudis, Dilip Giri, Monica Morrow, Domenick J. Falcone, Xi Kathy Zhou, Baoheng Du, et al. 2011. “Inflammation and Increased Aromatase Expression Occur in the Breast Tissue of Obese Women with Breast Cancer.” *Cancer Prevention Research (Philadelphia, Pa.)* 4 (7): 1021–29. https://doi.org/10.1158/1940-6207.CAPR-11-0110.

Ohno, Haruya, Kosaku Shinoda, Bruce M. Spiegelman, and Shingo Kajimura. 2012. “PPAR Agonists Induce a White-to-Brown Fat Conversion through Stabilization of PRDM16 Protein.” *Cell Metabolism* 15 (3): 395–404. https://doi.org/10.1016/j.cmet.2012.01.019.

Ollberding, Nicholas J., Yeonju Kim, Yurii B. Shvetsov, Lynne R. Wilkens, Adrian A. Franke, Robert V. Cooney, Gertraud Maskarinec, et al. 2013. “Prediagnostic Leptin, Adiponectin, C-Reactive Protein, and the Risk of Postmenopausal Breast Cancer.” *Cancer Prevention Research (Philadelphia, Pa.)* 6 (3): 188–95. https://doi.org/10.1158/1940-6207.CAPR-12-0374.

Osborn, Olivia, and Jerrold M. Olefsky. 2012. “The Cellular and Signaling Networks Linking the Immune System and Metabolism in Disease.” *Nature Medicine* 18 (3): 363–74. https://doi.org/10.1038/nm.2627.

Papa, V, V Pezzino, A Costantino, A Belfiore, D Giuffrida, L Frittitta, G B Vannelli, R Brand, I D Goldfine, and R Vigneri. 1990. “Elevated Insulin Receptor Content in Human Breast Cancer.” *Journal of Clinical Investigation* 86 (5): 1503–10.

Parida, Sheetal, Sumit Siddharth, and Dipali Sharma. 2019. “Adiponectin, Obesity, and Cancer: Clash of the Bigwigs in Health and Disease.” *International Journal of Molecular Sciences* 20 (10). https://doi.org/10.3390/ijms20102519.

Park, Eek Joong, Jun Hee Lee, Guann-Yi Yu, Guobin He, Syed Raza Ali, Ryan G. Holzer, Christoph H. Österreicher, Hiroyuki Takahashi, and Michael Karin. 2010. “Dietary and Genetic Obesity Promote Liver Inflammation and Tumorigenesis by Enhancing IL-6 and TNF Expression.” *Cell* 140 (2): 197–208. https://doi.org/10.1016/j.cell.2009.12.052.

Park, Jiyoung, Christine M. Kusminski, Streamson C. Chua, and Philipp E. Scherer. 2010. “Leptin Receptor Signaling Supports Cancer Cell Metabolism through Suppression of Mitochondrial Respiration in Vivo.” *The American Journal of Pathology* 177 (6): 3133–3144. https://doi.org/10.2353/ajpath.2010.100595.

Park, Jiyoung, and Philipp E. Scherer. 2013. “Endotrophin in the Tumor Stroma: A New Therapeutic Target for Breast Cancer?” *Expert Review of Anticancer Therapy* 13 (2): 111–13. https://doi.org/10.1586/era.12.164.

Park, Myung Hee, and Edith C. Wolff. 2018. “Hypusine, a Polyamine-Derived Amino Acid Critical for Eukaryotic Translation.” *Journal of Biological Chemistry*, September, jbc.TM118.003341. https://doi.org/10.1074/jbc.TM118.003341.

Pierce, Brandon L., Rachel Ballard-Barbash, Leslie Bernstein, Richard N. Baumgartner, Marian L. Neuhouser, Mark H. Wener, Kathy B. Baumgartner, et al. 2009. “Elevated Biomarkers of Inflammation Are Associated with Reduced Survival among Breast Cancer Patients.” *Journal of Clinical Oncology: Official Journal of the American Society of Clinical Oncology* 27 (21): 3437–44. https://doi.org/10.1200/JCO.2008.18.9068.

Pollak, Michael. 2008. “Insulin and Insulin-like Growth Factor Signalling in Neoplasia.” *Nature Reviews. Cancer* 8 (12): 915–28. https://doi.org/10.1038/nrc2536.

Renehan, Andrew G., Margaret Tyson, Matthias Egger, Richard F. Heller, and Marcel Zwahlen. 2008. “Body-Mass Index and Incidence of Cancer: A Systematic Review and Meta-Analysis of Prospective Observational Studies.” *Lancet (London, England)* 371 (9612): 569–78. https://doi.org/10.1016/S0140-6736(08)60269-X.

Renehan, Andrew G., Marcel Zwahlen, Christoph Minder, Sarah T. O’Dwyer, Stephen M. Shalet, and Matthias Egger. 2004. “Insulin-like Growth Factor (IGF)-I, IGF Binding Protein-3, and Cancer Risk: Systematic Review and Meta-Regression Analysis.” *Lancet (London, England)* 363 (9418): 1346–53. https://doi.org/10.1016/S0140-6736(04)16044-3.

Rosen, Evan D., and Bruce M. Spiegelman. 2014. “What We Talk About When We Talk About Fat.” *Cell* 156 (1–2): 20–44. https://doi.org/10.1016/j.cell.2013.12.012.

Seale, Patrick, Heather M. Conroe, Jennifer Estall, Shingo Kajimura, Andrea Frontini, Jeff Ishibashi, Paul Cohen, Saverio Cinti, and Bruce M. Spiegelman. 2011. “Prdm16 Determines the Thermogenic Program of Subcutaneous White Adipose Tissue in Mice.” *The Journal of Clinical Investigation* 121 (1): 96–105. https://doi.org/10.1172/JCI44271.

Seo, Bo Ri, Priya Bhardwaj, Siyoung Choi, Jacqueline Gonzalez, Roberto C. Andresen Eguiluz, Karin Wang, Sunish Mohanan, et al. 2015. “Obesity-Dependent Changes in Interstitial ECM Mechanics Promote Breast Tumorigenesis.” *Science Translational Medicine* 7 (301): 301ra130-301ra130. https://doi.org/10.1126/scitranslmed.3010467.

Shahar, Suzana, Rabeta Mohd Salleh, Ahmad Rohi Ghazali, Poh Bee Koon, and Wan Nazaimoon Wan Mohamud. 2010. “Roles of Adiposity, Lifetime Physical Activity and Serum Adiponectin in Occurrence of Breast Cancer among Malaysian Women in Klang Valley.” *Asian Pacific Journal of Cancer Prevention* 11 (1): 61–66.

Stern, Jennifer H., Joseph M. Rutkowski, and Philipp E. Scherer. 2016. "Adiponectin, Leptin, and Fatty Acids in the Maintenance of Metabolic Homeostasis Through Adipose Tissue Crosstalk." *Cell Metabolism* 23 (5): 770–84. https://doi.org/10.1016/j.cmet.2016.04.011.

Sugiura, K., and C. C. Stock. 1952. "Studies in a Tumor Spectrum. II. The Effect of 2,4,6-Triethylenimino-s-Triazine on the Growth of a Variety of Mouse and Rat Tumors." *Cancer* 5 (5): 979–91. https://doi.org/10.1002/1097-0142(195209)5:5<979::aid-cncr2820050514>3.0.co;2-j.

Ulanet, Danielle B, Dale L Ludwig, C Ronald Kahn, and Douglas Hanahan. 2010. "Insulin Receptor Functionally Enhances Multistage Tumor Progression and Conveys Intrinsic Resistance to IGF-1R Targeted Therapy." *Proceedings of the National Academy of Sciences of the United States of America* 107 (24): 10791–10798. https://doi.org/10.1073/pnas.0914076107.

Valli, Alessandro, Matteo Morotti, Christos E. Zois, Patrick K. Albers, Tomoyoshi Soga, Katharina Feldinger, Roman Fischer, et al. 2019. "Adaptation to HIF1α Deletion in Hypoxic Cancer Cells by Upregulation of GLUT14 and Creatine Metabolism." *Molecular Cancer Research* 17 (7): 1531–44. https://doi.org/10.1158/1541-7786.MCR-18-0315.

Wang, Y. Claire, Klim McPherson, Tim Marsh, Steven L. Gortmaker, and Martin Brown. 2011. "Health and Economic Burden of the Projected Obesity Trends in the USA and the UK." *Lancet (London, England)* 378 (9793): 815–25. https://doi.org/10.1016/S0140-6736(11)60814-3.

Weber, Matthias M., Christian Fottner, Sun Bin Liu, M. Christina Jung, Dieter Engelhardt, and Gustavo B. Baretton. 2002. "Overexpression of the Insulin-like Growth Factor I Receptor in Human Colon Carcinomas." *Cancer* 95 (10): 2086–95. https://doi.org/10.1002/cncr.10945.

Wei, Tai, Peng Ye, Xin Peng, Li-Ling Wu, and Guang-Yan Yu. 2016. "Circulating Adiponectin Levels in Various Malignancies: An Updated Meta-Analysis of 107 Studies." *Oncotarget* 7 (30): 48671–91. https://doi.org/10.18632/oncotarget.8932.

Witherspoon, Mavee, Qiuying Chen, Levy Kopelovich, Steven S. Gross, and Steven Lipkin. 2013. "Unbiased Metabolite Profiling Indicates That a Diminished Thymidine Pools Is the Underlying Mechanism of Colon Cancer Chemoprevention by Alpha-Difluoromethylornithine (DFMO)." *Cancer Discovery* 3 (9): 1072–81. https://doi.org/10.1158/2159-8290.CD-12-0305.

Zabala-Letona, Amaia, Amaia Arruabarrena-Aristorena, Natalia Martín-Martín, Sonia Fernandez-Ruiz, James D. Sutherland, Michelle Clasquin, Julen Tomas-Cortazar, et al. 2017. "MTORC1-Dependent AMD1 Regulation Sustains Polyamine Metabolism in Prostate Cancer." *Nature* 547 (7661): 109–13. https://doi.org/10.1038/nature22964.

Zhang, Maomao, Julie S. Di Martino, Robert L. Bowman, Nathaniel R. Campbell, Sanjeethan C. Baksh, Theresa Simon-Vermot, Isabella S. Kim, et al. 2018. “Adipocyte-Derived Lipids Mediate Melanoma Progression via FATP Proteins.” *Cancer Discovery*, January, CD-17-1371. https://doi.org/10.1158/2159-8290.CD-17-1371.

Zoncu, Roberto, Alejo Efeyan, and David M. Sabatini. 2011. “MTOR: From Growth Signal Integration to Cancer, Diabetes and Ageing.” *Nature Reviews. Molecular Cell Biology* 12 (1): 21–35. https://doi.org/10.1038/nrm3025.